The reconstruction of past climate variability in the NW Indian Ocean based on a coral proxy record from the Maldives

(109 Seiten, 44 Abbildungen, 8 Tabellen)

Dissertation
zur Erlangung des Doktorgrades
der Naturwissenschaften

vorgelegt beim Fachbereich Geowissenschaften
Goethe-Universität
in Frankfurt am Main

von
David Storz
aus Filderstadt
Frankfurt am Main, 2010

(D30)

vom Fachbereich 11 der

Goethe-Universität Frankfurt am Main als Dissertation angenommen.

Dekan: Prof. Dr. Robert Pütz

Gutachter: Prof. Dr. Eberhard Gischler

Prof. Dr. Wolfgang Oschmann

Datum der Disputation:

Abstract

Until now, the NW Indian Ocean was sparsely covered with coral proxy records, and records from the Maldives Archipelago do not exist. The first such coral proxy record from the central Maldives is presented in this study. It originates from a massive *Porites lutea* (Quoy and Gaimard, 1833) colony that was sampled March 2007 in the lagoon of Rasdhoo Atoll (4°N/ 73°W), which is located in the central Maldives. The record spans a period of 90 yrs and reaches back to 1917 AD with monthly to bimonthly resolution. This study investigates temporal variations of the skeletal stable oxygen ($\delta^{18}O$) and carbon ($\delta^{13}C$) isotopes, the strontium-to-calcium (Sr/Ca), and the annual extension-rates, and their relationship to historical climate variations 1917-2007.

Annual extension-rates show an increase over the 20th century, and are correlated with instrumental sea surface temperatures (SST). The interannual variation of the extension-rates within 2.5-4 years is driven by the El Niño-Southern Oscillation (ENSO). The amount of skeletal extension during the summer months is triggered by variations in the strength of the SW monsoon. Interannual and decadal variability in monsoon current activity (18-19 yrs) and rainfall over India are an expression of the summer monsoon strength. This is the reason why a statistical link between coral extension-rates and precipitation over India can be established. This implies that annual extension-rates in corals can be used as a new proxy for Indian monsoon variability on decadal resolution.

The $\delta^{18}O$ record exhibits the 20th century warming trend that is influenced by the effect of monsoon-induced cooling. $\delta^{18}O$ also reveals interannual ENSO triggered variability, which is due to ENSO-forced variations in SST and sea surface salinity (SSS). A decadal variation at 12-14 yrs cannot be linked to SST variations in the NW Indian Ocean, but with decadal variations of SSS. They could be caused by ENSO-forced variations of the monsoon currents during the mature phase of ENSO teleconnections in the Indian Ocean in boreal winter.

The Sr/Ca record does not indicate a significant warming, in spite of the observed SST rise at the sampling site. Changes in seawater Sr/Ca cannot be excluded. Nevertheless, interannual ENSO forcing is still evident. Evidence for the Pacific Decadal Oscillation (PDO) is found during 1917-1955. Afterwards, the Sr/Ca data indicate the disappearance of PDO forcing. By the combination of Sr/Ca and

$\delta^{18}O$ it is possible to detect ~80% of historical El Niño and La Niña events at the sample site. This study confirms the notion that interannual to multi-decadal climate fluctuations in the Pacific play a crucial role for climate variability in the Indian Ocean.

Kurzfassung

Bis jetzt gibt es im nordwestlichen Indischen Ozean nur sehr wenige Arbeiten, die historische Klimavariabilität mit Korallenarchiven rekonstruieren. In dieser Arbeit werden die ersten Korallenproxy-Aufzeichnungen von den Malediven vorgestellt. Sie stammen aus einem Kern einer massiven Koralle der Art *Porites lutea* (Quoy und Gaimard, 1833), welche in der Lagune von Rasdhoo (4°N/73°W), eines Atolls im zentralen Bereich des Archipels, im März 2007 beprobt wurde. Die Zeitreihe umfasst 90 Jahre, und reicht mit monatlicher bis zweimonatlicher Auflösung zurück bis in das Jahr 1917. Diese Arbeit untersucht die zeitlichen Variationen der stabilen Isotopenverhältnisse von Sauerstoff ($\delta^{18}O$) und Kohlenstoff ($\delta^{13}C$), und des Strontium/Calcium (Sr/Ca)-Verhältnis im Skelettmaterial, sowie der jährlichen Wachstumsraten (jährliche Dicke eines Inkrements) zwischen 1917-2007 und stellt diese in den Bezug zu historischen Klimavariabilität im nordwestlichen Indischen Ozean.

Die jährlichen Wachstumsraten nehmen über die Beobachtungszeit zu, was mit der Erwärmung des Meerwassers im nordwestlichen Indischen Ozean im 20. Jahrhundert erklärt werden kann. Es kann gezeigt werde, dass die zwischenjährlichen Variationen des Wachstums des Korallenskeletts innerhalb der Periodizität von 2.5-4 Jahren durch Variationen des Klimaphänomens El Niño-Southern Oscillation (ENSO) gesteuert werden. Ein Zusammenhang zwischen dem Korallenwachstum während des Sommermonsuns und dem Niederschlag über Südindien konnte gefunden werden, da das Wachstum in den Sommermonaten von der Stärke der Monsunströmungen gesteuert wird. Zwischenjährliche und dekadische Variabilität von Monsunniederschlägen und -strömungen sind Ausdruck der Monsunstärke. Die Ergebnisse zeigen daher, dass die jährliche Wachstumsrate der Koralle als neues Archiv für dekadische und zwischenjährliche Variationen der Sommermonsunstärke verwendet werden kann.

Die Zunahme der Meerwassertemperaturen über das 20. Jahrhundert zeigt sich auch in der Zeitreihe von $\delta^{18}O$, welche einen Trend zu leichteren Isotopenverhältnissen aufweißt. Der Effekt der windinduzierten Kühlung durch den Monsun im nordwestlichen Indischen Ozean hat einen Einfluss auf den Langzeittrend von $\delta^{18}O$. Außerdem unterliegt $\delta^{18}O$ ebenfalls zwischenjährlichen Schwankungen, die vom ENSO System gesteuert werden. Sie wurden durch die Variationen in den Meerwassertemperaturen (SST) und der Salinität verursacht. Es kann gezeigt werden, dass ein dekadisches Signal mit der Periodizität von 12-14 Jahren nicht temperaturgesteuert ist, sondern von dekadischen Schwankungen des Salzgehaltes herrührt, möglicherweise verursacht durch ENSO-gesteuerte Variationen der zonalen Strömungen während der Wintermonsunzeit.

Die Sr/Ca-Daten zeigen keinen Langzeittrend, wie man es eigentlich erwarten sollte, da eine signifikante Zunahme der SST durch die instrumentellen Klimadaten und $\delta^{18}O$ angezeigt wird. Es ist nicht auszuschließen, dass das Sr/Ca-Verhältnis im Meerwasser während des letzten Jahrhunderts variiert hat. Trotzdem zeigt die Sr/Ca Zeitreihe zwischenjährige Variabilität, die mit ENSO verbunden werden kann, und Hinweise auf die Pazifische Dekadische Oszillation (PDO), ein Klimaphänomen, welches die Klimavariabilität im Indio-pazifischen Bereich steuert. Die Sr/Ca-Zeitreihe zeigt, dass dieses Phänomen nach 1955 das Klima in den zentralen Malediven nicht mehr beeinflusst. Mit der Kombination von Sr/Ca und $\delta^{18}O$ ist es möglich, 80% der historische El Niño- und La Niña Ereignisse auf den Malediven zu rekonstruieren. Diese Arbeit bestätigt die Annahme, dass zwischenjährige bis dekadische Klimavariationen im Pazifik eine wichtige Rolle für Variabilität der SSTs im Indischen Ozean spielen.

Content

List of figures

List of tables

1. Introduction

Coral proxy records serve as excellent recorders of paleo-environmental conditions in tropical and subtropical near-shore waters (Gagan et al., 2000, Lough, 2004; Grotolli and Eakin, 2007). Isotopic and trace elements signatures vary in a predictable way as a result of environmental variations, such as SST, SSS, ocean circulation, precipitation and cloud cover. Multi-century climate records from tropical and subtropical oceans are either sparse or non-existent, or have various limitations (Reynolds et al., 2002; Rayner et al., 2003; Smith and Reynolds, 2004; Thompson et al., 2008). Due to relative short instrumental records, which do not reach back beyond the 18th century, the understanding of long-term climate variability requires the extension of climate records prior the 19th century. The investigation of coral records as high resolution climate archives is thus highly valuable for the understanding of recent climate variations and teleconnections in the tropics and beyond.

The W and NW Indian Ocean are sparsely covered with long multi-decadal to centennial coral isotopic records (Figure 1). Until the last decade, most climate proxy studies have been conducted in the Pacific Ocean (for locations and references see Gagan et al. [2000], and Grotolli and Eakin [2007]). The Pacific is the origin of interannual to multi-decadal climate variations, such as El Niño-Southern Oscillation (ENSO), and the Pacific Decadal Oscillation (PDO), which are influencing climate variability in the tropics and beyond. The Pacific Ocean is thus the "classical" field for historical proxy climate reconstructions.

The Indian Ocean is nevertheless also subject to interannual, decadal and multi-decadal climate forcing. The predominant climate phenomenon north of 10°S is the Indian Monsoon system, which is characterized by seasonal reversals of the surface wind system and a distinct seasonality of precipitation. The understanding and prediction of decadal and interannual variations of the Indian Monsoon are of high socio-economic interest. It is driven by the seasonal shift of the Inter-Tropical-Convergence Zone (ITCZ), due to differential heating of the Eurasian subcontinent and the Indian Ocean. The last decades of research showed that huge portions of climate variability in the Indian Ocean are mainly triggered by the Pacific. The Indian Ocean climate is affected by the ENSO phenomenon, centered in the tropical E Pacific. It forces the Indian monsoon as well as the monsoon system of East Africa

during years with ENSO anomalies (Hastenrath, 1988; Torrence and Webster, 1999). SST of the central equatorial Indian Ocean is clearly influenced by interannual ENSO variability via reversal of the Walker circulation pattern. Due to its connection to the western Pacific warm pool, warmest SSTs are found in non-El Niño years in the eastern part of the Indian Ocean. El Niño-events in the Pacific lead to a turnaround in the large-scale Walker circulation. The result is the reversal of zonal wind stress, and therefore in zonal SSTs. Hence, strong El Niño years cause higher-than-normal SSTs in the western equatorial Indian Ocean (Webster et al., 1999). ENSO is phase-locked to the annual cycle of the Indian monsoon. Its mature phase is found during the NE monsoon in the winter months (Webster and Yang 1992; Hung et al., 2004). An ENSO-like decadal climate mode in the Indian Ocean is proven to originate in the Pacific as well (Cobb et al., 2001, Pfeiffer and Dullo, 2006). On a multi-decadal timescale, the Pacific Decadal Oscillation (PDO) modulates climate in the Pacific and remotely in the Indian Ocean (Mantua et al., 1997). It is not proven yet that the PDO modulates ENSO variability but it seems to strengthen both El Niño – and La Niña states during PDO warm or cold phases, respectively (Mantua et al., 1997; Linsley et al., 2008). The definition of a PDO index is based on SST records in the N Pacific: a "cool" PDO regime prevailed from 1890-1924 and again from 1947-1976, while "warm" regimes dominated the remaining periods (Mantua and Hare, 2002). It is likely that the Indian Dipole is also driven by external Pacific forcing by the Pacific (e.g., Charles et al., 2003), despite the fact that some studies indicate an internal mode of climate atmosphere-ocean interaction unique to the Indian Ocean, (e.g., Saji et al., 1999; Webster et al., 1999). SST variations restricted to the in the equatorial Indian Ocean, and independent of Pacific forcing, are suggested to be one reason for decadal monsoon variability (Kucharski et al., 2006).

Coral proxy studies conducted in the NW and W Indian Ocean made important contributions to the understanding of Indian Ocean climate variability. The genus *Porites* is the common coral used for proxy-climate studies in the Indo-Pacific realm. The most common proxy for coral climate reconstructions is coral stable oxygen ($\delta^{18}O$). It is principally a function of variations of SST and SSS, i.e. seawater $\delta^{18}O$. Studies from the Seychelles (Charles et al., 1997), Kenya (Cole et al., 2000), Eritrea (Klein et al., 1997), La Réunion (Pfeiffer et al., 2004b), and the Chagos Archipelago (central tropical Indian Ocean, Pfeiffer et al., 2004a) revealed ENSO-driven interannual and decadal climate variability. Zinke et al. (2004) were able to detect in

the SW Indian Ocean several phases of stronger and weaker ENSO teleconnection since the mid of the 17th century with a record from Madagascar. Pfeiffer and Dullo (2006) found for the first time evidence for the impact of the Indian monsoon system by the detection of monsoon-wind induced cooling in a coral proxy record from the Seychelles. Until now, none of the coral records successfully tracked the temporal variability of the monsoon system. Recently, evidence for PDO-related oscillations in the Indian Ocean was found in a coral proxy record from the southern hemisphere (Madagascar and La Réunion, Crueger et al., 2009). Zinke et al. (2009) reconstructed with coral indices that were based on the published coral records from the Seychelles, Kenya, and Mayotte, teleconnections between SST variability, precipitation and surface air temperatures over East Africa and western India.

Interannual and decadal variations of $\delta^{18}O$ in coral proxy records are often dominated by variations in SST and/or SSS. The Sr/Ca in coral skeletons, negatively correlated to ambient SST, was introduced as a salinity-independent SST proxy (Corrège, 2006). High-resolution calibration studies for the genus *Porites* at different sites in the Indo-Pacific revealed its significant SST-dependence (e.g., Beck et al., 1992; Alibert and McCulloch, 1997; Corrège et al., 2000; Fallon et al., 2003). These studies usually cover relative short periods of several years to one decade. The accuracy of Sr/Ca as a thermometer underlies, however, on a variety of processes. This is best seen in the fact that for every single location, different Sr/Ca-SST calibrations are published (Corrège, 2006). The precondition of long-term historical SST reconstructions is the invariance of the seawater Sr/Ca ratio (e.g., Beck et al., 1992). Several studies have challenged the postulate of invariance of the Sr/Ca ratio in space and time (e.g., De Villiers, 1999; Sun et al., 2003; De Dekker et al., 2004). This subverts the idea of the application of coral Sr/Ca as a seawater independent SST proxy. Skeletal chemistry is influenced by physiological processes (e.g., Cohen et al., 2001, 2002; Meibom et al., 2003, 2006; Sinclair et al., 2006), and early diagenesis or calcite-filled borings in live-collected corals (Nothurft et al., 2007). Finally, heterogeneties in the distribution of Sr in coral skeletons (e.g., Allison et al., 2005; Cohen et al., 2001; 2002) also limit the accuracy of Sr/Ca as a SST proxy.

However, due to the ambiguous nature of coral $\delta^{18}O$, coral Sr/Ca is still an important proxy for past SST reconstructions (Corrège et al., 2006). In combination with $\delta^{18}O$, Sr/Ca was successfully used to separate the seawater $\delta^{18}O$ component from $\delta^{18}O$, and to reconstruct past SSS trends and variations (McCulloch et al., 1994;

Gagan et al., 1998; Hendy et al., 2002; Felis et al., 2009). Marshall and McCulloch (2001) used a decadal coral Sr/Ca record from the Indonesian Outflow region, in order to affirm the notion that the Pacific is triggering climate variations in the Indian Ocean. Long-term Sr/Ca records in the NW Indian are still missing. Pfeiffer et al. (2006) published the first short Sr/Ca record spanning 45 yrs from Peros Banhos, 10° to the south of Rasdhoo Atoll in the central Indian Ocean (Chagos Archipelago, 5°20'S/71°55'N). These authors were able to reconstruct strong El Niño events for 1950-1995. Pfeiffer et al. (2009) found significant correlations of three Sr/Ca records of the same location with gridded SST data. Higher correlations with a record of air temperatures of a local climate station demonstrate that the access on local climate data improves climatologic interpretations of coral records. First evidence for the PDO in coral proxy records from the NW and central Indian Ocean was found by Pfeiffer et al. (2009). They were able to track the shift from "cool" to "warm" PDO regime during the mid-1970s.

Until now, no coral proxy records from the Maldives archipelago, the largest reef area in the Indian Ocean, have been published. This study presents the first coral proxy record (δ^{18}O, δ^{13}C, Sr/Ca and extension-rates) from this area, covering the period 1917-2006 AD. The location of the Maldives has the potential to allow the investigation of the effect of wind-induced cooling in the vicinity of monsoon wind reversals. This study attempts to reconstruct monsoon-related SST patterns in the NW Indian Ocean and interannual to decadal climate variability in the Maldives. Coral extension-rates are often disregarded in proxy climate studies, and the investigation of annual extension in *P. lutea* as an archive for ENSO and/or monsoon-forced interannual to decadal climate variability is one focus of this study. The new multi-proxy record emphasizes the potential of corals for climate reconstructions in general, and of climate variability in the NW Indian Ocean in particular

2. Regional Setting

2.1. Geomorphology

The Maldives Archipelago in the NW Indian Ocean is amongst the largest carbonate platforms in the world (Figure 1). It is about 1.000 km long and up to 150 km^2 wide, encompassing an area of 107.500 km^2. In total, about 0.3% of this area is represented by some 1.300 small islands, only 10 of which are larger than 2 km^2. The maximum land elevation is 5 m above present seal level. The Maldives Archipelago is bounded bathymetrically by the 2.000 m contour, i.e., it rises steeply from the surrounding Indian Ocean seabed. Geomorphologically, the archipelago forms a double row of a total of 22 atolls, with the two rows separated by the up to 450 m deep Inner Sea basin (Figure 2). Rasdhoo Atoll (alternative diction "Rasdu", sometimes also called "Ross Atoll"; 4°N/73°W) is located in the western row of the Maldivian Atolls. It is an almost circular atoll with a maximum diameter of 9.25 km and a size of 62 km^2 (Figure 3). The marginal reef is continuous and surface-breaking, and three channels through it connect the interior lagoon with the open ocean. The reef rim surrounds a 40 m-deep lagoon with numerous coral patch reefs. The fore reef slope is very narrow except on the western side of the atoll. The slope ends in an almost vertical drop-off (Gischler et al., 2008). The coral study of Scheer (1974) reported 99 coral species at Rasdhoo. For comparison, Pillai and Scheer (1976) list a total of 241 species for the entire archipelago.

2.2. Climate and hydrology

The central Maldives are located in the vicinity of the Indian monsoon system. The climate is dominated by the seasonal reversal of the monsoon winds (Figure 4a and b). Over the Indian Ocean north of 10°S, they generally blow from SW during May-September (summer monsoon) and from NE during November-February (winter monsoon). Hence, the wind speed record (Figure 4c) shows a bimodal seasonal pattern with highest values in May and October/November at the onset and the end of the wet SW monsoon (sources, references and abbreviations of all used climate data sets are given in Table 1). The seasonal reversal of the monsoon winds force the

5

reversal of sea surface currents at the central Maldives (Figure 4d). The monsoon currents are the predominant oceanographic characteristic of the N Indian Ocean (Shankar et al., 2002; Figure 5). The SODA zonal current record, as an indicator for the strength of the monsoon currents, is used here due to the closeness to the equator. It is strongly correlated with the meridional current record ($r = 0.97$, $p < 0.0001$). In May and October/November the ITCZ moves over the central Maldives during its seasonal displacement. In these months the outgoing longwave radiation (OLR) is lowest, while it is highest January/February (Liebmann and Smith, 1996). The ITCZ movement is also reflected in the bimodal pattern of precipitation (Figure 6a). Salinity (SSS) fluctuates between 34.4 (February/March) and 35.4 psu (September) in the instrumental SSS record, does not exhibit a bimodal pattern and is not in phase with precipitation (Figure 6b). The relationship between SSS and precipitation in the seasonal cycle illustrates the decoupling of atmosphere and hydrological cycle in this region. This may be due to the forcing of seasonally reversing circulation in the upper ocean, caused by the seasonally reversing monsoon winds over the northern Indian Ocean (Schott and McCready, 2001; Shankar et al., 2002). With the onset of the summer monsoon, the currents introduce upwelled, saltier waters of the western Arabian Sea at the central Maldives. After the collapse of the summer monsoon currents, the winter monsoon currents influence the central Maldives by the introduction less salty waters from the Bay of Bengal (Eigenheer and Quadfasel, 1999; Figure 5). Additionally, wind stress evaporation during the SW monsoon in summer may also contribute to higher salinity during the wet summer monsoon season.

The maximum monthly SST is lagging maximum SSS by 6 months, and minimum monthly SST is lagging minimum SSS by 1-2 months (Figure 6b and c). The seasonal SST cycle shows the importance of the effect of monsoon-induced cooling in the NW Indian Ocean. Maximum SSTs occur in April, during the transition phase between the monsoons, shortly before the onset of the SW monsoon and average 29.5 °C. Minimum SSTs occur in January, in the dry NE monsoon season, and average 27.8 °C (ERSST dataset). Continuous long-term SST records from Rasdhoo Atoll are not available. Short in situ SST measurements were conducted at Rasdhoo for the period April 2005 to March 2006 by a SST logger installed at the reef slope of Kuramathi (8.7 m depth). Highest monthly SST occurred in this time span in April 2005 (30.4 °C) and lowest in January 2006 (27.3 °C). The timing of both events is in agreement with the instrumental record, but the seasonal cycle of 3.1 °C in this single

year was significant higher than observed in the gridded SST dataset though (2.2 °C; ERSST and HadISST1).

SST observations for the 2°x2° grid box surrounding the central Maldives show a mean seasonality of 1.7 °C (ERSST dataset, Figure 6c), in agreement with the 1°x1° gridded HadISST1 dataset. The close link between ENSO variations and SST variability throughout the Indian Ocean and in the central Maldives is illustrated in Figure 7. In this study, the Niño 3.4 index is used as a reliable proxy for the strength of ENSO, and is based on SST (ERSST) anomalies in the central Pacific (Figure 7a; Trenberth, 1997). The field correlation in Figure 7b shows the strong and significant positive correlation between SST variability and Niño 3.4 in the interannual band. The cross-spectral analysis between gridded SST of the central Maldives and Niño 3.4 reveals the typical modes of ENSO forcing in the interannual range of the SST spectrum. No significant coherence is found for SST and Niño 3.4 in the decadal band (ERSST, Figure 7c).

SST exhibit a significant long-term trend since 1917 (r = +0.79, p < 0.0001, e.g. ERSST). The ERSST and HadISST1 datasets indicate a SST rise of +0.7 °C since 1917. Available SODA SSS data since 1958 indicate a weak freshening trend (r = -0.32, p < 0.001), while the precipitation record of Male International Airport (70 km E of Rasdhoo) since 1975 does not show a secular trend.

No data on the isotopic composition of the precipitation on a seasonal time-scale is available. However, perennial monthly measurements in the northwestern and central Indian Ocean have been carried out at few locations, e.g., at Diego Garcia (7°20'S/72°25'E) with a mean annual range between -2 and -5‰ for $\delta^{18}O$ (reported relative to Vienna Standard Mean Ocean Water [VSMOW], Global Network of Isotopes in Precipitation [GNIP] database, International Atomic Energy Agency 1994). Ten measurements of seawater $\delta^{18}O$ composition in the lagoon and fore reef of Rasdhoo (sampled February 2009) show a mean $\delta^{18}O$ of 0.52‰ (+/- 0.12‰ SD, Table 2).

3. Material and methods

3.1. Sampling and measurements

Searching for and finding an appropriate *Porites* colony in Rasdhoo Atoll was quite lengthy and difficult because more than 90 % of the very large colonies were dead as a consequence of the 1998 bleaching event in the central Maldives (Wilkinson et al. 1999; Schuhmacher et al. 2005). A 95 cm long core (C1) was recovered from a colony of *P. lutea* in March 2007 on Rasdhoo Atoll. The colony is living on a patch reef in the central area of the lagoon. The coral head is 1 m high with the top between 0.5 and 1 m below sea level. The core was drilled parallel to the dominant axis of growth from the top of the head using a pneumatic drill device (Figure 8).

Slices with a thickness of five millimeter were cut from the core and cleaned in an ultrasonic bath of deionised water. X-ray radiographs were prepared from the slices in order to reveal growth directions, density variations and annual banding (Figure 9). Thin sections from the top, the middle and the bottom were visually analyzed in order to rule out the existence of diagenetic effects, such as recrystallization and/or non-skeletal growth of aragonite. No evidence for mineralogical alteration and secondary cementation is found. Coral slices were dried and then sampled by milling about 250 µg from the surface with a dental drill along the maximum axis of growth. The sampling resolution was 11-13 samples per cm along axis, i.e., a sample every 0.7 to 0. 9 mm on average was taken. This provides an almost monthly resolution due to an annual extension-rate of ~1 cm.

Powdered subsamples (60-120 µg) were reacted with 100 % H_3PO_4 at 72 °C using a Gas Bench II (Thermo Finnigan) according to the method outlined by Spötl and Vennemann (2006). Samples were analyzed for $\delta^{18}O$ and $\delta^{13}C$ at the Institute for Geosciences, University of Frankfurt on a Thermo Finnigan MAT253 mass spectrometer. The analytical error was 0.08‰ for $\delta^{18}O$ and 0.06‰ for $\delta^{13}C$, respectively. All coral isotope data are reported relative to the Vienna Peedee Belemnite (VPDB).

All Sr/Ca analytical work was done at the IFM GEOMAR, Universty of Kiel and samples were submitted in three charges (batches). The sample powder as obtained from micro-drilling and submitted in three sample charges was weighed into polycarbonate tubes and dissolved overnight with 1 ml 2% (v/v) subboiled nitric acid.

An aliquot from this digest solution was transferred to polypropylene tubes and made up to 10 ml 2% (v/v) nitric acid resulting in an approximate concentration of 10 (4-12) mg l^{-1} Ca. Multi-element stock solutions were gravimetrically prepared from SPEX Specpure grade single element standard solutions, acidified to 2 % (v/v) with subboiled nitric acid (quartz distilled), and stored in PFA (perfluoralkoxy) flasks. While Ca was kept at constant concentrations of approximately 10 mg l^{-1} in all calibration solutions Sr was added to 160, 180, 200, 220 µg l^{-1} covering the natural range of Sr/Ca (7.3-10.1 mmol/mol) ratios in biogenic carbonates and seawater. Two laboratory blank solutions with and without 10 mg l^{-1} Ca were included in the calibration series. We could not see any matrix effect from 10 or 50 mg l^{-1} Ca on the background signal of the other analyses. All sample preparation work and storage of measuring solutions in the autosampler during analysis were under Class-100 clean bench conditions. Only all-plastic labware was used for handling and treatment of the samples. The subsequent measurements were performed by ICP optical emission spectrometry (ICP-OES) using a CIROS^{CCD} SOP instrument with radial viewing of the plasma (Spectro Analytical Instruments, Kleve, Germany). The instrument was equipped with a MicroMist™- 200 micro-nebulizer with nominal 200 µl min^{-1} sample uptake and a water-cooled (4°C) Cinnabar™ cyclonic spraychamber (Glass Expansion, Australia). The wavelengths Ca: 317.933 nm and Sr: 407.771 nm were selected for quantitative analysis, and Ar: 597.159 nm was used as a monitor line for plasma temperature. The detector read-out was forced to be real simultaneous. Raw-data (in counts per second, cps) from 5 individual acquisitions per sample were exported to secondary spreadsheet software for further data reduction. We applied an intensity ratio calibration strategy as outlined by De Villiers et al. (2002) with a linear least-square regression function for the calculation of molar ratios (in mmol/mol) from intensity ratios (in cps/cps). The results were then externally normalized to our in-house coral standard "Mayotte 5a" with Sr/Ca = 8.819 mmol/mol). This standard was re-analyzed as a bracketing standard for every set of 6 unknown coral samples. It was also used for a step-wise drift correction (e.g., Schrag, 1999). More than 10% of samples were re-analyzed for the estimation of analytical precision. Every tenth sample was re-analyzed after one hour, and some samples were analyzed both at the beginning and end of an analytical session, and with the next sample batch after a month or so. The analytical error (1sigma) of the Sr/Ca measurements as estimated from these replicate measurements was 0.09%

RSD within-sample batch and 0.11% RSD between sample batches, or better than 0.01 mmol/mol Sr/Ca.

Between each of the charges an offset between of 0.02-0.03 mmol/mol exists. The Sr/Ca data are therefore given in zero mean values, in order to remove this discontinuity.

3.2. Coral chronology

Cyclic variation in the $\delta^{18}O$ record is assumed to be annual, with each cycle spanning around 1 cm. Sub-annual dating is based on the annual $\delta^{18}O$ cycles, where the most positive $\delta^{18}O$ value is assigned to be the coldest average month, which, for the central Maldives, is January. This introduces a noncumulative error of +/- 1-2 months in any given year due to variations in the timing of the lowest winter SSTs. Since $\delta^{18}O$ is a composite signal of both SST and seawater $\delta^{18}O$, the observation that SST minima lag precipitation and salinity minima by 1-2 months on average may induce further inaccuracy in the fixing of the anchor points. The chronology is thus tied to one anchor month January within each year. The $\delta^{18}O$ and $\delta^{13}C$ were interpolated to equidistant, monthly resolved time-series using the AnalySeries 2.0.4.2 software package (Paillard et al., 1996). The banding is caused by density variations in the skeleton with dense layers being formed during the summer months and less dense layers during winter. The proxy data chronology has been cross-checked with the dense bands; heavier $\delta^{18}O$ values clearly matched the winter layers in most cases. Skeletal portions with unclear density banding pattern (i.e. heavy stress bands) exist. Unclear annual banding is not necessarily a problem for the age model of a coral chronology. For instance, most equatorial Pacific *Porites* corals do not even reveal annual density bands, and the chronologies are established using the annual cycles in $\delta^{13}C$ (oral communication with Dr. Thomas Felis, MARUM, University of Bremen). The chronology is thus based on the proxy data. Prerequisite of this age model is constant linear extension within a given year.

3.3. Statistical treatment

For the spectral analyses of the coral and instrumental climate data the software AnalySeries 2.0.4.2 is used. Prior to spectral analyses, the individual time-series were detrended by removing the linear trend and normalizing to unit variance. The Blackman Tukey method was used (Blackman and Tukey, 1958), which is the classical method for spectral analyses. This procedure is very robust to spurious spectral features. The algorithm computes first the autocovariance of the data, and then applies a window (Barlett), and finally Fourier-transforms the covariance functions to compute a power spectrum (Paillard et al, 1996). The chosen window should not considerably affect the results for typical short and noisy time series. A further advantage of this method is the possibility to apply cross spectra for two time-series. This method provides the statistical tool to detect correlations between two time-series in the spectral range, when ordinary least square correlations are not significant. In order to improve statistical significance, all time-series analyses were repeated by applying the high-resolution Multi-taper Method and the Maximum Entropy Method, provided by the same software package (not shown).

4. Results

4.1. Oxygen isotopes

The monthly $\delta^{18}O$ of C1 is plotted in Figure 10a. The record of annual mean values shows a long-term trend towards more negative isotope values that is highly significant (r = -0.51; p < 0.001), the absolute offset since 1917 is -0.17‰. The annual mean $\delta^{18}O$ is -4.92‰ and the record fluctuates between -4.81 and -5.10‰ (Table 3). The $\delta^{18}O$ record exhibits a clear seasonality (defined as the difference of maximum and minimum value in a given year) with a mean value of 0.39‰.

Within the mean seasonal cycle (not to be confused with seasonality), lowest monthly $\delta^{18}O$ occur in August (Figure 11a). In comparison, the mean seasonal SST cycle of the gridded datasets indicates highest monthly SST in April, before the onset of the summer monsoon cooling.

The correlation between monthly $\delta^{18}O$ and ERSST is weak, but significant (r = -0.31, p < 0.001), and stronger than for HadISST1 (r = -0.22, p < 0.001). Higher correlations between annual mean $\delta^{18}O$ and gridded SST data were found. Again, $\delta^{18}O$ exhibits a stronger correlation with ERSST than HadISST1 (Table 4). A regression equation between $\delta^{18}O$ and SST yields a best fit line with highest slope (-0.13 ‰/°C) for the $\delta^{18}O$-SST relationship, when the ERSST dataset is used (Table 5). This slope is not consistent with published estimates (between -0.18 and -0.22 ‰/°C for *Porites* corals (e.g., Lough, 2004). Figure 12a compares the annual mean coral $\delta^{18}O$ of C1 with gridded SST from the ERSST datasets for the period of 1917-2006. When the linear trends in both records are removed, no significant correlation between annual mean $\delta^{18}O$ and SST exists. Coral $\delta^{18}O$ and SST follow the long-term warming trend in the central Maldives. Consequently, the correlation between proxy and SST is highest, when applied for the whole record. A correlation between annual mean $\delta^{18}O$ and SSS since 1958 is not significant (Table 4).

4.2. Strontium-to-calcium ratio

The monthly Sr/Ca record fluctuates between -0.07 and +0.07 mmol/mol (zero mean values, Figure 10b). The coral Sr/Ca record shows no long-term trend towards lower ("warmer") values (Figure 12b). The absence of a long-term trend in Sr/Ca disagrees with the SST rise in this region, since gridded instrumental SST data indicate a significant warming, accelerated since 1955. The records of annual mean $\delta^{18}O$ of C1 also show a long-term trend (Figure 10a). Since every single charge of the Sr/Ca record does not show an inherent long-term trend, it is unlike to address this discrepancy to an analytical artifact. The correlation between annual mean Sr/Ca and instrumental SST is therefore weaker (e.g., ERSST: r = -0.21; p = 0.05) than after removing the long-term trend (e.g. ERSST: r = -0.34, p < 0.01). It is stronger in the lower part of the record until 1955 (Table 6, Figure 12b). The correlation between annual mean Sr/Ca and Niño 3.4 is weak, but significant (r = -0.28, p < 0.01).

The mean seasonality is 0.13 mmol/mol. The range of published Sr/Ca-SST calibration slopes is wide and varies from 0.05-0.08 mmol/mol $°C^{-1}$ (Corrège, 2006). With an averaged value of 0.06 mmol/mol $°C^{-1}$ (Corrège, 2006), we would receive mean seasonal fluctuations of ~2.2°C at the sampling site. This value is higher than SST fluctuations observed in the gridded SST datasets (+1.7°C), and could indicate stronger site-specific SST variability. The mean seasonal Sr/Ca cycle shows most positive ("coldest") values in January and most negative ("warmest") values in August (Figure 11a), and corresponds to the seasonal cycles of $\delta^{18}O$ (Figure 11b). Both coincide in the timing of coolest and warmest months. The Sr/Ca record confirms the age model based on the assumption that heaviest $\delta^{18}O$ values are assigned to the January.

4.3. Carbon isotopes

The long-term trend of coral $\delta^{13}C$ shows a significant decrease towards lighter values since 1917 (Figure 13). The monthly record ranges between 0 and -2‰ and shows a distinct seasonality of 0.71‰ (+/- 0.26‰ SD). The seasonal cycle is in phase with $\delta^{18}O$ and, hence, responsible for a significant correlation between both records, even when long-term trends are removed (r = 0.25; p < 0.001). Most positive

coral $\delta^{13}C$ values are developed during the winter monsoon season in January/February in any given year, and highest values in August (not shown). A correlation between annual mean time-series of $\delta^{13}C$ and $\delta^{18}O$ is insignificant.

4.4. Annual extension-rates

The coral growth-rate refers in the literature sometimes either to the growth characteristic linear extension-rate, or to calcification-rate. To avoid confusion, the term "extension-rate" is used here instead of "growth-rate" for the distance between two $\delta^{18}O$ maxima in the seasonal cycle. The annual extension-rate in C1 is 9.9 mm/yr (+/- 2.1 mm/yr SD, Figure 14a). This value falls within the lower range of 6-16 mm/yr, observed for *Porites* corals (Lough and Barnes, 2000).

C1 shows a significant trend towards higher annual mean extension-rates throughout the record ($r = +0.37$, $p < 0.001$, if described linearly, Figure 14b). The absolute increase since 1917 is 3 mm/yr). The correlation of linear extension-rates with both instrumental SST datasets is similar and significant ($r = +0.48$, $p < 0.001$). In the lower part of the record, i.e., during the period between 1920 and 1955, the extension-rates exhibit a concave shape that resembles the SST record in this period at first glance ($r = +0.69$, $p < 0.0001$). Years with decreased extension-rates down to 5 mm/yr are found in especially in the upper part of the record, in 1982, 1992 and 1997-1998 may reduce the strength of the correlation after 1955 ($r = +0.45$; $p < 0.001$).

5. Discussion

5.1. Annual extension-rates

5.1.1. Trend and SST reconstruction

The annual extension-rates are based on the age model applied on the $\delta^{18}O$ record. The discussion is started with annual extension-rates, since they are later used in the discussion of geochemical proxies. The annual extension-rate record of C1 follows the warming trend of 0.7°C evident in the instrumental record. The positive correlation between the extension-rate record of C1 and SST for 1917-2006 is in agreement with the observation of Lough and Barnes (2000), who found a significant SST-dependence of annual calcification and extension in massive *Porites* corals. The absolute increase of annual mean extension since 1917 is about 3 mm/yr. This would roughly correspond to an increase of 4 mm/yr for each one-degree rise in SST. Lough and Barnes (2000) found for each one-degree rise in SST along the Great Barrier Reef a comparable increase of 3 mm/yr for individual *Porites* colonies. Hence, the significant long-term trend of the annual extension-rates can be explained as a consequence of the warming in the central Maldives. Years with decreased extension-rates reduces the correlation and should be linked to ecological stress. These events cannot be explained by SST anomalies alone (Chapter 5.4.).

In order to demonstrate the SST-sensitivity of annual extension-rates in *Porites* corals, Lough and Barnes (2000) compared mean annual extension-rates of 44 records from reef sites in the Indo-Pacific with the corresponding mean SST. The correlation between mean annual extension-rate is strong (r = +0.91, p < 0.0001; Figure 15). If the dominant factor of annual mean extension in C1 was SST (28.7 °C for 1917-2006; ERSST), both values should plot next to the regression graph in Figure 15. A temperature of 28.7 °C should correspond, following Lough and Barnes (2000), to an annual mean extension-rate of about 18 mm/yr in C1. This is significant higher than 9.9 mm/yr in C1. For comparison, Pfeiffer et al. (2004a) found in their coral proxy study with *P. lutea* an annual mean extension-rate of 14-15 mm/yr for the period 1875-1996. The annual mean SST at Peros Banhos (Chagos Archipelago) is 28.0 °C (1°x1°; Had1SST1 Hadley1SST dataset). Extension-rate record and SST plot in this case near the line of best fit in Figure 15.

This discrepancy between SST and expected annual mean extension-rate can be explained by the fact that the mean annual extension-rate in *Porites* depends, for a given period, not only on SST, but also on other environmental parameters, such as turbidity (Tomascik et al., 1994) and hydraulic energy (a measure of water motion due to waves and tidal currents, Scoffin et al., 1992). Turbidity is only important in shelf environment with continental influence. Evidence for strong water motions in the lagoon of Rasdhoo Atoll was found by Gischler (2006). This author revealed tidal currents as crucial controlling factor for sediment deposition at Rasdhoo Atoll. Fine sediment is winnowed by strong tidal currents in the eastern part of the atoll adjacent to channels through the marginal reefs, leading to an asymmetric distribution of modern carbonate sediments at this site (Figure 16). It is therefore likely that the hydrological conditions described by Gischler (2006) permanently affected the growth strategy of the coral colony, which thus sacrificed extension for increased skeleton density to produce a more robust skeleton.

This example implies that mean annual extension-rate of pre-instrumental *Porites* records cannot be used without the knowledge of past environmental conditions as a proxy or "paleothermometer" for the calculation of past ambient SST. Due to the prevailing site-specific conditions at Rasdhoo Atoll, one would consequently estimate a ~2.5° lower mean SST for the recorded period at the location, as given in the gridded SST records.

The empirical relationship between annual mean extension-rates and skeleton density for the Indo-Pacific locations is negative; the increase of annual mean extension causes the decrease in skeleton density (Lough and Barnes, 2000). Following this relationship, one could estimate a mean skeletal density of 1.4 g/cm^3 in C1.

5.1.2 Interannual and decadal climate variability

The Indian Ocean SSTs are externally forced by the ENSO, centered in the central Pacific (Webster et al., 1998; Murtugudde et al., 2000). The extension-rate record shows at first glance a high interannual variability (Figure 14). Since the annual extension-rates are influenced by ambient SST variations, one could expect also evidence for ENSO signature in this record. A cross-spectral analysis reveals several spectral peaks from sub-decadal to interannual range (Figure 17), centered

at ~3.7 yrs, ~3.1, ~2.8 and 2.3 yrs. These peaks are the typical modes of the ENSO-driven interannual variability, which are also evident in the gridded SST record of the central Maldives (compare with Figure 7c). The cross-spectrum (lower panel of Figure 17) demonstrates significant spectral coherence between annual extension-rates and the annual mean Niño 3.4 index for these peaks. The ENSO mode of 5-6 yrs, found in the SST spectrum, is only evident with lower spectral coherence in the cross-spectrum. The ENSO mode of ~3.7 yrs is the strongest interannual mode in the extension-rate record, i.e., yielding the largest amount of spectral power. This is in agreement with the dominance of this period in the SST record. Figure 18 illustrates the strong in-phase relationship between extension-rates and SST within the band of 3-4 yrs. Both time-series reveal the amplification of the 3-4 yrs band after ca. 1950, and the weakening of this mode towards the end of the record. Weaker ENSO driven teleconnections at the central Maldives agrees with the observation that the state of the ENSO system was weaker for 1920-1950, and as a consequence, the ENSO teleconnection into remote areas such as the Indian Ocean thus degraded (Kumar et al., 1999). The significant in-phase relationship also implies the accuracy of the applied age model.

The extension-rate record reveals a phase shift of about 6 months to one year to ENSO-forced SST anomalies in the central Pacific. This effect can be demonstrated by the application of field correlations between the extension-rate record of C1 and gridded SST for the Indo-Pacific realm (Figure 19). The "center action" of the ENSO system is the Eastern Pacific, but Yu and Reinecker (1999) and Murtugudde et al. (2000) reported that towards the end of ENSO events, such as the 1997/98 event and earlier events, warming propagated from west to east, resulting in extreme SST anomalies in the E Indian Ocean. This could be seen as part of the propagating ENSO wave described by Tourre and White (1997) and White and Cayan (2000). In the analysis of Figure 19 the extension-rate record and SST datasets were high-pass filtered in order to eliminate slow variations or trends. If the extension-rate record lags the SST fields by one year, the correlations throughout the NW Indian Ocean and the geographical center of ENSO forcing in the eastern equatorial Pacific is negative (Figure 19a). This does not agree with the empirical relationship between annual extension of *Porites* corals and SST. In the reversed case, i.e., if SST lags the extension-rate record by one year, SST fields with positive correlation are produced in parts of the NW Indian Ocean, but not in the Pacific

17

(Figure 19b). A lag of 6 months between SST and extension-rate produces fields with positive correlation throughout the whole Northern Indian Ocean between extension-rates and SST fields in central eastern equatorial Pacific (Figure 19c).

Studies investigating climate-induced variations in coral growth are relatively rare. ENSO-related growth variability was also found in a *Porites* head in the "center of action" in the central Pacific (French Polynesia, Bessat and Buigues, 2001), in this case for the annual calcification-rate. Interannual ENSO signature is also found in a coral record from the Arabian Sea (Tiwari and Rao, 2001). ENSO-forced interannual variability outside the Indo-Pacific has been found, however, not for *Porites*, in an endemic coral taxon in the southwestern-south Atlantic (Evangelista et al., 2007),

The period of ~2.3 yrs in the Blackman Tukey spectrum is the typical mode of the Quasi-biennial oscillation (QBO), a phenomenon that was originally observed between westerly and easterly equatorial stratospheric winds (Reed et al., 1961; Baldwin et al., 2001). The QBO significantly influences the Indo-Pacific realm and is found in a variety of meteorological records of precipitation, rainfall, wind-speed and SST (Conversi and Hammed, 1998). The exact nature of the connection between the stratospheric and atmospheric QBO remains unresolved (Dean and Kemp, 2004). The QBO yields periods between 2.1 and 2.4 yrs and is also evident in other climate archives, such as varved sediments and tree rings (Dean and Kemp 2004). Tiwari and Rao (2001) found the QBO of 2.3 yrs in an extension-rate record from the Gulf of Kutch (Northern Arabian Sea). A QBO modulation was also reported by Charles et al. (1997) in the coral $\delta^{18}O$ record from the Seychelles. Local Rainfall and gridded wind speed records from the central Maldives also yield a QBO signature.

ENSO forcing explains only fluctuations in the interannual band of the extension-rate record. The extension-rate record reveals furthermore spectral power in the quasi-decadal range at ~8.6 yrs. This signal can be explained by SST variations, since both records share spectral coherence in this range (Figure 20), and are in phase with each other (Figure 21). This period within 8-9 yrs appears to be an "endemic" pattern of climate variability in the NW Indian Ocean. It should not been associated with the Indian Ocean Dipole, since it is suggested that this mode is principally a product of strong ENSO-like teleconnections over the Indian Ocean (Charles et al., 2003). A coral-based Dipole index established by these authors and based on coral $\delta^{18}O$ records yields a period of 12-13 yrs.

5.1.3. Monsoon current variability

SST-driven interannual and quasi-decadal variability is only one characteristic of the extension-rate record. The extension-rate record yields a clear variability in the decadal to multi-decadal rang at first glance (Figure 14). After 1958, a significant decadal variability centered at ~18.3 yrs, and a period centered at ~6.6 yrs is evident in the power spectrum. Both periods are not found in the earlier part of the time-series (Figure 22). They do not belong to the typical ENSO modes found in the record, and are supposed to be not connected to SST variability at the central Maldives. Beside SST variations, the annual extension might also be affected by variations in hydraulic energy at the sampling site (Scoffin et al., 1992). The SODA zonal currents record (0.5°x0.5) for 1958-2004 illustrates the seasonal reversion of the zonal currents for the NW and SW monsoons in the central Maldives including Rasdhoo Atoll (Figure 23). The dataset indicates a two-time higher current velocity during the SW monsoon. Variations in the monsoon current activity should be stronger in the lagoon of Rasdhoo Atoll due to the strong tidal currents and the limited space in the lagoon. Interannual and decadal variations in the hydrological energy in the lagoon, especially in the summer months, might have consequences for the coral growth.

In order to demonstrate that coral growth is affected by variability of the summer monsoon currents, cross correlations were applied for the annual extension-rate record with (1) the mean NE monsoon (November-February) current record, (2) the SW monsoon (May-September) current record, and (3) the difference between NW and SW monsoon currents as an intra-annual gradient. This analysis led to two conclusions:

(1) *No link between NE monsoon currents and extension-rates.* Expectedly, the spectrum of the annual mean NE monsoon record does not share spectral coherence with the extension-rates for the signals within 18-19 yrs and 6-7 yrs (Figure 24a). Spectral coherence is found for periods centered at ~4.5 and ~2.9 yrs, but cross-phase analysis shows that the current record lags the extension-rate record for these periods by 2 yrs, which disproves causality (not shown).

(2) and (3) *Link between SW monsoon and extension-rates.* The cross-spectrum between the time-series of the SW monsoon current and the extension-rate record reveals both spectral alignment and significant coherence for the periods

centered at ~18 yrs and in the interannual range (Figure 24b). The generated time-series of seasonal differences between summer and winter-monsoon shows stronger spectral coherence at 18-19 yrs (Figure 25a). Almost 80 % of the variance of annual extension in this range can be explained by the variance in this generated dataset within the range of ~18.3 yrs. Weaker spectral coherence at ~6.6 yrs could be due to the fact that this band is also part of interannual SST variability, and both parameters could interfere with each other. No temporal lag between both time-series is found (Figure 25b and c).

Stronger current velocities during the SW monsoon and consequently a higher level of hydraulic energy imply enhanced ecological stress for the coral. Signals at ~18.3 yrs and ~6.6 yrs are suggested to be modulated by variations in formation of the growth band during summer. Coral growth responds to phases with higher SW monsoon currents with the production of denser summer layers, and as the consequence, reduced seasonal extension. This is especially the case, when summer months with higher-than normal SW currents follows winter monsoon with weak monsoon current activity. The same analysis repeated with mean winter/spring SST, and summer/autumn SST reveals no significant differences to the cross spectrum in Figure 20 (not shown). Solar radiation is also seen as an important environmental parameter that promotes the seasonal timing of intra-annual growth. In *P. lutea* colonies, the sub-annual extension- and calcification-rate are positively correlated with changes in seasonal solar radiation (Sun et al., 2008). No statistical link to winter/spring OLR is found with the extension-rates (both not shown). This is in agreement with Lough and Barnes (2000), who showed that light availability is of minor importance for annual mean growth in *Porites* corals. This implies that that the strength of the SW monsoon currents is the principal factor, which determines annual growth in C1.

Shallow water lagoon environments may enhance broad-scale environmental variations. SST and current variations in the lagoon of Rasdhoo are likely larger than indicated by gridded instrumental climate records. These records average over a wider geographical range including different marine settings. However, since long-term in-situ SST and current measurements are not available, this is still speculative. Extension-rate records from corals thriving in lagoon environments with weak or steady current activity might be better suited for the reconstruction of pre-instrumental SST variability. Otherwise one has to expect the interference of non-

SST signals. For instance, Tiari and Rao (2001) found no monsoon-related decadal or interannual spectral peaks in their time-series analysis of extension-rates and described their ENSO signals to be driven by SST. However, these authors used a coral of the genus *Favia* as climate archive and did not give a description on the sampling site. A different growth strategy of this coral and possible different environmental conditions should be considered.

An example for the successful application of extension-rates for the reconstruction of multi-decadal SST variations is the study of Saenger et al. (2009). These authors used a *Siderastrea* coral to reconstruct the strength of Atlantic Multidecadal Oscillation beyond instrumental times. It was even possible to calibrate extension-rates with SST and to calculate absolute SST values for pre-instrumental times. Gischler et al. (2009) published Pleistocene extension-rate records for the genus *Montastraea*, Florida Keys, which also yield multi-decadal to interannual variations, possibly linked to climate oscillations.

For further ecological and environmental interpretations of the long-term growth trend in C1, the annual mean calcification-rate (product of skeleton density and annual extension) would be of interest. It depends on a variety of environmental parameters (Sun et al., 2008), and is in the focus of reef research, since its reaction to global warming and ocean acidification is crucial for the health of reef systems (Bessat and Buigues, 2001; De'ath et al., 2009). Long-term changes in the calcification-rate in corals could be caused by the progressive acidification of the oceans due to the release of anthropogenic CO_2 by combustion of fossil fuels (De'ath et al., 2009). Due to the increase of annual mean extension, a potential decrease of the calcification-rate in C1 throughout the last decades could have been accompanied by the progressive decline in skeletal density. This trend is likely modified by the decadal, monsoon-induced variations in annual extension. Acidification and the decline of calcification could favor bioerosion in reef systems in the future. Corals could loose their commonness in these ecosystems (De'ath et al., 2009).

5.1.4. Reconstruction of rainfall over India

Both predominant periods, centered at 18-19 yrs and 6-7 yrs in the spectrum of extension-rates, are associated with variations in the strength of the monsoon system. Decadal variations in the strength of the Indian monsoon system are forced by endemic Indian Ocean SST variations, rather than by ENSO (Kucharski et al., 2006). Monsoon Current variations are an expression of this dynamics. The All Indian Monson index (AIR, Sontakke and Singh, 1996; Figure 26a) is a further parameter, which is triggered by the strength of the monsoon system. It is a reliable indicator for the strength of the SW monsoon over the Indian subcontinent (Sontakke and Singh, 1996). A cross-spectral analysis between AIR and the extension-rate reveals significant coherence within 18-19 yrs and 6-7 yrs (Figure 26b). The extension-rate record shares with the annual mean May-September AIR index almost 92% of variance within the band of 18-19 yrs, and 85 % within 6-7 yrs. Annual extension-rates lags the AIR index by 2 yrs within 18-19 yrs indicating a short response time between SW monsoon current variability and rainfall over India (Figure 26c). This demonstrates that C1 recorded the strength of the monsoon-system, by the sensitivity of coral growth to current variability during the summer months.

Since the extension-rate record shows a statistical link to AIR, a field correlation is applied with land precipitation datasets. In order to remove background noise, a high-pass filter was applied prior to analysis (Figure 27a). These correlations are negative over fields on the Indian subcontinent, the Arabian Peninsula, and in Africa north to the Ethiopian highlands. The extension-rate record can therefore be used as a proxy of rainfall variability for these regions, shown exemplarily for the Ghats region, southern India (Figure 27b). The correlation is strong and significant for 1958-2006. The negative correlation is in agreement with the proposed mechanism of teleconnection: periods of stronger summer monsoon causes higher rainfall in the Ghats region, and higher monsoon current activity in the central Maldives. Higher hydraulic energy in the lagoon during summer reduced growth in C1. In contrast, precipitation fields over Kenya are positive correlated with C1 and reveal a dipole character to the Indian subcontinent. This characteristic between equatorial Africa and Indian reflects the temporal variations in the strength of the ITCZ. Phases of higher monsoon strength over the Indian subcontinent are accompanied with drier conditions over equatorial Africa (Janicot, 2009). Beside precipitation, C1 shows no

correlation to air temperatures over India. For comparison, Zinke et al. (2009) succeeded a statistical link between a constructed coral $\delta^{18}O$ index (Seychelles, Kenya, Mayotte) land temperatures, beside and rainfall, over India, equatorial East Africa and southeast Africa.

5.1.5. Sub-annual extension

The mean seasonal cycles of $\delta^{18}O$, Sr/Ca yield an annual mean cycle, which shows coolest SST in January and warmest SST in July and August. Based on linear sub-annual growth, both proxies do not indicate the effect of monsoon-induced cooling within their seasonal cycles, which leads to a decline of SST after April/May. This creates actually a lag of, on average, 3 months between the reconstructed and instrumentally measured warmest month in the seasonal cycle. This offset (indicated with an arrow in Figure 28) is the result of non-linear skeletal extension on sub-annual scale, with accelerated monthly extension during winter and spring and slowed monthly extension during the remaining time. This temporal difference enables the conduction of a rough estimation of summer and winter extension-rates, since it is assumed that the Sr/Ca seasonal cycle is principally driven by SST. If it is assumed that the Sr/Ca minimum, which is assigned to August by the model of linear annual growth, is rather formed on average in April/May, the offset implicates that the mean sub-annual extension-rates between January and April/May is twice as high as in the remaining year. This effect explains the weak correlation between monthly Sr/Ca, $\delta^{18}O$ and gridded SST. This observation underlines the significance of the current activity on the growth of C1 on sub-annual scale during the SW monsoon.

5.2. Oxygen isotopes

5.2.1. Interannual and decadal climate variability

The extension-rate record demonstrates the presence of ENSO forcing in the coral time-series. Since coral $\delta^{18}O$ depends on interannual variations of both SST and SSS, this could reduce the sensitive of $\delta^{18}O$ for ENSO variability, due to possible overlay of both parameters. ENSO reaches its mature phase in boreal winter

between November and February (e.g., Hung et al., 2004). A cross-spectrum of November-February $\delta^{18}O$ and Niño 3.4 reveals distinct spectral peaks and corresponding coherence centered at 12-14 and ~2.8 yrs (Figure 29). Weaker spectral peaks are found in the typical ENSO modes of ~5.3, ~3.7 and ~2.8 yrs. This interannual variability illustrates again the strong coupling between the Pacific and the Indian Oceans. Additionally, significant coherence within 12-14 yrs between $\delta^{18}O$ and Niño 3.4 suggests Pacific climate forcing in this decadal band. This is consistent with the finding of Cole et al. (2000), Cobb et al. (2001) and Pfeiffer and Dullo (2006). This decadal signal cannot be explained by ENSO forced SST variations. SST does not yield this signal in the power spectrum (Figure 7).

The presence of an ENSO-like decadal variation in the power spectrum of $\delta^{18}O$ is the result of the fact that $\delta^{18}O$ is also influenced by SSS variations. Since annual mean $\delta^{18}O$ only weakly correlates with annual mean gridded SST (r = -0.41, p < 0.001; ERSST), $\delta^{18}O$ must also be affected by SSS variability of ambient seawater. Indeed, coral $\delta^{18}O$ shows stronger variations that cannot explained SST variations in the gridded dataset. The lagoon of Rasdhoo was definitely subject of stronger SST variations than evident in the broad-scale averaged SST record, but the onset of decadal fluctuations after ca. 1950 is remarkable (Figure 12a). This is also demonstrated by a wavelet-analysis, in which a decadal signal started to occur after this year (Figure 30).

The nature of the ENSO-like variability of 12-14 yrs in coral $\delta^{18}O$ can be illustrated with the application of a cross-spectrum between this proxy and gridded SST and SSS. For 1958-2004, for which the SSS data are available at SODA, no spectral coherence is expectedly found between $\delta^{18}O$ and SST in the decadal ENSO band of 12-14 yrs (Figure 31a). Moreover, spectral coherence is found between $\delta^{18}O$ and SSS within this range (Figure 31b). This relation between $\delta^{18}O$ and ENSO variability is confirmed by repeating this analysis for the Niño 3.4 index, SST and SSS records (Figure 31c and d). This analysis indicates that SSS is the driver for the 12-14 yrs fluctuations in $\delta^{18}O$. In the interannual range, $\delta^{18}O$ and both instrumental records show analogue peaks centered at ~5.3 yrs and ~3.7 yrs, matching the dominant ENSO modes.

Since the annual extension-rates in C1 are subject to interannual and decadal variability, one could speculate that growth-related metabolism effects could be the origin of climate signals in coral $\delta^{18}O$. However, several reasons argue against a

predominant role of growth-effects for the origin these signals in coral $\delta^{18}O$. First, studies conducted with the genus *Porites* show that $\delta^{18}O$ can be influenced by annual mean extension-rate below a critical threshold level of 6 mm/yr (Felis et al., 2003). The annual mean extension-rate in C1 is 9.9 mm/yr and significantly higher than this value. Second, a linear correlation between annual mean $\delta^{18}O$ and extension-rates is insignificant (r = -0.17, p = 0.31), and no spectral coherence is found between both records in the interannual range (not shown). Finally, the ENSO-like signal of 12-14 yrs is not found in the extension-rate record (Figure 17). No correlation between annual mean $\delta^{13}C$ and $\delta^{18}O$ indicates that metabolic effects did not exert control on $\delta^{18}O$ (Guilderson and Schrag, 1999).

The lack of the decadal ENSO-like variation in the extension-rate record supports the idea that this signal is not forced by SST. The origin of this oscillation is subject of debate (e.g., Latif and Barnett, 1994; Pierce et al., 2000; Evans et al., 2001; Timmermann et al., 2003). The decadal mode of ENSO variability is not connected with SST anomalies in the eastern equatorial Pacific (Latif et al., 1997). Cobb et al. (2001) found a clear coherence between coral $\delta^{18}O$ records from the Seychelles and Palmyra (central Pacific) in the range of this ENSO mode. Pfeiffer and Dullo (2006) speculated that interactions between trade and monsoon winds in the Indian Ocean are the origin of this ENSO-like signal on a decadal scale. Reason et al. (1996) showed that decadal variations in the wind over the Pacific may introduce decadal variations in the Indian Ocean via the Indonesian Throughflow. Climate models and instrumental records indicate that wind stress and the monsoon current are strongly varying with ENSO variability in the Indian Ocean along the equator (Manghnani et al., 2003). Consequently, both the record of COADS wind speed (2°x2°) and SODA zonal currents (0.5°x0.5°) for November-February reveal an ENSO-like period of 12-14 yrs (not shown). Possibly decadal SSS and consequently coral $\delta^{18}O$ variations could be linked to decadal wind driven changes in the strength of the winter monsoon current by ENSO. Evidence for ENSO-forced variability of Indian Ocean currents is also found in a coral $\delta^{18}O$ record from La Réunion, SW Indian Ocean. There, La Niña events are triggering the strength of inflow of the Southern Equatorial Current are found as interannual signals in the record (Pfeiffer et al., 2004b).

5.2.2. Long-term SST trend and monsoon-induced cooling

A link between decadal monsoon variability and Indian Ocean $\delta^{18}O$ proxy records was not possible to establish in the previous studies. Coral $\delta^{18}O$ records from Kenya (Cole et al., 2000), and the Seychelles (Charles et al., 1997, 2003) showed a clear influence by ENSO, Cole et al. (2000), Charles et al. (1997) and Charles et al. (2003) relied on AIR as a measure for monsoon strength. Charles et al. (1997) claimed that decadal variations in their coral $\delta^{18}O$ record from the Seychelles should be explained by variations of the Indian monsoon strength, since the AIR index also yields variations in the decadal range (Chapter 5.1.4.). Stronger rainfall over the Indian subcontinent could be associated with more positive $\delta^{18}O$ (i.e., cooler SST). Enhanced convection over Indian should lead to stronger low-level winds and increased cooling of the W Indian Ocean through evaporation and wind-induced mixing (Charles et al., 1997). In contrast, Cole et al. (2000) found no statistical link between their own $\delta^{18}O$ record from Kenya and the $\delta^{18}O$ record of Charles et al. (1997) from the Seychelles with AIR. However, Webster and Yang (1992), and Vinayachandran (2004) showed that rainfall indices are not the best measures to characterize the monsoon-strength in the NW Indian Ocean, due to the complex atmosphere-ocean interactions. Felis et al. (2000) showed a counterexample for a coral $\delta^{18}O$ record outside of the NW Indian Ocean, which shows a relationship to the AIR index. These authors found a connection between AIR and $\delta^{18}O$ in the interannual range in a *Porites* coral from the northern Red Sea, which can be explained by the monsoon-desert mechanism of Rodwell and Hoskins (1996), where variations in the strength of the Asian monsoon via teleconnections are proposed to have a control on Saharan and Mediterranean subsidence and therefore aridity.

A good measure for the decadal variations of monsoon strength in the Indian Ocean is instead the SW monsoon current variability (Chapter 5.1.3). But decadal variations in the SW monsoon strength are not recorded by the coral $\delta^{18}O$ record of C1 (Figure 29). A significant correlation between the AIR index and the coral $\delta^{18}O$ record of C1 from the central Maldives does therefore not exists, similar to the $\delta^{18}O$ record of Pfeiffer and Dullo (2006) from the Seychelles, and no spectral coherence in a cross-spectrum between both time-series was found (not shown). Instead of relying on rainfall indices as a measure for the strength of the Indian monsoon in the Indian Ocean, Pfeiffer and Dullo (2006) found a clear link between a coral proxy record from

the Seychelles and the monsoon wind system. The strength of the δ^{18}O-climate correlation depends on the annual cycle of the monsoon year; their record primarily reflects wind-induced cooling of the SW monsoon season.

The secular depletion in δ^{18}O can be explained with the SST rise at the sampling site. Monsoon wind-induced cooling could affect the secular warming trend found in coral δ^{18}O of C1. The absolute decrease of ~0.17‰ during 1917-2006 corresponds to a warming of ~0.7 °C in the gridded SST dataset of the central Maldives. Reduced correlation between δ^{18}O with SST ($r = -0.41$, $p < 0.001$) is addressed to interannual SSS variations. This explains the relative low slope of 0.13 ‰/°C for the empirical δ^{18}O-SST relationship.

In order to show that the long-term trend of δ^{18}O is affected by monsoon-induced cooling, a field correlation between the monthly anomalies of the δ^{18}O record and SST datasets in the Indian Ocean is applied. It reveals strongest correlations and, in particular, lowest p-values in an area that approximately corresponds to the area of the seasonal wind reversals (Figure 32a). An averaging of several records of an area may diminish effects of site-specific or region-specific SSS fluctuations, and enhance the significance of the long-term trend. In order to proof this, published monthly δ^{18}O records of *Porites* colonies from the Seychelles (Charles et al., 1997) and Kenya (Cole et al., 2000), locations in the central and western vicinity of the monsoon wind field, are combined (by averaging the monthly values for the period 1917-1995) with C1 to coral indices. Figure 32b illustrates the result of a field correlation between the coral index of C1 and the Seychelles record. An elongate SST-field in direction of the monsoon-winds is found off of E Africa. The corresponding field of p-values again maps a circular area, which is associated with the area of monsoon-induced upwelling in the southwest Arabian Sea. The index consisting of C1, Seychelles and Kenya maps the predominant wind fields during the SW and NE monsoons in the entire N Indian Ocean (Figure 32c). Highest p-values are found off of E Africa and the Arabian Peninsula.

This analysis suggests that the δ^{18}O record from the Maldives follows the long-term warming trend of this monsoon-influenced area in the NW Indian Ocean, despite of its location in the vicinity of this area. With the construction of the combined coral proxy record, it was possible to improve the proxy-climate correlation. Hence, it was even possible to reconstruct the rudimentary orientation of the seasonal wind field and to track the area of cold upwelled waters. The Arabian Sea is

cooled by monsoon winds by wind-induced evaporation and upwelling (Rao and Sivakumar 2000; Vinayachandran 2004). This demonstrates that information about monsoon-induced cooling is also inherent in the long-term trend of coral proxy records. This example illustrates the potential of corals to reconstruct broad scale SST trends. Coral indices are thus a reliable recorder for long-term SST trends, especially when existing SST records are unreliable, such as during the 1940-60s (Pfeiffer et al., 2008, Thompson et al., 2008).

5.3. Strontium-to-calcium ratio

5.3.1. Seasonal cycle and long-term trend

The mean seasonality of 0.06 mmol/mol corresponds to a seasonality of ~2.2°C in the lagoon of Rasdhoo Atoll. This indicates that the seasonal SST variations at this site are sufficiently captured by gridded SST datasets. This is supported by the fact that in-situ SST measurements at Kuramathi showed a clearly higher SST variation during 2005/2006. The seasonality of Sr/Ca should not be reduced by decelerated growth during the SW monsoon season, since lowest and highest monthly SST occurs January and May. The mean seasonal cycle of δ^{18}O is more obtused than that of Sr/Ca, which is likely caused by the fact that δ^{18}O is also influenced by seasonal variations in rainfall and SSS.

Compared to δ^{18}O and extension-rates, no long-term trend in Sr/Ca is found. The correlation with SST is best 1917-1955, and weaker afterwards (Table 6). This suggests that Sr/Ca is also influenced by non-temperature effects. Longer instrumental records of local ambient temperatures (either air or seawater) are, however, not available. We have already excluded diagenetic effects or secondary calcite-filled micro-holes caused by boring activity (Nothdurft et al., 2007, Chapter 3). The effect of coral growth on the incorporation of Sr^{2+} in the skeleton is believed to be negligible in *Porites* in most conducted studies (e.g., Alibert and McCulloch, 1997; Wei et al., 2000; Mitsugushi et al., 2003; Corrège et al., 2004; Allison and Finch, 2004). Effects of coral growth in C1 can be likely ruled out, since correlation between annual extension-rates and annual mean Sr/Ca is insignificant. Additionally, no spectral coherence is found between both time-series (not shown). Several studies

have challenged the postulate of invariance of Sr content in the world oceans (e.g. De Villiers, 1999; De Deckker et al., 2004). Sun et al. (2003) showed that calibrations between SST and coral Sr/Ca are better, when the Sr/Ca-ratio of the ambient seawater is involved in the empirical equations. This effect may explain discrepancies between coral Sr/Ca records from different parts of the ocean (De Villiers, 1999). It is suggested that Celestite ($SrSO_4$)-secreting Acantharia (suborder of the Radiolaria) are one reason for the invariant Sr distribution in the seawater (De Deckker, 2004). They are common in the upper 400 m at low latitudes of the oceans, and are most abundant between 14°-25° S (De Dekker, 2004). They contribute substantially to changes in seawater Sr/Ca by extracting Sr^+ for the formation of their skeleton. In the deeper ocean, the organisms dissolve and the Sr/Ca of seawater regains its conservative nature (De Villiers, 1999; De Dekker, 2004). In order to proof this suggestion, however, temporal and spatial abundance analysis of Acantharia in the region would be necessary.

Quinn et al. (2005) addressed discrepancies between the long-term trends in Sr/Ca and $\delta^{18}O$ to variable Sr/Ca ratios in the ambient surface-water in a *Porites* coral at a site in the W Pacific (Rabaul, Papua New Guinea). The Sr/Ca ratio in the study of Quinn et al. (2005) suggested an unrealistic cooling of 0.7 °C, but still revealed clear connections to ENSO variability. The possibility of short-term changes in seawater Sr was also suggested by Smith et al. (2006), who addressed interannual variation in skeletal Sr/Ca in a coral record from South Florida to variations of ambient seawater. Monthly resolution records of the $^{87}Sr/^{86}Sr$ ratio in *Porites* cores from southern Taiwan indicate a stronger mixing between surface and subsurface waters during El Niño years. This is caused the intrusion of a branch of the Kuroshio Current during these phases (Liu et al., 2009). Hydrological dynamics become a crucial aspect in the understanding of Sr/Ca variations in corals (Hu et al., 2009). These examples show that variations of seawaterSr/Ca at the sample site cannot be excluded. Since current variability plays an important role at the sampling site, a correlation between the coral Sr/Ca record and the monsoon current records was applied. A significant link to current variability was, however, not found.

Since a weak but significant correlation with annual mean SST (ERSST) exists, it is suggested that a SST component is still involved in the formation of the Sr/Ca signal. Based on this, the potential of Sr/Ca as a recorder for climate variability will be tested.

The correlation between the annual mean Sr/Ca record and $\delta^{18}O$ of C1 (also when the linear trend is removed) is also weak and insignificant. This could be also addressed to the strong interannual variations of salinity and SST at the location site.

5.3.2. Interannual Sr/Ca variability

The annual Sr/Ca spectrum reveals typical interannual ENSO peaks within the range at 2.7-3.0 yrs and in the typical ENSO band of 3.5-3.7 yrs, found in SST, extension-rates and $\delta^{18}O$ (Figure 33a). The decadal signal at 10-12.5 yrs slightly rising over the low resolution spectrum and is found neither in SST, nor in $\delta^{18}O$ and annual mean extension-rates datasets, and is possibly of non-SST origin. Highest coherence between the Sr/Ca record and Niño 3.4 at ~3.7 yrs demonstrates the sensitivity of Sr/Ca to capture the predominant mode of SST variability at the sampling site (Figure 33b). The evidence for interannual ENSO forcing can also be illustrated by the application of correlation between the interannual variability in Sr/Ca and in SST fields in the Indo-Pacific realm (Figure 34). The proxy record maps the "center of origin" of the ENSO system in the eastern tropical Pacific.

5.3.3. Pacific Decadal Oscillation

The predominant characteristic of the Sr/Ca record is its concave shape 1917-1955 (Figure 12). This pattern resembles the instrumental SST record at first glance; a correlation of annual mean Sr/Ca and SST (not de-trended) is obviously stronger than for the whole record (Table 6). The regression slope between gridded SST (ERSST) and Sr/Ca is -0.18 mmol/mol °C^{-1}, which is three-times lower than the mean regression slope of -0.06 mmol/mol °C^{-1} (Corrège, 2006; Figure 35). This could indicate a higher sensitivity of SST variations at the sampling site compared to the gridded SST dataset. One possible origin for varying slopes for the Sr/Ca-SST regression reported in coral proxy studies is indeed the choice of SST datasets (Corrège, 2006). Gridded SST datasets provide sometimes arguable SST records (e.g., Thompson et al., 2008). Differences between the ERSST and HadISST1 records for the central Maldives are obvious, when one regard the r-values for the correlation between Sr/Ca and SST for 1917-1953 (Table 6). Still, the lowest reported

regression slope value is -0.08 mmol/mol $°C^{-1}$ (Allison and Finch, 2004), which could also indicate the presence of a non-SST effect.

The gridded SST follows the PDO index during 1917-1955 at first glance (Figure 36). The annual mean Sr/Ca record consequently resembles the annual mean PDO index in 1917-1955 (Figure 37a). In the mid-1950s, the PDO signature disappeared similar to the gridded SST record, after the transition of the positive (warm) into the negative (cool) PDO regime at the end of the 1940s (Mantua et al., 1997). The multi-decadal peak (34-35 yrs) in the spectral-analysis should be addressed to the PDO signature during 1917-1950 (Figure 33).

The weakening of PDO-forcing in the central Maldives after 1950s can be illustrated in Figure 38 by the synopsis of field correlations applied for the PDO index, the coral Sr/Ca record and gridded SST for the central Maldives (ERSST), and SST fields in the Indo-Pacific realm. The impact of PDO is evident 1917-1955, but not afterwards (Figure 38a). Reversely, no or only few SST fields in the Pacific Ocean with significant correlation to Sr/Ca and central Maldivian SST are evident after the 1950s (Figure 38b and c). The permanent characteristic for both periods is the meridional dipole structure in the N and S Pacific, caused by the opposite SST development during PDO "warm" and "cold" phases (Mantua et al., 1997). During 1917-1955, the field correlation of Sr/Ca and SST reveals the spatial characteristic of the dipole in the N Pacific (Figure 38b). High correlations are found between Sr/Ca and SST in the coastal area off of North America and in the N Pacific. The dipole nature is also found for the SST dataset of the central Maldives in these decades (Figure 38c). Pfeiffer et al. (2009) also found for their combined Sr/Ca record from Chagos (71°E, 5°S) similar PDO-related SST fields in the Pacific, in their case for the period 1950-1995.

Beside SST, the PDO also reveals a strong linkage to sea level pressure (SLP) and precipitation in the Pacific (Deser et al., 2004). During 1917-1955, the PDO index reveals a significant correlation with SLP fields in the N Pacific, which can be reconstructed by the Sr/Ca record in this period (Figure 38). This underlines the interpretation of PDO forcing in the lower part of the time-series.

This climate link between the central Maldives and the Pacific for 1917-1955 can also be shown by using climate archives only. Beside our Maldivian Sr/Ca record, we used a Geoduck clam record (*Panopea abrupta*) deriving from the NE Pacific (122°W/48°N), which is a valuable SST proxy from the "center of action" of

PDO variability (Strom et al., 2004). Both records reveal a significant correlation for 1917-1955, while afterwards this correlation disappeared (Figure 37b). Pfeiffer et al. (2009) found a significant correlation between their combined Sr/Ca record and the same growth index for the period 1950-1995 at Chagos Archipelago.

The absolute amount of the transition in Sr/Ca would indicate a SST decline of ~2 °C (assuming a Sr/Ca-SST slope of -0.06 mmol/mol°C^{-1}) between 1942 and 1949. The two gridded SST datasets indicate, however, a drop of ~0.8 °C. Since in situ SST data of this period are missing, this discrepancy is difficult to resolve. Pfeiffer et al. (2009) found in their Sr/Ca records for the PDO shift in the mid-1970s at Chagos also discrepancies in the estimation of the amount of SST rise. Only one record indicates a warming, which is consistent with gridded SST.

5.4. The relationship between PDO, Indian Monsoon variability, and decadal ENSO-like variability in the coral record

The combination of the coral proxies Sr/Ca, extension-rates, and δ^{18}O can be used to demonstrate changes of climatic teleconnections with the Pacific in the decadal range. These proxy records reveal three conspicuous aspects: First, the coral record experienced PDO variabilty 1917-1955, which is confirmed by coral Sr/Ca. A correlation between extension-rates and Western Ghat precipitation is weaker during this interval than afterwards. PDO disappeared after the mid-1950s, and the correlation between annual extension-rate and Western Ghat Precipiation increased.

The annual extension-rates (Figure 40) benefited during the warm PDO phase 1922-1945 by warmer conditions. No correlation exists between the PDO index and the extension-rates in this period. This lack of correlation could be caused by the interactions of both SST and SW monsoon current variability. This should also be the origin for the weaker correlation between annual extension and rainfall over South India until 1955 (Figure 27). The shift from PDO to non-PDO dominance in the extension-rate record may explain the rise of years of reduced extension, observed for instance in 1982, 1992 and 1999 (Figure 40a). Most of these events coincide with more rain over the Western Ghat region (Figure 40b). Years with accelerated excursions occur in the majority of the cases in phases of weaker rainfall over the

Indian subcontinent. This is exemplary for the years with strong SW monsoon rainfall 1955-1995, where no positive excursion is found (Figure 40a).

Krishnan and Sugi (2003) found signatures of PDO on the summer monsoon over India. Their finding suggests an inverse relationship between the strength of PDO variations associated with the strength of monsoon rainfall. The majority of dry monsoon events appear during the PDO warm phases (Krishnan and Sugi, 2003), and the majority of wet monsoon events during the PDO cool phases. Sen Roy (2006) found also a negative relationship between PDO and rainfall during the dry NE monsoon.

The PDO disappears in the mid-1950s in the proxy and SST records during the period of the onset of decadal ENSO-like variation in $\delta^{18}O$ (Figures 12a, 30, 36). This could be a hint for changed teleconnection patterns between the NW Indian Ocean and the Pacific. The causes and mechanism of multi-decadal teleconnections originating in the Pacific associated with the PDO are still being investigated (e.g., Deser et al., 2004; D'Arrigo and Wilson, 2006). Evidence for remote PDO-forcing of SST and SLP by the flow of the South Equatorial Current and the flow through the Mozambique Channel is found in $\delta^{18}O$ records from Madagascar and La Réunion (Crueger et al., 2009). It is speculated that the proposed disappearance of PDO signature at the central Maldives is due to temporal changes in the influence of the dynamics of the Indonesian Throughflow and the Equatorial Currents. Changes in the hydrodynamics may also cause a change in seawater Sr/Ca after 1955 (Figure 12b). To address this question, more proxy records from C1 are needed, such as radiocarbon ($\Delta^{14}C$) and boron isotopes that can be applied as tracer for ocean circulation and water masses (see Grotolli and Eakin [2007], and references therein; Hönisch et al., 2004).

The temporal variability of the spatial pattern of the PDO in the N Indian Ocean is poorly understood (D'arrigo and Wilson, 2006). Still, Pfeiffer et al. (2009) found PDO signature in coral Sr/Ca records of the central Indian Ocean (Chagos Archipelago), and D'arrigo and Wilson (2006) found evidence for PDO teleconnection for 1870-1988 between a tree-ring record from Asia and the coral-proxy record from Kenya (Cole et al., 2000).

5.5. Reconstruction of ENSO events

The combination of Sr/Ca and $\delta^{18}O$ is usually used to reconstruct the seawater component of $\delta^{18}O$, which is correlated to SSS (Corrège, 2006). Two things are necessary for the reconstruction of past SSS: long in-situ SST data from the lagoon in order calibrate Sr/Ca with SSS, and the proof that Sr/Ca is not biased by non-SST effects. Both pre-conditions are not fulfilled. The combination of Sr/Ca and $\delta^{18}O$, however, could be used as detectors for historical ENSO events at the NW Indian Ocean, since Sr/Ca features an interannual component that is driven by SST (Figures 33 and 34).

El-Niño events lead to a warming of 0.5 °C-1.5 °C in the NW Indian Ocean (Reason et al., 2000). The magnitude of interannual ENSO anomalies is small, and the signal to noise ratio relative low (Annamalai et al., 1999). Therefore, Sr/Ca and $\delta^{18}O$ were filtered using a Hamming filter to remove the decadal components, short period noise and to highlight interannual variability in the ENSO band of 2.5 to 7 yrs. For the period 1917-2006, 21 La Niña and El Niño events were identified in agreement with SST (Figure 41). The 1997/98 El Niño event and the subsequent La Niña event of the following year show strong positive and negative excursion in the Sr/Ca record. Two possible events in the lower part of the record are not noted in the ENSO tabulation of Kousky and Bell (2000), and three are noted and detected in SST, but not found in both proxies. The strong El Niño event in 1982/83 was not identified with the proxy records. In total, about 80% of historical ENSO events were detected with in the coral proxies.

This confirms the notion of a SST component in the Sr/Ca record, but also the usefulness of $\delta^{18}O$, which depends on SST and SSS, as a proxy for historical SST variations. The band-passed filtered records of Sr/Ca and $\delta^{18}O$ indicate three-time higher SST fluctuations in the lagoon than the gridded SST record (Table 7). Higher SST fluctuations could be expected for the lagoon environment, but the influence of SSS fluctuations in the lagoon on $\delta^{18}O$, and the impact of non-SST effects on Sr/Ca are unknown. Therefore, a fluctuation (twice standard deviation) of 1 °C for the ENSO band SST variability in the lagoon could be overestimated.

The infrequency of ENSO events in the period 1920-1950 can be explained by weaker ENSO teleconnections during this period than in later decades (Kumar et al., 1999).

5.6. Carbon Isotopes

Although the primarily focus of this study are the extension-rates, coral $\delta^{18}O$ and Sr/Ca, it is important to briefly discuss the $\delta^{13}C$. Both $\delta^{18}O$ and $\delta^{13}C$ are in the seasonal cycle in phase with each other. Most positive coral $\delta^{13}C$ values are developed during the winter monsoon season in January/February in any given year, when SST is lowest and the seasonal solar radiation highest. Heavier $\delta^{13}C$ probably reflect the level of highest photosynthetic activity of the hosted zooxanthellae coincident with the most enriched ^{13}C portions of the coral skeleton (e.g., Swart 1983; Sun et al. 2008). It is likely that a major portion of the seasonal $\delta^{13}C$ cycle can be addressed to seasonal differences in light availability. Lighter $\delta^{13}C$ occur in August and not in early spring as indicated by OLR, as a consequence of the sub-annual slowing of skeletal extension (Chapter 5.1.5). The long-term trend towards lighter values in $\delta^{13}C$ is usually attributed to the Suess effect, i.e., the steady anthropologically induced release of lighter CO_2 into the atmospheric reservoir via combustion of fossil fuels (Figure 42).

Coral $\delta^{13}C$ depends on a variety of abiotic and biotic factors (e.g., Grotolli, 2002; Maier et al., 2003). Therefore, $\delta^{13}C$ records have always been considered to allow a less-straight forward environmental interpretation than $\delta^{18}O$. However, since ENSO is significantly influencing the ambient environment it is expectable to detect at least a weak ENSO signature in $\delta^{13}C$. A cross spectrum of mean November-February $\delta^{18}O$ and $\delta^{13}C$ reveals spectral alignment and coherence for the typical interannual ENSO mode centered at ~3.7 yrs (not shown). Similarities of both isotope proxies in the interannual or decadal range are not uncommon for coral proxy records (Lough, 2004). Following Lough (2004), this pattern can be addressed either to a direct climatological or an indirect biological origin, such as ENSO-triggered light availability caused by variations of interannual cloud coverage, or by coral growth-rates kinematics. An example for the latter process is the fact that coral $\delta^{13}C$ features variability within 8-9 yrs in the power spectrum. This signal yields spectral coherence with the annual extension-rates in this band (Figure 43). This proxy thus indirectly reflects the quasi-decadal SST variations at the sampling site.

Finally, coral $\delta^{13}C$ can also be influenced by $\delta^{13}C$ of the water column dissolved inorganic carbon (DIC, Lamb and Swart, 2008). Between equatorial upwelling and monsoon-driven circulation, the coral may be exposed to different

isotopic signatures in DIC. No link between monsoon current variability and Spectral peaks in δ¹³C resembling spectral peaks in the SW and NE monsoon spectrum is, however, evident.

6. Summary and conclusion

This study used annual extension-rates, $\delta^{18}O$, Sr/Ca and $\delta^{13}C$ to reconstruct historical climate variations for the period 1917-2006 (Table 8). Since no coral proxy record from the Maldives exists, this study fills this gap in the Indian Ocean

Because of its vicinity to the monsoon system, the Maldives are affected by the seasonal reversals of monsoon currents and winds. Due to strong hydraulic energy of the ambient seawater, the mean annual extension is comparably low.

A significant increase in the annual extension-rates can be linked to the warming in the NW Indian Ocean. The annual extension-rates are triggered by SST variations in the interannual range that are linked to the ENSO forcing. Variations with a periodicity of 8-9 yrs are caused by Indian Ocean SST variations.

Decadal variability with a period of 18-19 yrs in the extension-rate record is an expression of the variability of the Indian monsoon system, but cannot be linked to Pacific climate variability. Phases of stronger Indian monsoon cause higher-than-normal-rainfall anomalies over the Indian subcontinent, and stronger SW monsoon current activity. These currents affect the skeletal extension in the summer months. Corals likely sacrifice extension for calcification in order to obtain a more robust skeleton in phases of stronger SW monsoon currents. Due to this causality, it is possible to reconstruct rainfall over southern India.

This study thus underlines the potential of extension-rates, to reconstruct past climate variations. Extension-rate records are usually disregarded in proxy climate studies, since it is believed that they are affected by a variety of effects. The principal environmental factors are, however, SST (Lough and Barnes, 2000) and current variability (Scoffin et al., 1992), which is confirmed by this study. The application of annual extension-rates as a proxy for the monsoon variability was feasible because of two factors: the geomorphology of Rasdhoo Atoll and the position of the coral colony in the lagoon. For the interpretation of fossil extension-rates, this implies that information on the coral habitat and the geomorphology is needed. Lagoon habitats may amplify decadal and interannual SST and current variations. In terms of Rasdhoo Atoll, one could suggest the existence of "climate facies". The dominance of SST-driven interannual and decadal variability in extension-rate records could be found in coral records deriving from the mudstone facies, where hydraulic energy is negligible or weak. The habitat of the investigated colony of this study might be an

intermediate area, with both SST and current forcing (Figure 44). The hard bottom area adjacent to the tidal channels might be dominated by the decadal variations of the monsoon currents. This idea is still highly speculative and introduces a two-dimensional approach on coral proxy studies. More studies on coral records from individual lagoons are needed in order to establish extension-rate records in *Porites* as a proxy for climate variations beyond the onset of instrumental climate records.

Coral $\delta^{18}O$ reveals an overall depletion trend in the 20th century. This proxy also yields an interannual ENSO variability, and a decadal ENSO-like signal of 12-14 yrs, which is driven by SSS variability. It is suggested that variations in the strength of the winter monsoon currents are responsible for this variation. The effect of monsoon-induced cooling is found in the long-term trend of $\delta^{18}O$.

In contrast, coral Sr/Ca does not feature a long-term trend. This could be explained by a non-climatologic effect. This proxy also features an interannual ENSO signature, and show PDO forcing 1917-1955. The disappearance of PDO signature after the mid-1950s reveals temporal variability of the spatial PDO component in the NW Indian Ocean, or at least, at the central Maldives. A warm PDO phase is suggested to lead to more favorable conditions for coral growth in the investigated core. Afterwards, coral growth is more affected by phases of higher-than normal SW monsoon strength.

By the combination of Sr/Ca and $\delta^{18}O$, it is possible reconstruct past ENSO events at the central Maldives. The correlation with SST is strong during this time, but disappeared afterwards. Because non-SST factors are inherent, and long in situ SST datasets of the lagoon are not available, it is not possible to reconstruct past SSS variability.

Coral $\delta^{13}C$ records a long-term depletion trend, which is addressed to the Suess effect. This signal reflects the impact of the anthropogenic combustion of fossil fuels on the atmospheric and oceanic carbon reservoir.

7. Zusammenfassung und Schlussfolgerung

Diese Arbeit präsentiert Korallenproxy-Zeitreihen von den Malediven, einer der größten rezenten Karbonatplattformen der Welt. Da bisher keine historischen Korallenaufzeichnungen von diesem Archipel existieren, versucht diese Arbeit, die bestehende Lücke zu füllen. Als Klimaarchiv wurde die Korallenart *Porites lutea* verwendet, eine massive Korallenspezies, welche häufig für die Rekonstruktion historischer Klimavariationen im Indo-Pazifik Verwendung findet. Der Korallenkern stammt von Rasdhoo (4°N/73°E), einem kleinen Atoll aus dem zentralen Bereich des Archipels. Die Länge der Aufzeichnungen ist 90 Jahre, von 1917 bis März 2007, mit monatlicher bis zweimonatlicher Auflösung. Diese Arbeit beschreibt und diskutiert die zeitlichen Muster der geochemischen Proxies $\delta^{18}O$, Sr/Ca und $\delta^{13}C$, sowie der jährlichen Wachstumsrate (Dicke eines Inkrements) während dieser Zeit und setzt sie in Beziehung zu historischer Klimavariabilität im nordwestlichen Indischen Ozean.

Mit der Untersuchung und Diskussion der jährlichen Wachstumsraten versucht diese Arbeit, einen Beitrag für das bessere Verständnis der zeitlichen Variation dieses Parameters in *Porites* Korallen zu leisten. Daher wird versucht, eine weitere Lücke zu schließen, denn Wachstumsraten in Korallen als Indikator für Klimavariationen wurden bisher in Korallenproxy-Studien kaum beachtet. Es gibt wenige Arbeiten, die mit den jährlichen Wachstumsraten Klimavariabilität zu rekonstruieren versuchen. Die mittlere Wachstumsrate 1917-2006 im untersuchten Korallenkern ist mit 9.9 mm/Jahr relativ niedrig für einen Standort in den Tropen mit einer mittleren Jahrestemperatur von 28,7 °C, im Vergleich zu anderen publizierten Studien (Lough und Barnes, 2000). Da dieser Wert außerhalb des empirischen Zusammenhangs zwischen Wachstumsrate und mittlerer SST von 44 Korallenkolonien im Indo-Pazifik liegt (Lough und Barnes, 2000), muss ein anderer Faktor auch auf das Korallenwachstum wirken. Scoffin et al. (1992) fand einen Zusammenhang zwischen Wachstumsraten und hydraulischer Energie des Meerwassers am Standort von *Porites* Korallen in Thailand. Je höher die Strömungen, desto geringer der Wachstum der Korallen. Die Koralle erhöhte wahrscheinlich die Kalzifikationsrate und daher Robustheit des Skeletts auf Kosten des jährlichen Wachstums. Über den genauen Verlauf und der Stärke der Gezeitenströmungen in der Lagune von Rasdhoo Atoll ist nichts bekannt, aber aufbauend auf der karbonatfaziellen Arbeit von Gischler (2006) kann angenommen

werden, das der Standort der beprobten Koralle sich noch im Einflussbereich der Gezeitenströme befindet. Der Einfluss der hydraulischen Energie auf das Wachstum vermindert aber nicht die Fähigkeit der Korallen, Temperaturtrends und Temperaturvariabilität aufzuzeichnen. Als Folge der Erwärmung im nordwestlichen Indischen Ozean seit 1917 kann man die Zunahme der Wachstumsraten beobachten. Außerdem ist es möglich, mit Spektralanalysen zu zeigen, dass zwischenjährliche Schwankungen, die einer Periodizität von 3-4 Jahren aufweisen, durch das ENSO - System gesteuert werden, welches die Temperaturen des Indischen Ozeans im zwischenjährlichen Bereich steuern. Damit zeichnet die Koralle Klimavariationen auf, die ihr Zentrum im östlichen Pazifik haben. Daneben reflektiert das Wachstum der Koralle auch eine Variabilität im Bereich von 8-9 Jahren, welche nicht auf ENSO zurückgeführt werden kann, und eher einer internen Klimavariabilität im Indischen Ozean entspricht.

Da gezeigt wurde, dass Wasserenergie ein wichtiger Faktor für das Wachstum der untersuchten Korallen ist, sollte es wahrscheinlich sein, dass die Korallen Variationen der Strömungsenergie in der Lagune speichern. Das Korallenwachstum zeigt für die Periode 1958-2004, für welche es Daten der Monsunströmungen gibt (SODA Datenbank, Carton et al., 2005), einen Zusammenhang mit der Variabilität der Stärke des Sommermonsunströmungen. Beide Zeitreihen zeigen eine deutliche spektrale Kohärenz innerhalb der Periodizität von 18-19 Jahren und eine innerhalb von 6-7 Jahren. Es ist denkbar, dass die Fähigkeit der Koralle, Monsunvariabilität aufzuzeichnen, auf die besondere Lage der Koralle in der Lagune und der besondere Geomorphologie des Atolls mit ihren zwei Gezeitenkanälen zurückgeführt werden kann. Entsprechend den Sedimentfazies, welche von Gischler (2006) in der Lagune von Rasdhoo kartiert worden sind, könnten die Klimasignaturen in den Wachstumsraten der Korallenkolonien eine Standortabhängigkeit zeigen, da die Sedimentfazies an der jeweiligen Lokalität die hydraulische Energie anzeigen. Daher sollte die Karbonatfazies bei der Untersuchung vorindustrieller *Porites* Kerne bekannt sein, bevor Wachstumsraten und andere Wachstumsparameter untersucht werden.

Die Variabilität der Monsunströmungen ist ein Ausdruck der Variabilität des Monsunsystems. Dies gilt auch für den Regenfall über Indien, welcher gewöhnlich als Indikator für die Stärke des Monsuns gilt (Sontakke und Singh, 1996). Daher besteht ein Zusammenhang zwischen Niederschlag über Südindien, Südarabien,

Nordostafrika und Kenia, und dem Wachstum der Koralle. Am Beispiel der Aufzeichnung des Sommermonsunniederschlags in der westlichen Ghat Region in Südindien kann gezeigt werden, das die Korrelation zwischen beiden Zeitreihen oberhalb des zwischenjährlichen Bereichs stark und signifikant ist, besonders ab der Mitte der 1950er Jahre.

Damit ist es in dieser Arbeit das erste Mal gelungen, zeitliche Variabilität des Monsunsystems im Indischen Ozean mit einer Korallenzeitreihe zu erfassen. Es wurde gezeigt, dass die Monsunstärke in Form der Strömungsvariabilität in der Koralle aufgezeichnet werden kann. Die dekadischen Variationen des Monsuns können dagegen mit δ^{18}O-Aufzeichnungen von Korallen aus verschieden Lokalitäten im nordwestlichen Indischen Ozean nicht rekonstruiert werden (siehe Cole et al., 2000; Pfeiffer und Dullo, 2006). Diese Arbeit bestätigt, dass δ^{18}O-Zeitreihen nicht dazu verwendet werden können, die zeitliche Variabilität des Indischen Monsuns zu rekonstruieren. Die atmosphärischen-ozeanischen Wechselwirkungen sind zu komplex, und der Regenfall über Indien spiegelt diese Dynamik nur unzureichend wieder (Webster und Yang, 1992; Vinayachandran, 2004). Dagegen ist es möglich, mit der δ^{18}O-Zeitreihe Gebiete der Monsunkühlung zu rekonstruieren. Dazu wurde eine Feldkorrelation mit geografisch gemittelten SST im Indo-Pazifik durchgeführt. Eine Kombination mit publizierten Korallenzeitreihen von den Seychellen (Charles et al., 1997) und Kenia (Cole et al., 2000) zu einem Korallenindex erhöht die Korrelation mit SST Feldern im nordwestlichen Indischen Ozean und zeichnet den Bereich der Monsunkühlung deutlicher nach. Es wird spekuliert, dass der Langzeittrend der SST der Monsunkühlung unterworfen ist.

Die relative niedrige Korrelation von δ^{18}O und instrumentellen SST für die 1917-2006 zeigt, dass die Salinität eine wichtige Rolle in der Variabilität von δ^{18}O in der Koralle spielt. Die δ^{18}O-Zeitreihe zeigt zwischenjährliche und dekadische Variabilität im Varianzspektrum auf, die im Zusammenhang mit SST- und Salinitätsschwankungen stehen, die durch ENSO verursacht wurden. Die bereits bekannte zwischenjährliche Variabilität von 3-4 Jahren tritt auf, sowie eine dekadische Schwankung von 12-14 Jahren, die nicht mit Variationen der SST erklärt werden können. Diese Variation ist im Bereich der typischen Periodizität der dekadischen ENSO Signals, und könnte durch Variationen der Wintermonsunströmungen verursacht worden sein, welche vom Pazifik über die

Passatwinde angetrieben wird. Die dekadische Variabilität tritt ab den 1950er Jahren in Erscheinung.

Das Sr/Ca-Verhältnis zeigt eine signifikante Korrelation mit SST zwischen 1917-1955. Nach 1955 ist die Korrelation schwach und folgt die der Erwärmung in der Region. Es kann nicht ausgeschlossen werden, dass das Sr/Ca Verhältnis im Meerwasser variiert hat. Räumliche Variationen des Sr/Ca-Verhältnisses in der obersten Wassersäule wurde in verschiedenen Studien beschrieben (de Villiers, 1999; Sun et al., 2003; De Dekker, 2004; Smith et al., 2005; Quinn et al., 2005). Neueste Arbeiten bringen Variationen des Sr/Ca Verhältnisses mit der Hydrodynamik in Verbindung (Hu et al., 2009). Trotz der geringen Korrelation mit SST zeigt die Sr/Ca-Zeitreihe zwischenjährliche Variationen, die mit ENSO verbunden werden können. Der Sr/Ca-Verlauf zeigt eine deutliche Korrelation mit dem PDO Index 1917-1955. Dies kann durch Feldkorrelationen bestätigt werden, welche außerdem die Dipolstruktur der PDO im nördlichen Pazifik rekonstruiert. Sr/Ca und SST zeigen außerdem, dass dieses Phänomen nach 1955 in den zentralen Malediven nicht mehr präsent ist.

Die Existenz der PDO in den zentralen Malediven bis 1955 könnte erklären, warum die Korrelation mit dem Regenfall über Südindien bis 1955 niedriger ist. Das Wachstum der Koralle könnte in dieser Zeit von der PDO Warmphase (1922-1947) profitiert haben, denn wärmere SST könnten dem Effekt stärkerer Monsunströmungen während der Sommermonsunzeit entgegengewirkt haben. Nach 1955 kommt es mehrmals zu Jahren, in denen der Wachstum rapide abnahm. Diese Jahre fallen häufig in Phasen, in welchen der Niederschlag über Indien während des Sommermonsuns hoch, dass heißt die Aktivität des Indischen Monsuns, höher war.

Die Kombination von Sr/Ca und δ^{18}O kann benutzt werden, um historische ENSO Ereignisse zu rekonstruieren. ENSO-Ereignisse in den zentralen Malediven sind definiert als Hoch- und Tiefpunkte (El Niño- und La Niña- Ereignisse) im ENSO Index Nino 3.4 und im instrumentellen SST Datensatz. In Kombination mit Tabellen über ENSO Ereignisse können ca. 80% dieser Ereignisse mit beiden geochemischen Proxies rekonstruiert werden.

Die Zeitreihen von Sr/Ca, δ^{18}O und der Wachstumsrate zusammengenommen geben möglicherweise den Hinweis darauf, dass sich die Stärke der PDO-Komponente im Indischen Ozean und damit die Art des Einflusses der Pazifischen Klimavariabilität in den zentralen Malediven verändert hat. Es ist auffällig, dass die

dekadischen ENSO Variabilität Mitte der 1950er Jahre beginnt, in der Zeit, in welcher die PDO Signatur in Sr/Ca und SST sich verliert. Es wird spekuliert, ob diese Beobachtungen mit der Aktivität und Dynamik der Äquatorströmungen im Zusammenhang steht.

Der Proxy $\delta^{13}C$ zeigt einen Langzeittrend hin zu leichterer Isotopie. Dieser Trend wird häufig in karbonatischen Klimaarchiven der letzten 100 Jahre beobachtet und mit der deutlichen Zunahme der Verbrennung fossiler Brennstoffe durch den Menschen seit der industriellen Revolution in Verbindung gebracht. Durch den vermehrten Eintrag von isotopisch leichterem $^{12}CO_2$ kommt es zur Veränderung des $\delta^{13}C$ der Atmosphäre und folglich des Ozeans, aus welchem die Koralle ihr Kohlenstoff für den Aufbau des Korallenskeletts bezieht.

References

Alibert C, and McCulloch MT (1997) Strontium/calcium ratios in modern *Porites* corals from the Great Barrier Reef as a proxy for sea surface temperature: calibration of the thermometer and monitoring of ENSO. Paleoceanography 12: 345-363

Allan RJ, and Ansell TJ (2006) A new globally complete monthly historical mean sea level pressure dataset (HadSLP2): 1850-2004. J Clim 19: 5816-5842

Allison N, and Finch AA (2004) High-resolution Sr/Ca records in modern *Porites lobata* corals: effects of skeletal extension-rate and architecture. Geochem Geophys Geosyst 5: Q05002, [doi:10.1029/2004GC000696]

Allison N, Finch AA, Newville M, and Sutton SR (2005) Strontium in coral aragonite: 3. Sr coordination and geochemistry in relation to skeletal architecture. Geochi Cosmochim Acta 69: 3801–3811

Annamalai H, Slingo JM, Sperber KR, and Hodges K (1999) the mean evolution and variability of the Asia Monsoon: comparison of the ECMWF and NCEP/NCAR reanalysis. Mon Weath Rev 127: 1157-1186

Baldwin MP, Gray LJ, Dunkerron TJ, Hamilton K, Haynes PH, Randel WJ, Holton JR, Alexander MJ, Hirota I, Horinouchi T, Jones DBA, Kinnersley JS, Marquardt C, Sato K, and Takahashi M (2001) The quasi-biennial oscillation. Revi Geophys 39: 179-229

Beck JW, Edwards RL, Emi I, Taylor FW, Recy J, Rougiere F, Joannot P, and Henin C (1992) Sea-surface temperature from coral skeletal strontium/calcium ratios. Science 257: 644-647

Bessat F, and Buigues D (2001) Two centuries of variation in coral growth in a massive *Porites* colony from Moorea (French Polynesia): a response of ocean-atmosphere variability from south central Pacific. Palaeogeogr Palaeoclimatol Palaeoecol 175: 381-392

Blackman RB, and Tukey JW (1958) The measurement of power spectra from the point of view of communication engineering. Dover Publications, New York, 190 p

Böhm F, Haase-Schramm A, Eisenhauer A, Dullo WC, Joachimski MM, Lehnert H, and Reiter J (2002) Evidence for preindustrial variations in the marine surface water carbonate system from coralline sponges. Geochem Geophys Geosyst 3: [doi:10.1019/2001GC000264]

Carton JA, Giese BS, and Grodsky SA (2005) Sea level rise and the warming of the oceans in the SODA ocean reanalysis. J Geophys Res [doi:110, 10.1029/2004JC002817]

Charles CD, Hunter DE, and Fairbanks RG (1997) Interaction between the ENSO and the Asian monsoon in a coral record of tropical climate. Science 277: 925-928

Charles CD, Cobb K, Morre MD, and Fairbanks RG (2003) Monsoon-tropical ocean interaction in a network of coral records spanning the 20th century. Mar Geol 201: 207-222

Cobb KM, Charles CD, and Hunter DE (2001) A central tropical Pacific coral demonstrates Pacific, Indian and Atlantic decadal climate teleconnections. Geophys Res Lett 28: 2209-2212

Cohen AL, Lane GD, Hart SR, and Lobel PS (2001), Kinetic control of skeletal Sr/Ca in a symbiotic coral: implications for the paleotemperature proxy. Paleoceanogr 16: 20-26

Cohen AL, Owens KE, Layne CD, and Shimizu N (2002) The effect of algal symbionts on the accuracy of Sr/Ca paleotemperatures from coral. Science 277: 331-333

Cole JE, Dunbar RB, McClanahan TR, and Muthiga NA (2000) Tropical Pacific forcing of decadal SST variability in the western Indian Ocean over the past two centuries. Science 287: 617-619

Conversi A, and Hammed S (1998) Common signals between physical and atmospheric variables and zooplankton biomass in the subarctic Pacific. ICES J Mar Sci 55: 739-747

Corrège, T (2006) Sea surface temperature and salinity reconstructions from coral geochemical tracers. Palaeogeogr., Palaeoclim., Palaeoecol. 232: 408-428

Corrège T, Delcroix T, Récy J, Beck JW, Cabioch G, and Le Cornec F (2000) Evidence for stronger El Niño Southern Oscillation (ENSO) events in a mid-Holocene massive coral. Paleoceanogr. 15: 465–470

Corrège T, Gagan MK, Beck JW, Burr GS, Cabioch G, and Le Comec F (2004) Interdecadal variation in the extent of South Pacific tropical waters during the Younger Dryas event. Nature 428:927-929

Crueger T, Zinke J, and Pfeiffer M (2009) Patterns of Pacific decadal variability recorded by Indian Ocean corals. Int J Earth Sci 98: 42-52

D'arrigo R, and Wilson B (2006) On the Asian expression of the PDO. Int J Clim 26: 1607-1617

Dean MD, and Kemp SL (2004) A 2100 year BP record of the Pacific Decadal Oscillation, El Niño-Southern Oscillation and Quasi-Biennial Oscillation in marine production and fluvial input from Saanich Inlet, British Columbia. Palaeogeogr Palaeoclimatol Palaeoecol 213: 207-229

Deser C, Phillips A, Hurrell J (2004) Pacific interdecadal climate variability: linkages between the tropics and North Pacific during boreal winter since 1900. J Clim 17: 3109-3124

De Deckker P (2004) On the celestite-secreting Acantharia and their effect on seawater strontium to calcium ratios. Hydrobiol 517: 1-13

De Villiers S (1999) Seawater strontium and Sr/Ca variability in the Atlantic and Pacific oceans. Earth Plan Sci Lett 171: 623-634

De Villiers S, Greaves M, and Elderfield H (2002) An intensity ratio calibration method for the

accurate determination of Mg/Ca and Sr/Ca of marine carbonates by ICP-AES. Geochem Geophys Geosys 3: 1001, doi:10.1029/2001GC000169.

De'ath G, Lough JM, and Fabricius KE (2009) Declining coral calcification on the Great Barrier Reef. Science 323: 116-119

Eigenheer A, and Quadfasel D (1999) Seasonal variability of the Bay of Bengal circulation inferred from TOPEX/Poseidon altimetry, J Geophy Res 105 (C2): 3243-3252

Evangelista H, Godiva D, Sifeddine A, Leao ZMAN, Rigozo NR, Segal B, Ambrizzi T, Kampel M, Kikuchi RKP, and Le Cornec F (2007) Evidences linking ENSO and coral growth in the Southwestern-South Atlantic. Clim Dyn 29: 869-88

Evans MN, Cane MA, Schrag DP, Kaplan A, Linsley BK, Villalba R, and Wellington GM (2001) Support for tropically-driven Pacific decadal variability based on paleo-proxy evidence. Geophys Res Lett 28: 3689-3692

Fallon SJ, McCulloch MT, and Alibert C (2003) Examining water temperature proxies in *Porites* corals from the Great Barrier Reef: a cross-shelf comparison. Coral Reefs 22: 389-404

Felis T, Pätzold J, and Loya Y (2003) Mean oxygen-isotope signatures in *Porites* spp. corals: inter-colony variability and correction for extension-rate effects. Coral Reefs 22: 328-336

Felis T, Pätzold J, Loya Y, Fine M, Nawar AH (2000) A coral oxygen isotope record from the northern Red Sea documenting NAO, ENSO, and North Pacific teleconnections on Middle East climate variability since the year 1750. Paleoceanogr 15: 679-694

Felis T, Suszuki A, Kuhnert H, Dima M, Lohmann G, and Kawahata H (2009) Subtropical coral reveals abrupt early-twentieth-century freshening in the western North Pacific Ocean. Geology 39: 527-530

Gagan MK, Ayliffe LK, Beck JW, Cole JE, Driffel ERM, Dunbar RB, and Schrag DP (2000) New views of tropical paleoclimates from corals. Quat Sci Rev 19: 45-64

Gagan MK, Ayliffe LK, Hopley D, Cali JA, Mortimer GE, Chappell J, and McCulloch MT, Head MJ (1998) Temperature and surface-ocean water balance of the mid-Holocene tropical western Pacific. Science 279: 1014-1017

Gischler E (2006) Sedimentation on Rasdhoo and Ari Atolls, Maldives, Indian Ocean. Facies 52: 341-360

Gischler E, Hudson JH, and Pisera A (2008) Late Quatenary reef growth and sea level in the Maldives (Indian Ocean). Mar Geol 250: 104-113

Gischler E, Hudson JH, and Storz D (2009) Growth of Pleistocene massive corals in south Florida: low skeletal extension-rates and possible ENSO, decadal, and multi-decadal cyclicities. Coral Reefs 28: 823-830

Grigg RW (1981) Coral reef development at high latitudes in Hawaii. Proc 4th Int Coral Reef Sym, Manila 1: 687-693

Grotolli AG (2002) Effect of light and brine shrimp on skeletal $\delta^{13}C$ in the Hawaiian coral *Porites compressa*: A tank experiment. Geochim Cosmochim Acta 66: 1955-1967

Grotolli AG, and Eakin CM (2007) A review of modern coral $\delta^{18}O$ and $\Delta^{14}C$ proxy records. Earth-Sci Rev 81: 67-91

Guilderson TP, and Schrag DP (1999) Reliability of coral isotope records from the western Pacific warm pool: A comparison using age-optimized records. Paleoceanogr 14: 457-464

Hastenrath S (1988) Climate and circulation of the tropics. Reidel, Dordrecht, Netherlands, p 455

Hendy EJ, Gagan MK, Alibert CA, McCulloch MT, Lough JM, and Isdale PJ (2002) Abrupt decrease in tropical Pacific sea surface salinity at end of Little Ice Age. Science 295: 1511-1514

Hönisch B, Hemming NG, Grottoli AG, Amat A, Hanson GN, and Bijma J (2004) Assessing scleractinian corals as recorders for paleo-pH: Empirical calibration and vital effects. Geochimica Cosmochim Act 68: 3675-3685

Hu C, Shen C, Chiu C, Chang C, Chiang H, Shen C, Lee D, Chen Y (2009) The influence of hydrological dynamics on *Porites* coral skeletal Sr/Ca thermometry. 2009 AGU Fall meeting, 14th-18th December, San Francisco, California, USA. Poster Presentation PP11A-1297

Hung CW, Liu X, and Yanai M (2004) Symmetry and asymmetry of the Asian and Australian summer monsoons. J Clim 17: 2413-2425

International Atomic Energy Agency (1994) Environmental isotope data No. 10: world survey of isotopic concentration in precipitation (1988-1991). IAEA, Vienna, p. 213

Janicot, S (2009) A comparison of Indian and African monsoon variability at different time scales. C R Geosci 341: 575-590

Klein R, Tudhope AW, Chilcott CP, Pätzold J, Abdulkatim Z, Fine M, Fallick AE, and Loya Y (1997) Evaluating southern Red Sea corals as a proxy record for the Asian monsoon. Eart Planet Sci Lett 148: 381-394

Kousky VE, and Bell GD (2000) Causes, predictions and outcome of El Niño 1997-1998. In: Chagnon SA (ed) El Niño 1997-1998. Oxford Univ. Press, New York, pp 28-48

Krishnan R, and Sugi M (2003) Pacific decadal oscillation and variability of the Indian summer monsoon rainfall. Clim Dyn 21: 233-242

Kucharski F, Molteni F, and Yoo JH (2006) SST forcing of decadal Indian Monsoon rainfall variability. Geophys Res Lett 33: L03709, doi:10.1029/2005GL025371

Kumar KK, Rajagopalan B, and Cane MA (1999) On the weakening relationship between the Indian monsoon and ENSO. Science 283: 2156-2159

Lamb K, and Swart PK (2008) The carbon and nitrogen values of particulate organic material from Florida keys: a temporal and spatial study. Coral Reefs 27: 352-362

Latif M, and Barnett TP (1994) Causes of decadal climate variability over the North Pacific and North America. Science 266: 634-637

Latif M, Kleeman R, and Eckert C (1997) Greenhouse warming, decadal variability, or El Niño? An attempt to understand the anomalous 1990s. J Clim 10: 2221-2239

Liebmann B, and Smith CA (1996) Description of a complete (interpolated) outgoing long-wave radiation dataset. Bull Am Meteorol Soc 77: 1275-1277

Linsley BK, Zhang PP, Kaplan A, Howe SS, and Wellington GM (2008) Interdecadal-decadal climate variability from multicoral oxygen isotope records in the south Pacific convergence zone region since 1650 A.D. Paleoceanogr PA2219 [doi:10.1029/2007PA001539]

Liu YW, Chiang HW, Shen CC, Lee DC, and Chen YG (2009) Natural variation of ^{87}Sr/^{86}Sr in coral *Porites* from southern Taiwan. 2009 AGU Fall meeting, 14th-18th December, San Francisco, California, USA. Poster Presentation PP11A-1299

Lough JM (2004) A strategy to improve the contribution of coral data to high -resolution paleoclimatology. Palaeogeogr Palaeoclimatol Palaeoecol 204: 115-143

Lough JM, and Barnes DJ (2000) Environmental controls on growth of the massive coral *Porites.* J Exp Mar and Ecol 245: 225-242

Maier C, Pätzold J, and Bak RPM (2003) The skeletal isotopic composition as an indicator of ecological and physiological plasticity in the coral genus *Madracis.* Coral Reefs 22: 370-380

Manghnani V, Subrahmanyam B, Xie L, and Morrison JM (2003) Numerical simulation of seasonal and interannual Indian Ocean upper layer circulation using Miami Isopycnic Coordinate Ocean Model. J Geophys Res 108: 3240 [doi:10.1029/2002JC001567]

Mantua NJ, and Hare SR (2002) The Pacific decadal oscillation. J Oceanogr 58: 35-44

Mantua NJ, Hare SR, Zhang Y, Wallace JM, and Francis RC (1997) A Pacific interdecadal climate oscillation with impacts on salmon production. Bull Am Meteorol Soc 78: 1069-1079

Marshall JF, and McCulloch MT (2001) Evidence for El Niño and the Indian Ocean Dipole from Sr/Ca derived SSTs for modern corals at Christmas Island, eastern Indian Ocean. Geophys Res Lett 28: 3453-3456

McCulloch MT, Gagan MK, Mortimer GE, Chivas AR, and Isdale PJ (1994) A high resolution Sr/Ca and δ^{18}O coral record from the Great Barrier Reef, Australia, and the 1982-1983 El Niño. Geochim Cosmochim Acta 58: 2747-2754

Meibom A, Stage M, Wooden J, Constantz BR, Dunbar RB, Owen A, Grumet N, Bacon CR, and Chamberlain CP (2003) Monthly strontium/calcium oscillations in symbiontic coral aragonite: biological effects limiting the precision of the paleotemperature proxy. Geophys Res Lett 30: 1418, doi: 10.1029/2002GL016864

Meibom A, Yurimoto H, Ciuf JP, Domart-Coulon I, Houlbreque F, Constantz B, Dauphin Y, Tambutte E, Tambutte S, Allem D, Wooden J, and Dunbar RB (2006) Vital effect in coral skeletal composition display strict three-dimensional control. Geophys Res Lett: 33 doi: 10.1029/2006GL025968

Mitchel TD, and Jones PD (2005) An improved method of constructing a database of monthly climate observations and associated high-resolution grids. Int J Clim 25: 693-712

Mitsuguchi T, Matsumoto E, and Uchida T (2003) Mg/Ca and Sr/Ca ratios of *Porites* coral skeleton: evaluation of the effect of skeletal growth rate. Coral Reefs 22: 381-388

Murtugudde R, McCreary JP, and Busalacchi AJ (2000) Oceanic processes associated with anomalous events in the Indian Ocean with relevance to 1997–1998. J Geophys Res 105: 3295-3306

Nothdurft, LD, Webb GE, Bostrom T, and Rintoul L (2007) Calcite-filled borings in the most recently deposited skeleton in live-collected *Porites* (Scleractinia): Implications for trace element archives. Geochi Cosmochim Acta 71: 5423–5438

Paillard D, Labeyrie L, and Yiou P (1996) Macintosh program performs time series analysis. Eos Trans AGU 77: 379

Pelejero C, Calvo E, McCulloch MT, Marshall JF, Gagan, MK, Lough JM, and Opdyke BN (2005) Preindustrial to modern interdecadal variability of coral reef pH. Science 309: 2204-2207

Pfeiffer M, and Dullo WC (2006) Monsoon-induced cooling of the western equatorial Indian Ocean as recorded in coral oxygen isotope records from the Seychelles covering the period of 1840-1994 AD. Quat Sci Rev 25: 993-1009

Pfeiffer M, Dullo WC, and Eisenhauer A (2004a) Variability of the intertropical convergence zone recorded in coral isotopic records from the central Indian Ocean. Quat Res 61: 245-255

Pfeiffer M, Timm O, and Dullo WC (2004b) Oceanic forcing of interannual and multidecadal climate variability in the southwestern Indian Ocean: Evidence from a 160 year coral isotopic record (La Réunion, 55°E, 21°S). Paleoceanogr 19: doi: 10.1029/2003PA000964.

Pfeiffer M, Timm O, Dullo WC, and Garbe-Schönberg D (2006) Paired coral Sr/Ca and $\delta^{18}O$ records from the Chagos Archipelago: Late twentieth century warming affects rainfall variability in the tropical Indian Ocean. Geology 34: 1069-1072

Pfeiffer M, Dullo WC, Zinke J, Cahyarini SY, Timm O, Weber ME, and Ricken W (2008) Tropical Indian Ocean Temperatures from Modern *Porites* Corals - Evaluating 20th Century Warming Trends from Geochemical Proxies and Instrumental data. Int. Conf., 160th ann. meet. Dt. Ges. Geowiss,, 98th ann. meet. Geol. Ver., Sept. 29-Oct. 2, 2008, Aachen, Germany. Abstr. Vol.. Schr. Dt. Ges. Geowiss., p. 77

Pfeiffer M, Dullo WC, Zinke J, and Garbe-Schönberg D (2009) Three monthly coral Sr/Ca records from the Chagos Archipelago covering the period of 1950-1995 A.D.: reproducibility and implications for quantitative reconstructions of sea surface temperature variations. Int J Earth Sci 98: 53-66

Pierce DW, Barnett TP, and Latif M (2000) Connections between the Pacific Ocean Tropics and midlatitudes on decadal time scales. J Clim 13: 1173-1194

Pillai CS, and Scheer G (1976) Report on the stony corals from the Maldive archipelago. Zoologica 126: 1-81

Quinn TM, Taylor FW, and Crowley TJ (2005) Coral-based climate variability in the Western Pacific Warm Pool since 1867. J Geophys Res 111: C11006, [doi:10.1029/2005JC003243]

Rao RR, and Sivakumar R (2000) Seasonal variability of near-surface thermal structure and heat budget of the mixed layer of the tropical Indian Ocean from a new global ocean temperature climatology. J Geophys Res 105: 995-1015

Rayner NA, Parker DE, Horton EB, Folland CK, Alexander LV, Rowell DP, Kent EC, and Kaplan A (2003) Global analyses of sea surface temperatures, sea ice, and night marine air temperatures since the late nineteenth century. J Geophys Res 108: No. D14, 4407 [doi:10.1029/2002JD002670]

Reason CJC (2000) Multidecadal climate variability in the subtropics/mid-latitudes of the southern hemnisphere oceans. Tellues A 25: 203-223

Reason CJC, and Allan RJ (1996) Evidence for the influence of remote forcing on interdecadal variability in the southern Indian Ocean. G Geophys Res 101: 11867-11882

Reed RJ, Campbell WJ, Rasmussen LA, and Rogers DG (1961) Evidence of a downward-propagating annual wind reversal in the equatorial stratosphere. J Geophys Res 66: 813-818

Reynolds RW, Rayner NA, Smith TM, Stokes DC, and Wang W (2002) An improved in situ and satellite SST analysis for climate. J Climate 15: 1609-1625

Rodwell MJ, and Hopkins BJ (1996) Monsoons and the dynamics of deserts. Q J R Meteorol Soc 122: 1385-1404

Saenger C, Cohen AL, Oppo DW, Halley RB, and Carilli JE. 2009. Surface-temperature trends and variability in the low latitude North Atlantic since 1552. Nature Geosci: [doi:10.1038/ngeo552]

Saji NH, Goswani BN, Vinayachandran PN, and Yamagata T (1999) A dipole in the tropical Indian Ocean. Nature 401: 360–363

Scheer G (1974) Investigation of coral reefs at Rasdu Atoll in the Maldives with the quadrat method according to phytosociology. Prc 2nd Int Coral Reef Symp, Brisbane 2: 655-670

Schott FA, and McCready JP Jr. (2001) The monsoon circulation of the Indian Ocean, Progr

Oceanogr 51: 1-123

Schrag DP (1999) Rapid analysis of high-precision Sr/Ca ratios in corals and other marine carbonates, Paleoceanogr 14: 97–102

Schuhmacher H, Loch K, Loch W, and See WR (2005) The aftermath of coral bleaching on a Maldivian reef – a quantitative study. Facies 51: 80-92

Scoffin TP, Tudhope AW, Brown BE, Chansang H, and Cheeney RF (1992) Patterns and possible environmental controls of skeletogenesis of *Porites lutea*, South Thailand. Coral Reefs 11: 1-11

Sen Roy S (2006) The impacts of ENSO, PDO, and local SSTs on winter precipitation in India. Phys Geogr 27: 464-474

Shankar D, Vinayachandran PN, and Unnikrishnan AS (2002) The monsoon currents in the north Indian Ocean. Progr Ocean 52: 63-120

Sinclair, DJ, Williams B, and Risk M (2006) A biological origin for climate signals in corals - trace element "vital effects" are ubiquitous in Scleractinian coral skeletons, Geophys. Res. Lett. 33: L17707*,* [doi:10.1029/2006Gl027183]

Smith JM, Quinn TM, Helmle KP, and Halley RB (2006) Reproducibility of geochemical and climatic signals in the Atlantic coral *Montastraea faveolata*. Paleoceanogr 21: [doi:10.1029/2005PA001187]

Smith TM, and Reynolds RW (2004) Improved extended reconstruction of SST (1854-1997). J Clim 17: 2466-2477

Sontakke NA, and Singh N (1996) Longest instrumental regional and all-India summer monsoon rainfall series using optimum observations: reconstruction and update. The Holocene 6: 315-331

Spötl C, and Vennemann T (2003), Continuous-flow isotope ratio mass spectrometric analysis of carbonate minerals. Rapid Communications in Mass Spectrometry 17: 1004-1006

Strom A, Francis RC, Mantua NJ, Miles EL, and Peterson DL (2004) North Pacific climate recorded in growth rings of geoduck clams: a new tool for paleoenvironmental reconstruction. Geophys Res Lett 31: L06206, [doi:10.1029/2004GL019440]

Sun D, and Su R, McConnaughey TA, Bloemendal J (2008) Variability of skeletal growth and $\delta^{13}C$ in massive corals from the South China Sea: Effects of photosynthesis, respiration and human activities. Chem Geol 255: 414-425

Sun Y, Sun M, Lee T, and Nie B. (2003), Influence of seawater Sr content on coral Sr/Ca and Sr thermometry. Coral Reefs 24: 23-29

Swart PK (1983) Carbon and oxygen fractionation in scleractinian corals: A review. Earth Sci Rev 19: 51-80

Swart PK (2000) The oxygen isotopic composition of interstitial waters: evidence for fluid flow and recrystallization in the margin of the Grand Bahama Bank. In: Swart PK, Eberli GP, Malone MJ, Sarg JF (eds) Proceedings of the Ocean Drilling Program, Scientific Results 166: 152-165

Thompson, DWJ, Kennedy JJ, Wallace JM, and Jones PD (2008) A large discontinuity in the mid-twentieth century in observed global-mean surface temperature. Nature 453: 646-649

Timmermann A, Jin FF, and Abshagen J (2003) A nonlinearity theory for El Niño bursting. J Atmos Sci 60: 152-165

Tiwari K, and Rao KNN (2001) Signature of ENSO signals in the coral growth rate record of Arabian Sea and Indian Monsoons. Pure Appl Geophys 161: 413-427

Tomascik T, Suharsono B, and Mah AJ (1994). Case histories: a historical perspective and anthropogenic impacts in the Indonesian Archipelago with a focus on the Seribu, Java Sea. In: Ginsburg RN (Ed.), Proceedings of Colloquium on Global Aspects of Coral Reefs: Health, Hazards and History 1993, Rosenstiel School of Marine and Atmospheric Science, University of Miami, pp. 304-310

Torrence C, and Webster PJ (1999) Interdecadal changes in the ENSO-monsoon system. J Clim 12: 2679-2690

Tourre YM, and White WB (1997) Evolution of the ENSO signal over the Indo-Pacific domain. J Phys Ocean 27: 683-696

Trenberth KE (1997) The definition of El Niño. Bull Am Meteorol Soc 78: 2771-2777

van Oldenborgh GJ, and Burgers G (2001) The effects of El Niño on precipitation and temperature, an update. KNMI preprint 2001-07. The KNMI Climate Explorer is available at http://climexp.knmi.nl

Vinayachandran PN (2004) Summer cooling of the Arabian Sea during contrasting monsoons. Geophys Res Lett 31: L13306 [doi:10.1029/2004GL019961]

Webster PJ, and Yang S (1992) Monsoon and ENSO: selectively interactive systems. Quart J Royal Meteorol Soc 118: 877-926

Webster PJ, Magaña VO, Palmer TN, Shukla J, Tomas RA, Yanai M, and Yasunari T (1998) Monsoons: processes, predictability, and the prospects for prediction. J Geophys Res 103: 14451-14510

Webster PJ, Moore MA, Loschnigg JP, and Leben RR (1999) Coupled ocean-atmosphere dynamics in the Indian Ocean during 1997-98. Nature 401: 356-359

Wei G, Sun M, Li X, and Nie BC (2000) Mg/Ca, Sr/Ca and U/Ca ratios of a *Porites* coral from Sabya Bay, Hainan Island, South China Sea and their relationships to sea surface temperature. Palaeogeogr Palaeoclimatol Palaeoecol 162: 59-74

White WB, Cayan DR (2000) A global El Niño-Southern Oscillation wave in surface temperature and pressure and its interdecadal modulation from 19000 to 1997. J Geophys Res 101 105: 11223-11242

Wilkinson C, Lindén O, Cesar H, Hodgon G, Rubens J, and Strong AE (1999) Ecological and socioeconomic impacts of the 1998 coral mortality in the Indian Ocean: an ENSO impact and a warning of future change? Ambio 28: 188-19

Woodruff SD, Diaz HF, Elms JD, and Worley SJ (1998) COADS Release 2 data and metadata enhancements for improvements of marine surface flux fields. Phys Chem Earth 23: 517-526

Yu L, and Reinecker MM (1999) Mechanism of the Indian Ocean warming during the 1997-98 El Niño. Geophys Res Lett 26: 735-738

Zinke J, Dullo WC, Heiss GA, and Eisenhauer A (2004) ENSO and Indian Ocean subtropical dipole variability is recorded in a coral record off southwest Madagascar for the period 1659-1995. Earth Planet Sci Lett 228: 177-194

Zinke J, Pfeiffer M, Timm O, Dullo WC, and Brummer GJA (2009) Western Indian Ocean marine and terrestrial records of climate variability: a review and new concepts on land – ocean interactions sinde AD 1660. Int J Earth Sci (Geol Rundsch) 98: 115-133

Zinke J, Pfeiffer M, Timm O, Dullo WC, and Davies GR (2005) Athmospheric-Ocean dynamics in the western Indian Ocean recorded in corals. Philos Trans R Soc A 363: 121-142

Figures
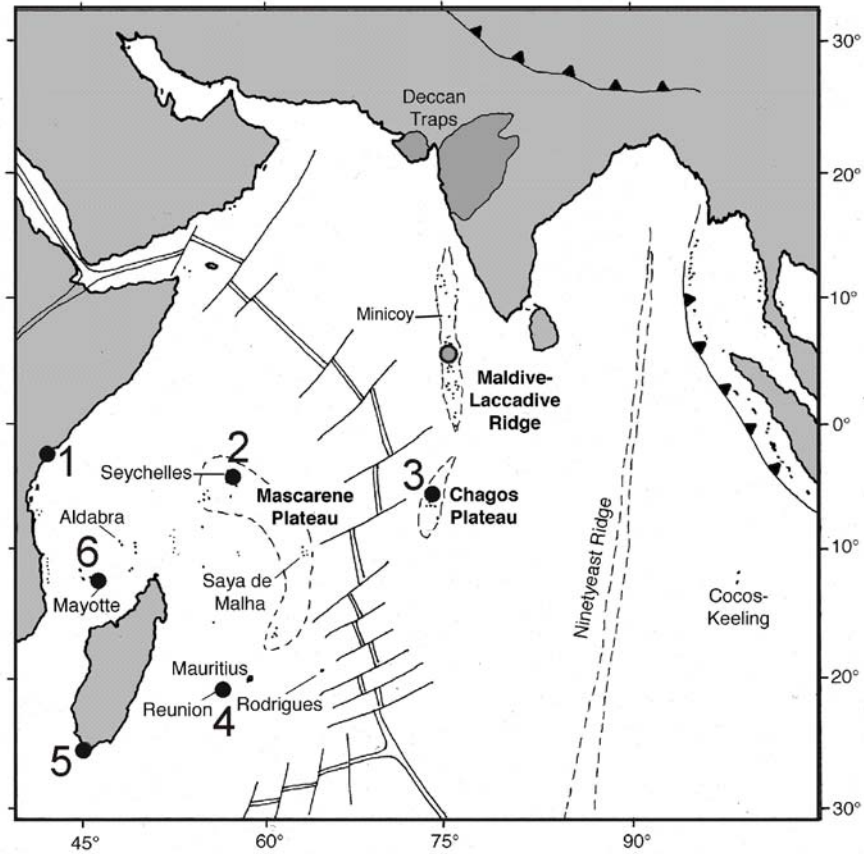
Figure 1: Geological setting of the Indian Ocean, with the location of the Maldives in the NW Indian Ocean (modified from Gischler, 2006). Grey circle: central Maldives. Black circles: Locations of published historical coral proxy records (longer than 30 yrs) in the NW and W Indian Ocean. 1: Kenya (Cole et al., 2000); 2: Seychelles (Charles et al., 1997; Pfeiffer and Dullo, 2006); 3: Chagos Archipelago (Pfeiffer et al., 2004a; 2006; 2009); 4: La Reunion (Pfeifer et al., 2004b); 5: Madagascar (Zinke et al., 2004), 6: Mayotte (Zinke et al., 2005).
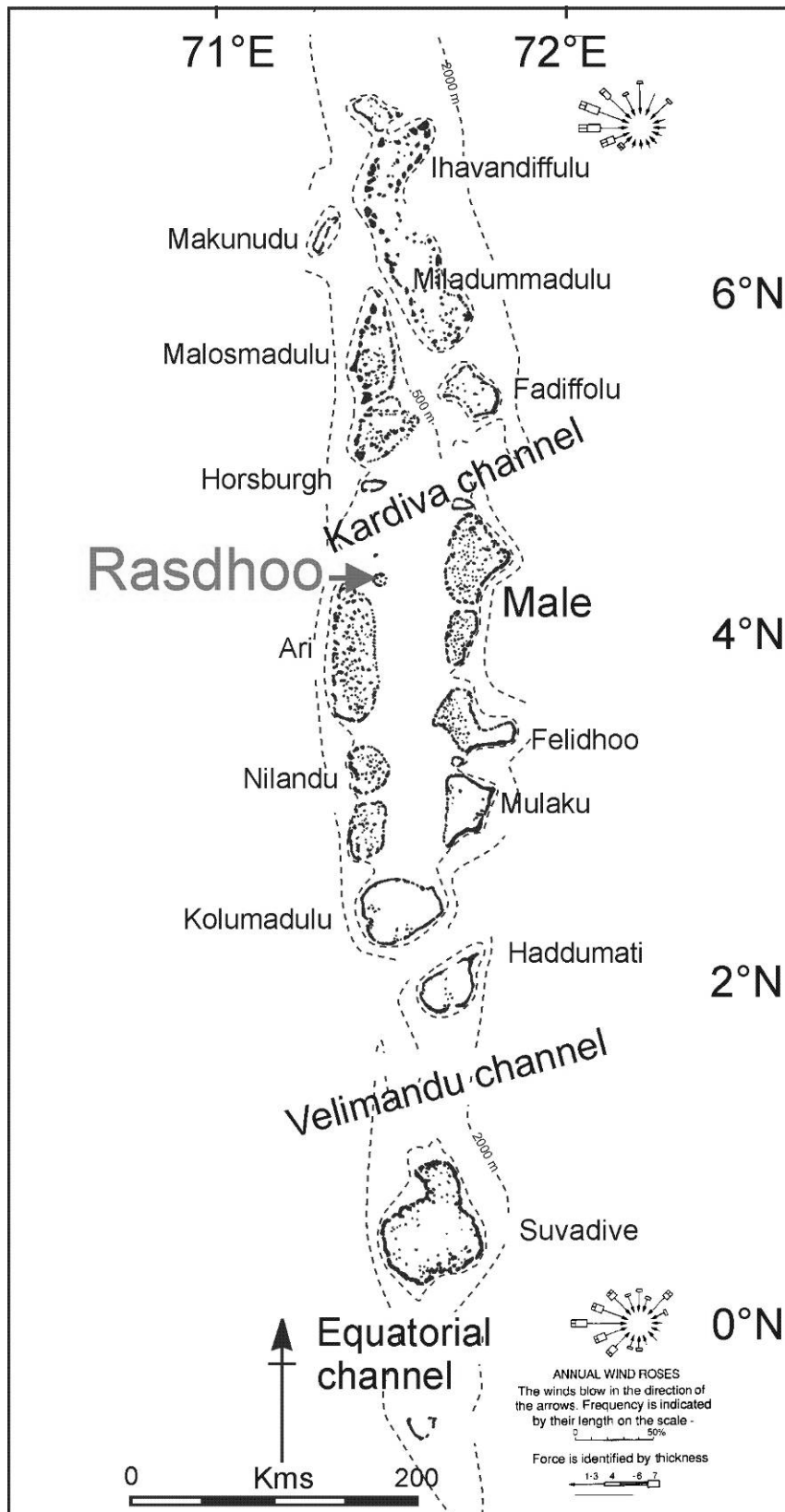
Figure 2: The Maldives Archipelago including predominant wind directions. Rasdhoo Atoll is located in the central area of the archipelago. Modified from Purdy and Bertram (2003).
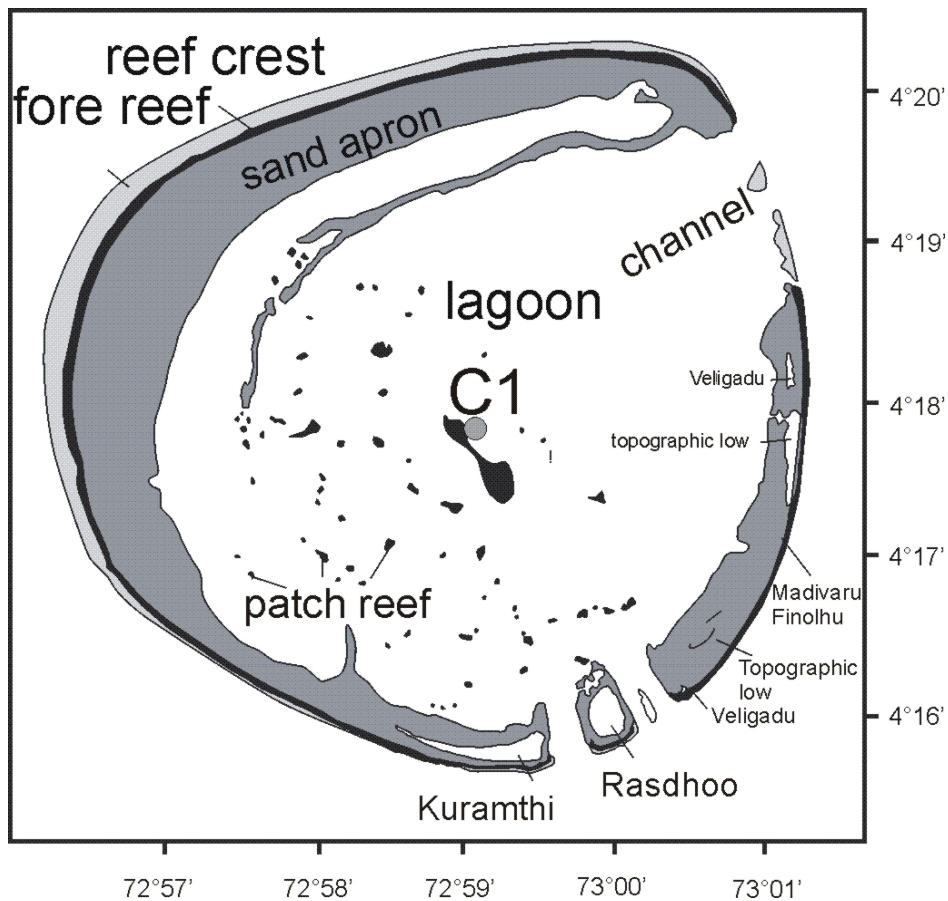
Figure 3: Position of the sampled colony C1 in the lagoon of Rasdhoo Atoll (latitude/longitude: 04°17''97N/72°58'49''), water depth of the colony: 1 m. Note that the fore reef on the eastern side is too narrow to show on figure. Maps are redrawn after Gischler et al. (2008).
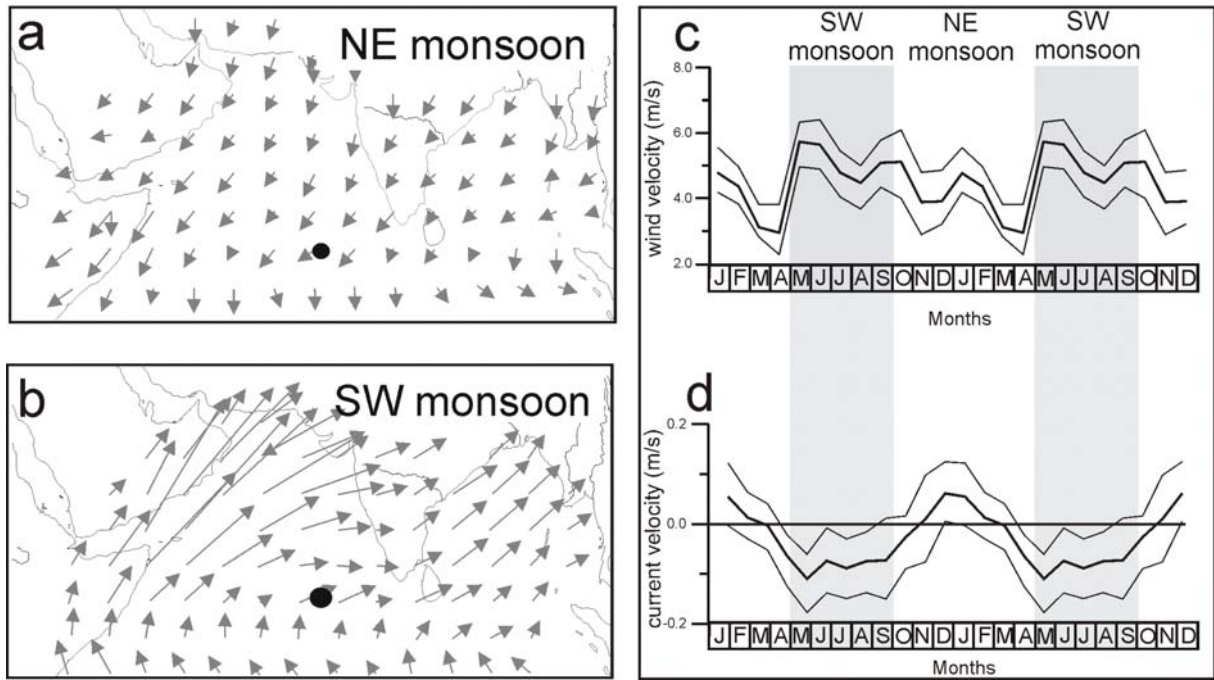
Figure 4: (a) and (b) Schematic representations of the seasonally reversed monsoon wind field for January and July, respectively. Redrawn after Shankar et al. (2002), black dot: central Maldives, (c) two mean seasonal cycles of the monthly gridded COADS wind speed record since 1977 (Woodruff et al., 1998), (d) two mean seasonal cycles of monthly gridded SODA zonal currents record since 1958. Note that positive velocities correspond to zonal velocity vectors orientated towards east, predominant during the NE monsoon season, while negative velocities accordingly correspond to vectors orientated towards west, predominant during the SW monsoon season. Thin lines indicate standard deviation.
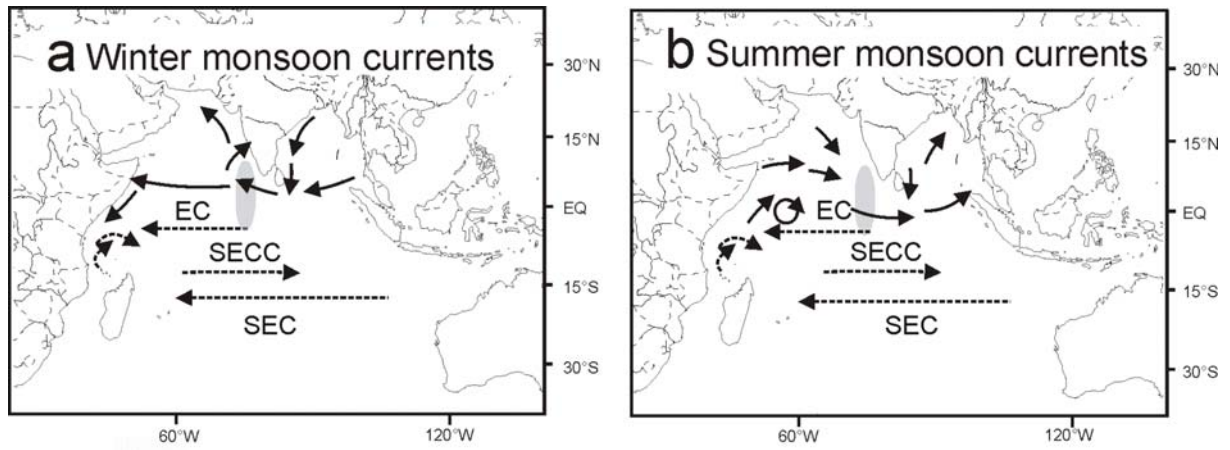
Figure 5: Monsoon currents in the Northern Indian Ocean for (a) January during the NE monsoon and (b) July during the SW monsoon. Current system redrawn after Shankar et al. (2002), EC: Equatorial Current; SECC: South Equatorial Counter Current: SEC: South Equatorial Current. Grey ellipsoid represents Maldives-Laccadive Ridge.
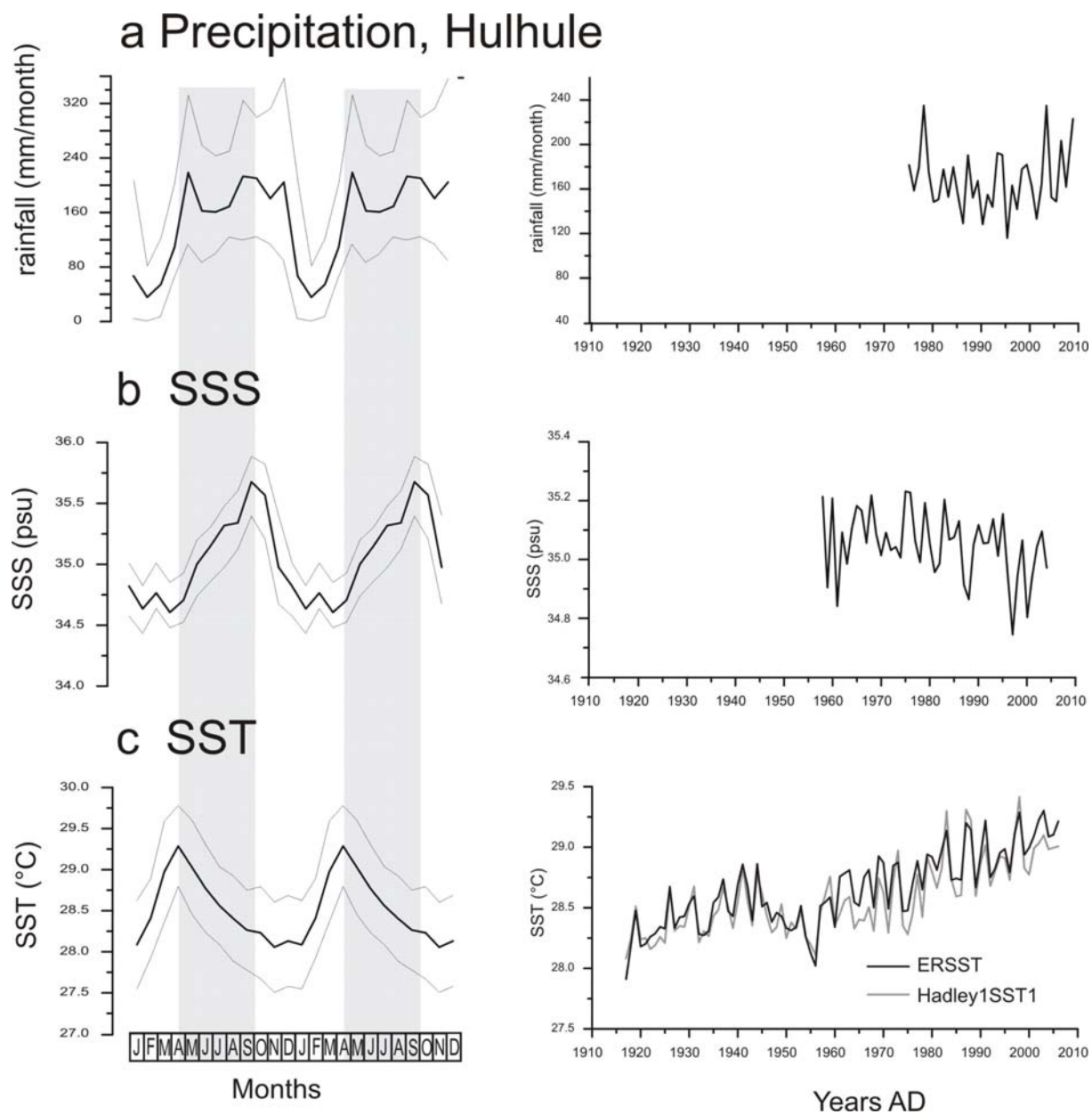
Figure 6: Mean seasonal cycle and time-series of (a) precipitation, (b) SSS and (c) HadISST1 and ERSST datasets. Shaded areas indicate SW monsoon season. References, sources and gridded area climate records are given in Table 1.
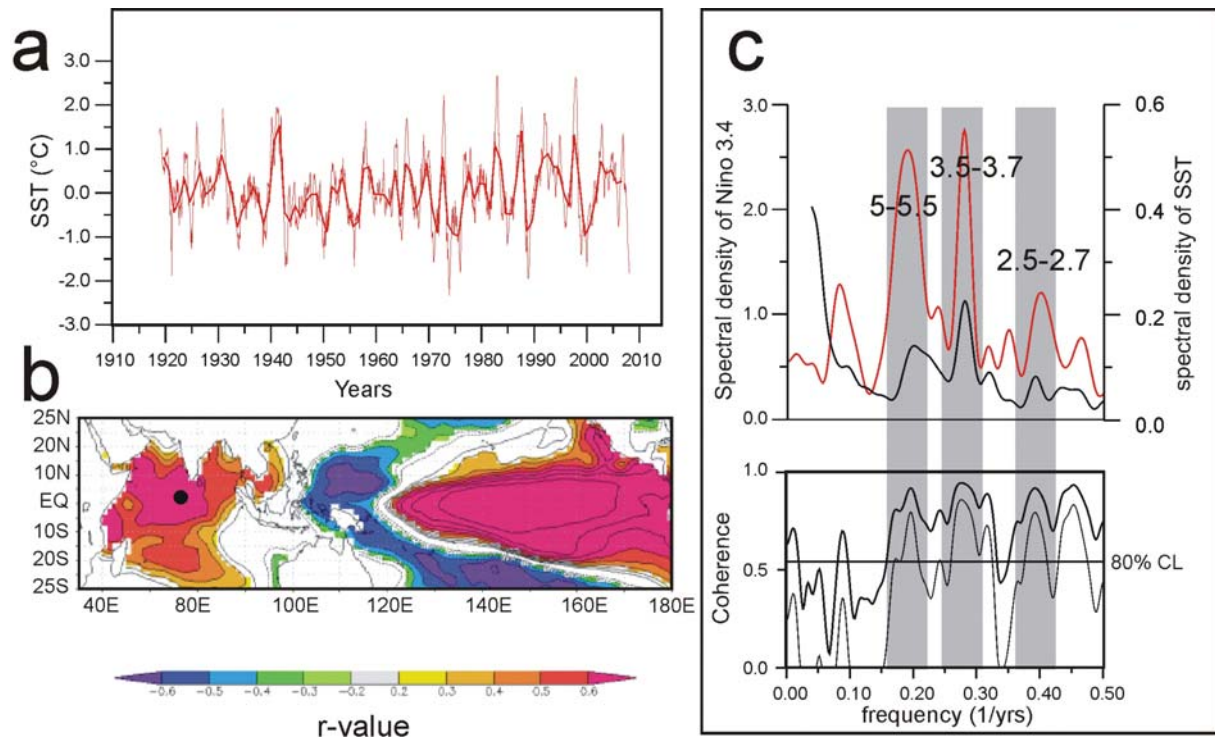
Figure 7: (a) Monthly and annual record of the ENSO index Niño 3.4 (based on ERSST). (b) R-values of running correlations between the 12-months averaged high-pass filtered (year-on-year difference) record of Niño 3.4, and SST fields (based on ERSST) in the Indo-Pacific, based on a grid of 2°x2° for the period 1917-2007. Black circle indicates the central Maldives. A high-pass filter (year-on-year difference) was used in order to highlight the interannual variability by removing trends or slow variations. Correlations stronger than r = +0.4 or r = -0.4 are significant at 99%, based on a two-sided student t-test. P-values < 0.2 have been masked out. Analysis was run with the KNMI climate explorer web application (van Oldenborgh and Burges, 2001; http://climexp.knmi.nl). (c) Blackman-Tukey cross-spectrum between annual mean Niño 3.4 and gridded SST (ERSST) from the central Maldives including Rasdhoo Atoll for the period 1917-2006. The top panel shows the variance spectra for both records, and the bottom panel shows the coherence (the correlation coefficient as the function of frequency between the records). Thin line on the bottom panel indicates the one sided lower error at 90%. Coherence values > 0.8 indicate that over 64% (0.8^2) of the variance at these periods is linearly correlated. Shaded area indicates the period of highest spectral coherence. Numbers are given in years. The bandwidth is 0.04 (number of lags: 41). The criteria for this are that the variance peaks are aligned (in the top panel) and that the corresponding coherence exceeds the 80% confidence level (CL).

Figure 8: Sampling of core C1 with a pneumatic drill device in the lagoon of Rasdhoo March 2007. The top of the *Porites* colony is 1 m below sea level.
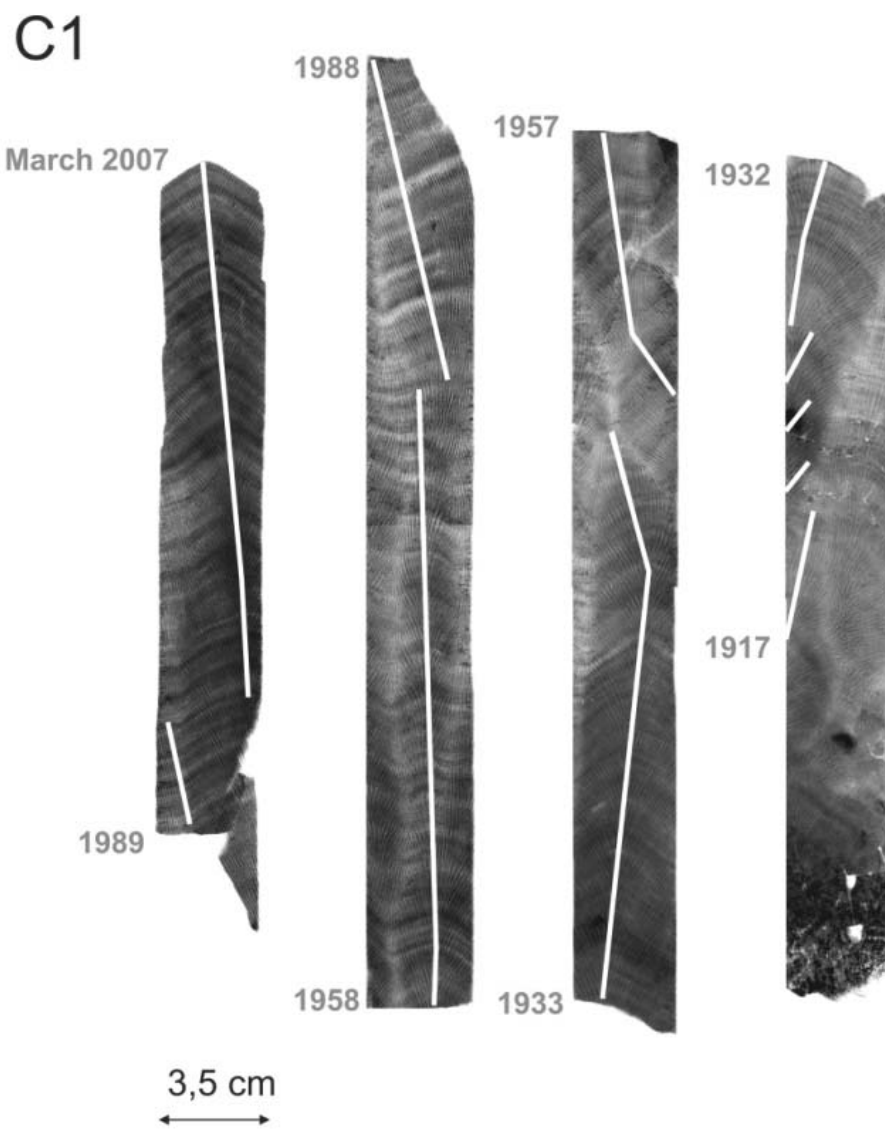
Figure 9: Radiograph of core C1 including the sampling transects.
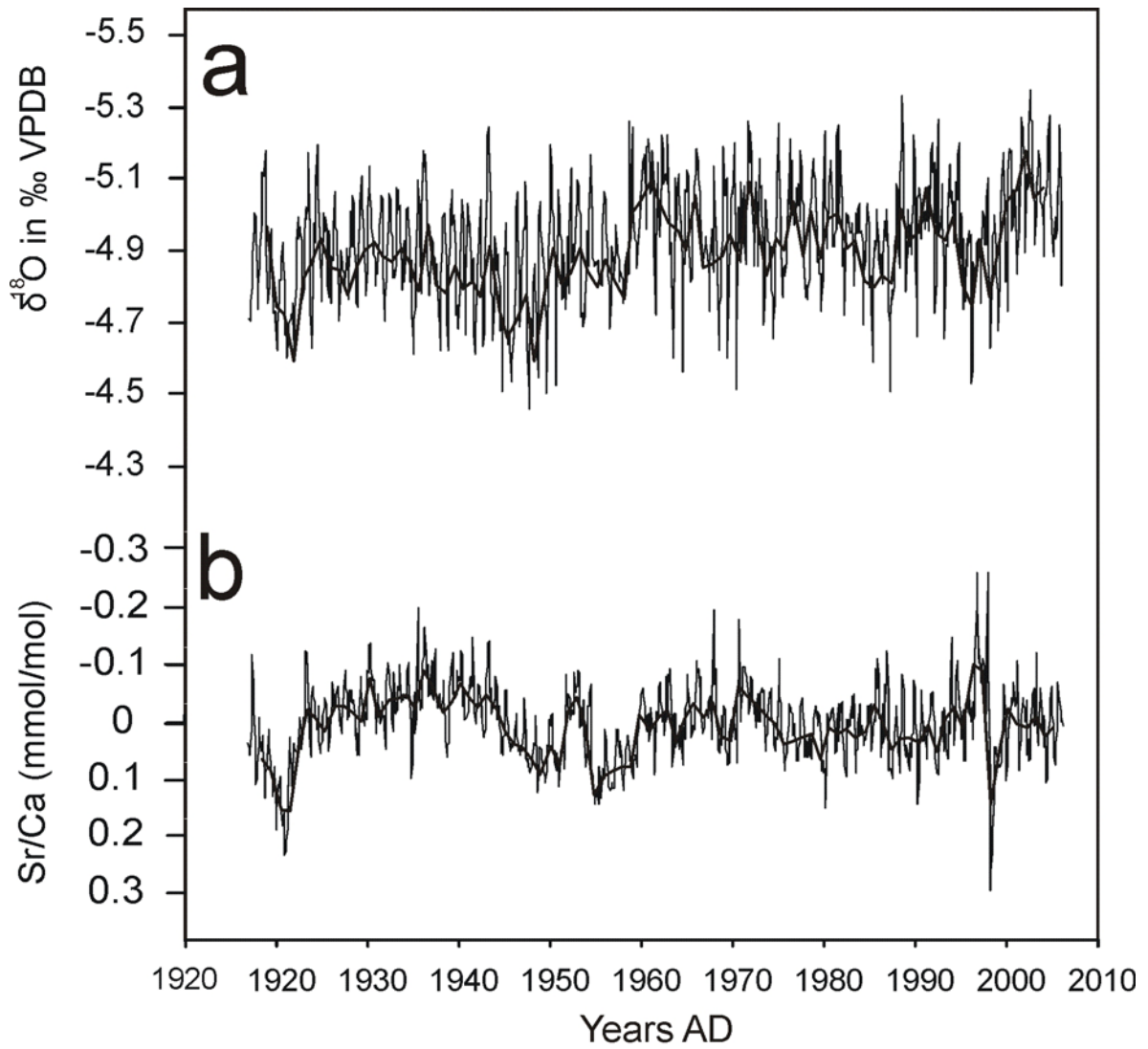
Figure 10: Synopsis of (a) monthly and annual mean δ18O (bold) and (b) monthly and annual mean (bold) Sr/Ca (record is scaled with zero mean).
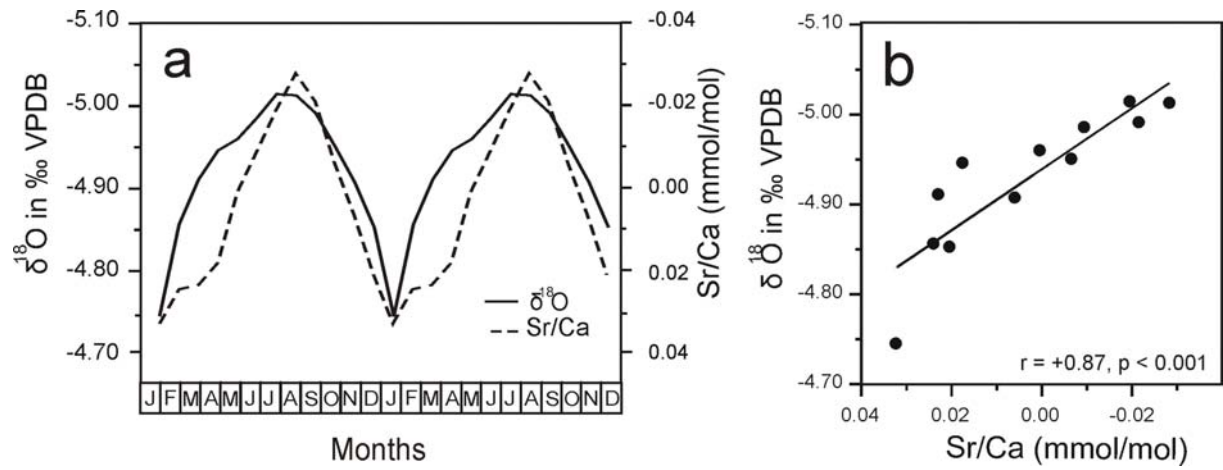
Figure 11: (a) Two mean seasonal cycles on monthly resolution for $\delta^{18}O$ and Sr/Ca. Values of each month are averaged for the period 1917-2006. Standard deviation for $\delta^{18}O$ is 0.13‰, and for Sr/Ca 0.06 mmol/mol. (b) Correlation between mean monthly $\delta^{18}O$ and Sr/Ca of the seasonal cycle.
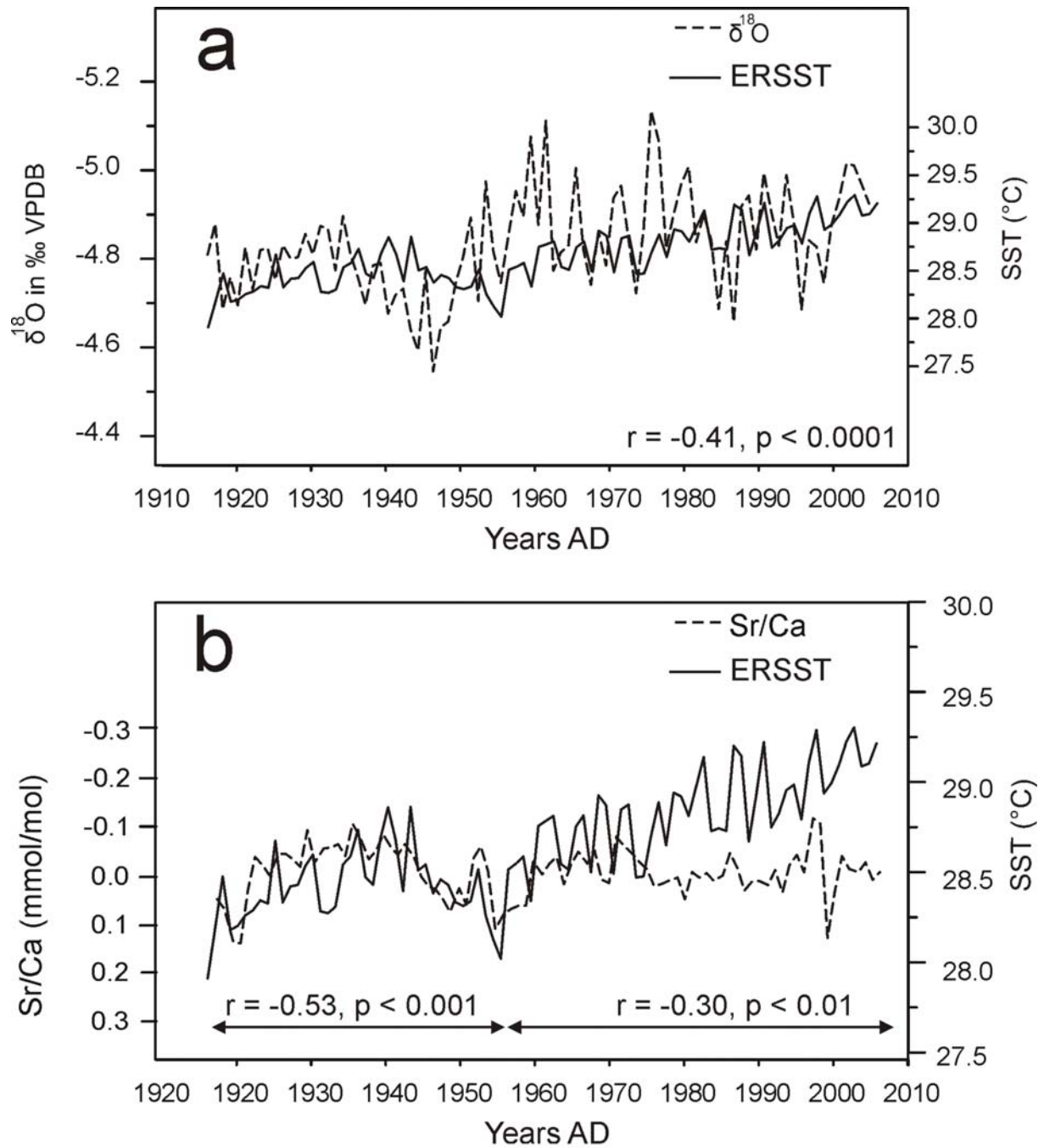
Figure 12: (a) Comparison of mean annual δ^{18}O with mean annual SST (ERSST) for the period of 1917-2006. Additionally, the correlation between time-series is given. (b) Comparison of mean annual Sr/Ca with mean annual SST (ERRST). Correlations are given for the periods 19-17-1955 and 1955-2007, respectively. Note that in (a) δ^{18}O is scaled after the empirical δ^{18}O-SST relationship of -0.20 ‰/°C (e.g., Grotolli and Eakin, 2007).
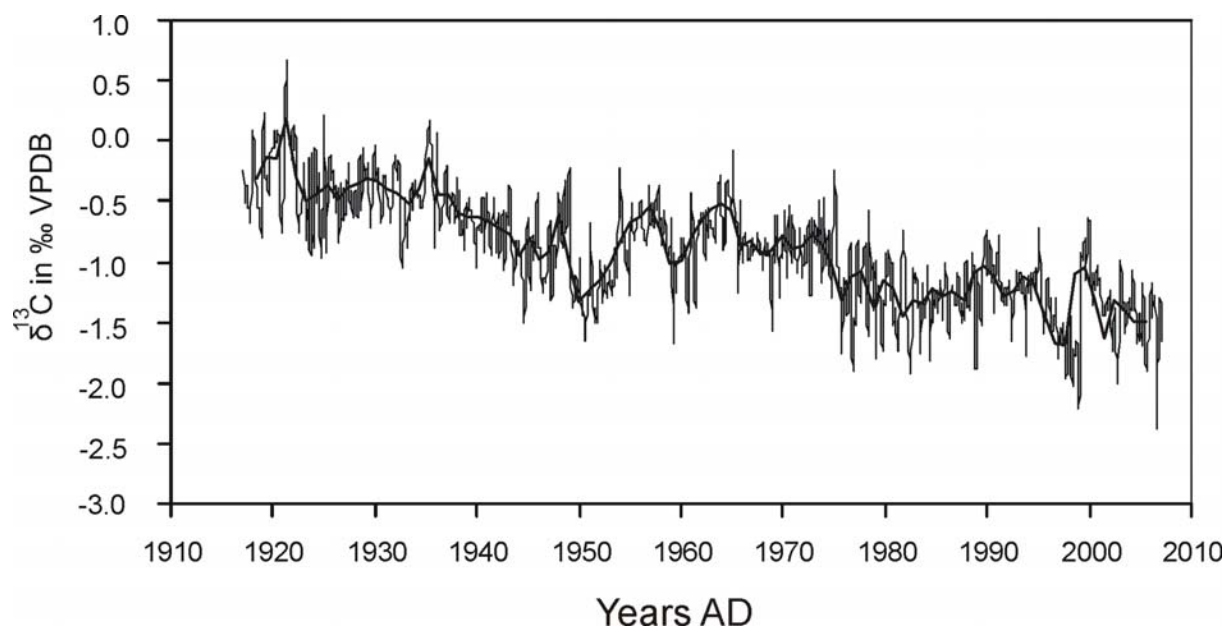
Figure 13: Monthly and annual mean (bold) record of $\delta^{13}C$ for the period 1917-2006 in C1.
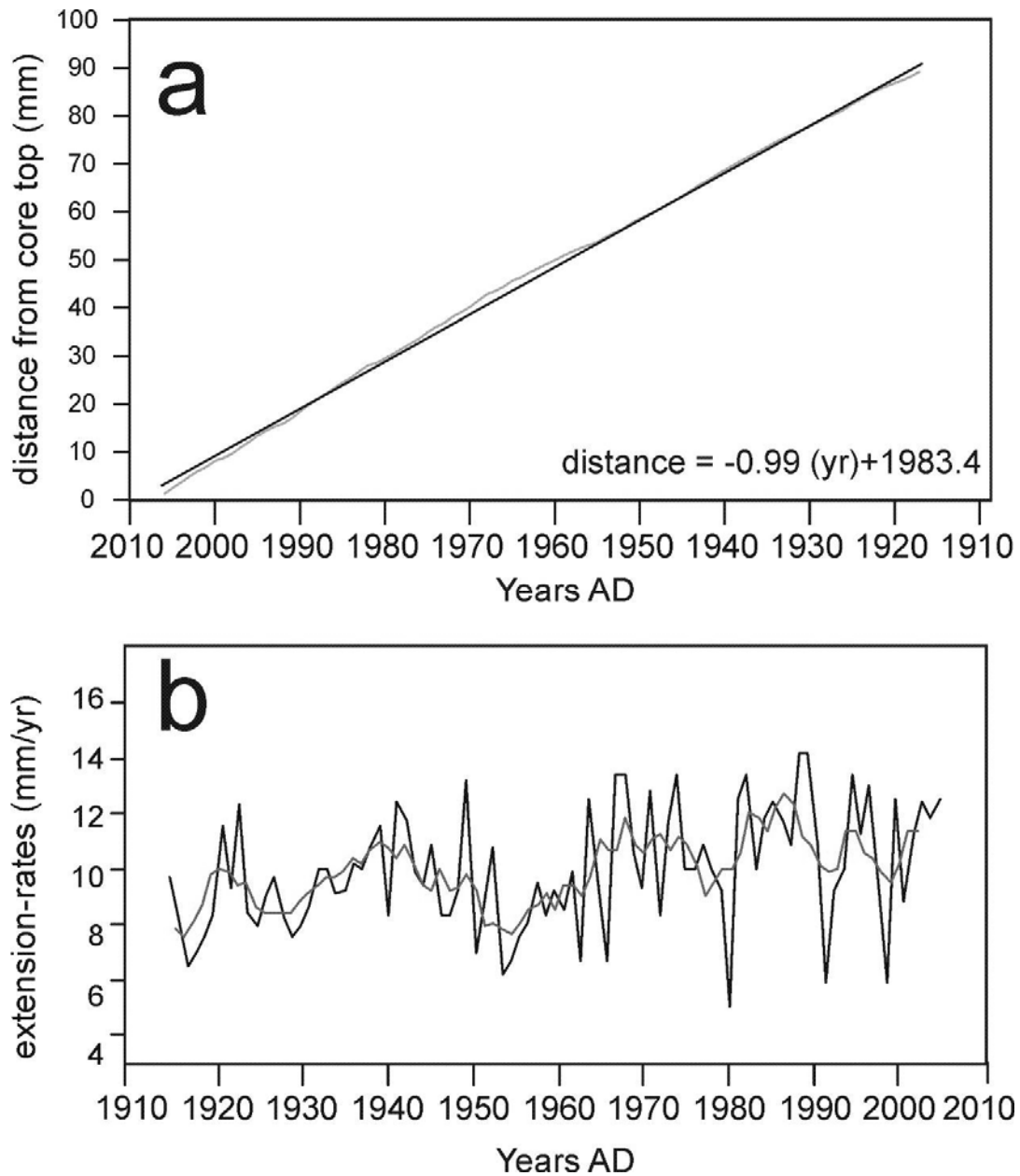
Figure 14: (a) Distance of each January value (i.e., $\delta^{18}O$ maxima in a seasonal cycle) from the top of core C1. Grey: Graph through the 89 time-distance points. Black: Interpolation by linear regression. The absolute value of the linear regression slope is the mean annual extension-rate of the record. (b) Annual extension-rate record, grey line indicates 5-yrs running mean average.

67
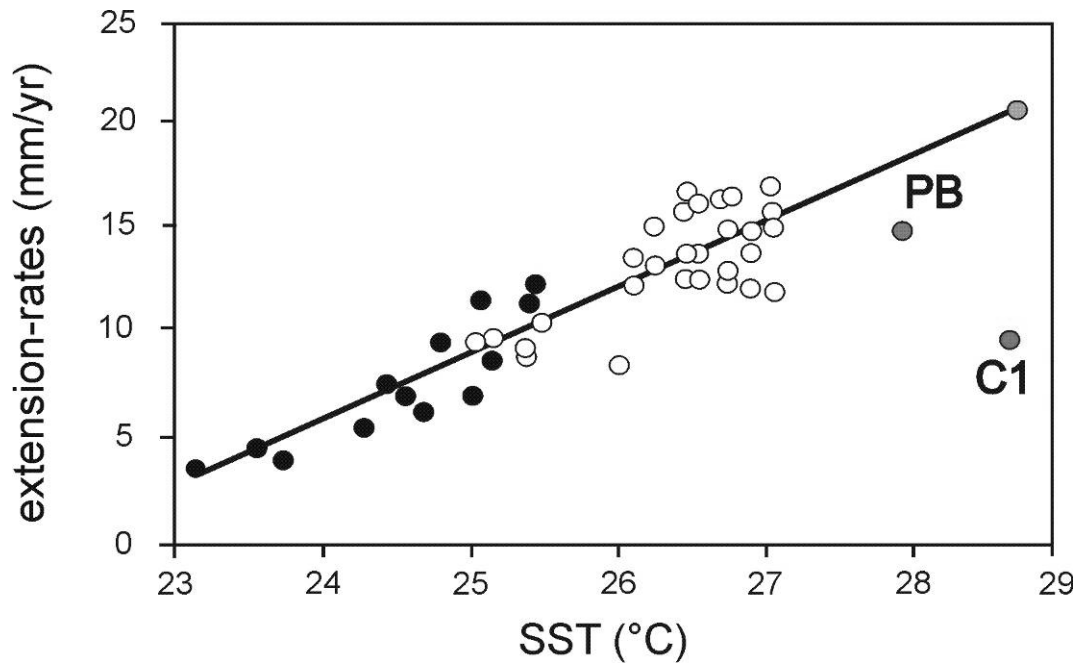
Figure 15: Scatter diagram of growth data averaged over colonies of the 46 Indo-Pacific reefs, and C1 versus annual average SST. Black circles: reefs from the Hawaiian Archipelago (Grigg, 1981); white circles: Great Barrier Reefs; grey circle: reef from Phuket, Thailand (Scoffin et al., 1992). PB: coral record from Peros Banhos, Chagos Archipelago (Pfeiffer at al., 2004a). Regression line is shown showing the statistically significant link. This figure is redrawn from Lough and Barnes (2000).
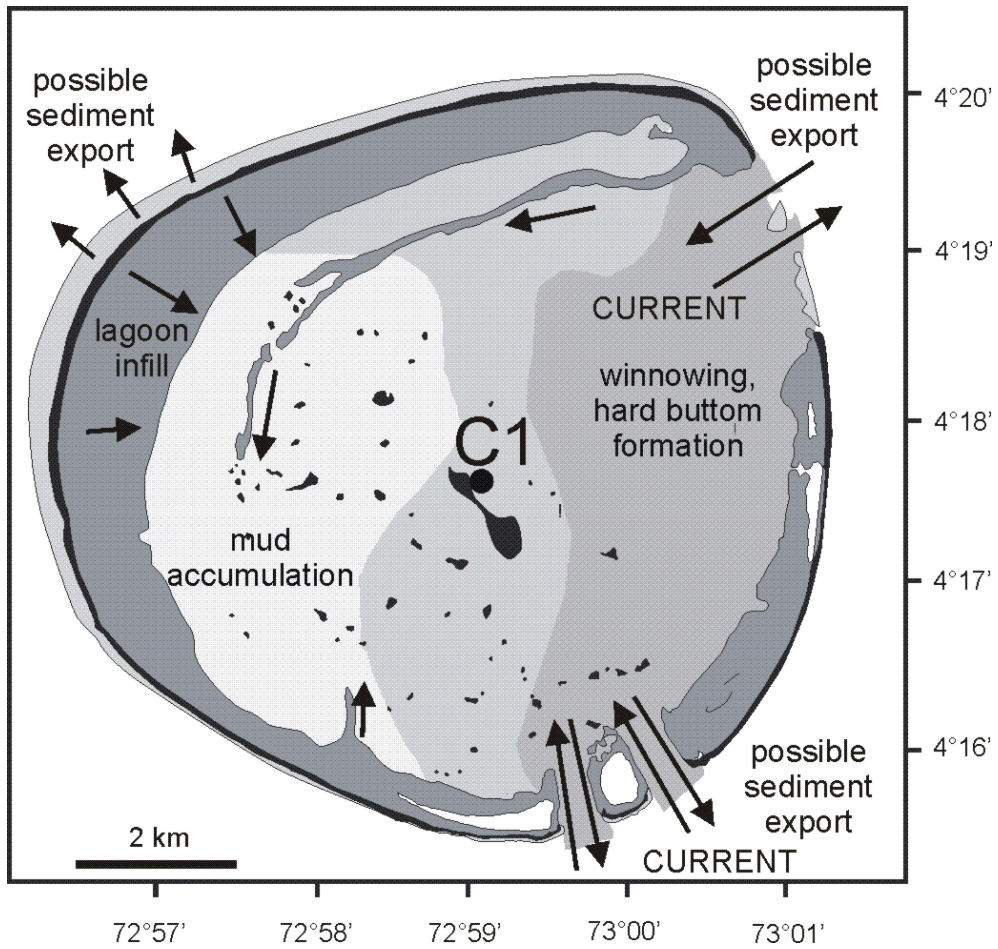
Figure 16: Facies map of Rasdhoo Atoll, including sediment dynamics and the location of C1. Dark grey area: hard bottom facies, medium grey area: mollusc wackestone-packestone facies, light grey area: mudstone facies. Redrawn after Gischler (2006): his figures 10 and 12.
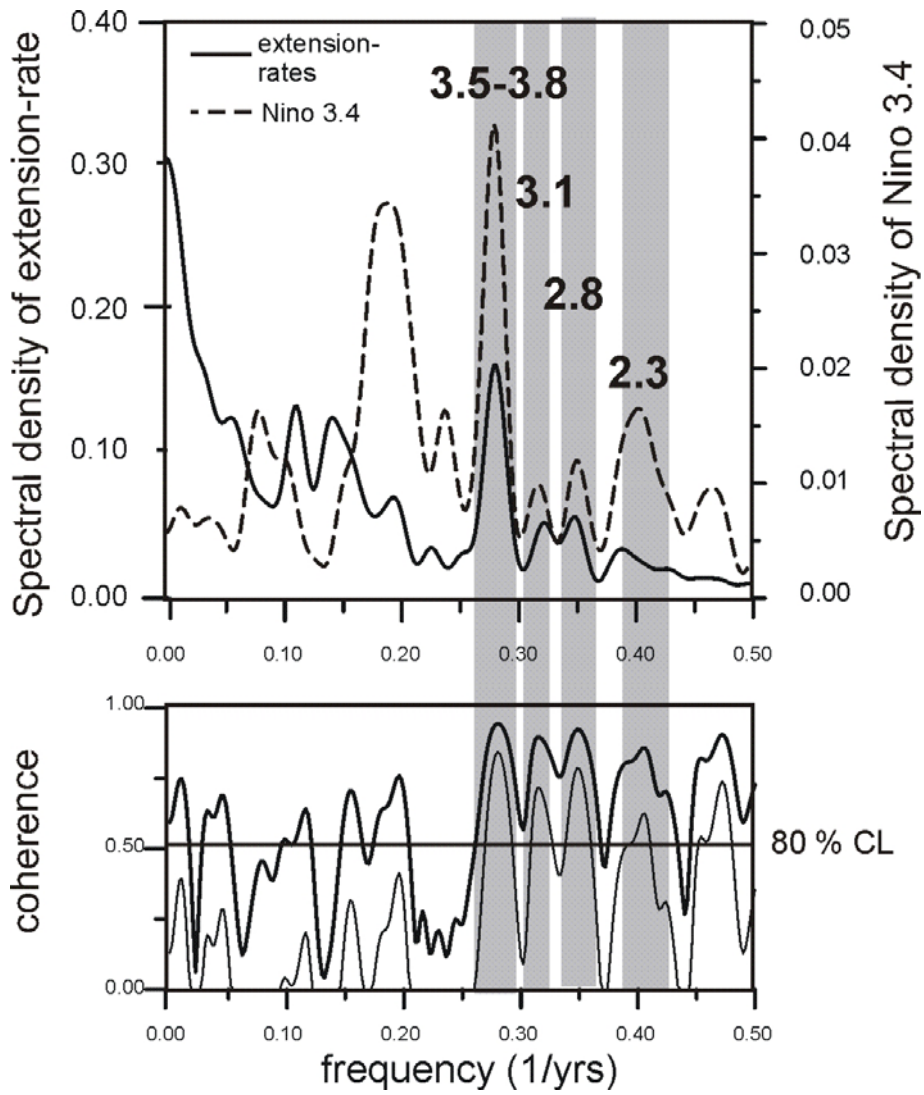
Figure 17: Cross spectrum between annual extension-rates of C1 and annual Niño 3.4 for the period 1917-2006. Shaded areas indicate periods of statistical significance. Numbers are given in years. See Figure 7c for legend.
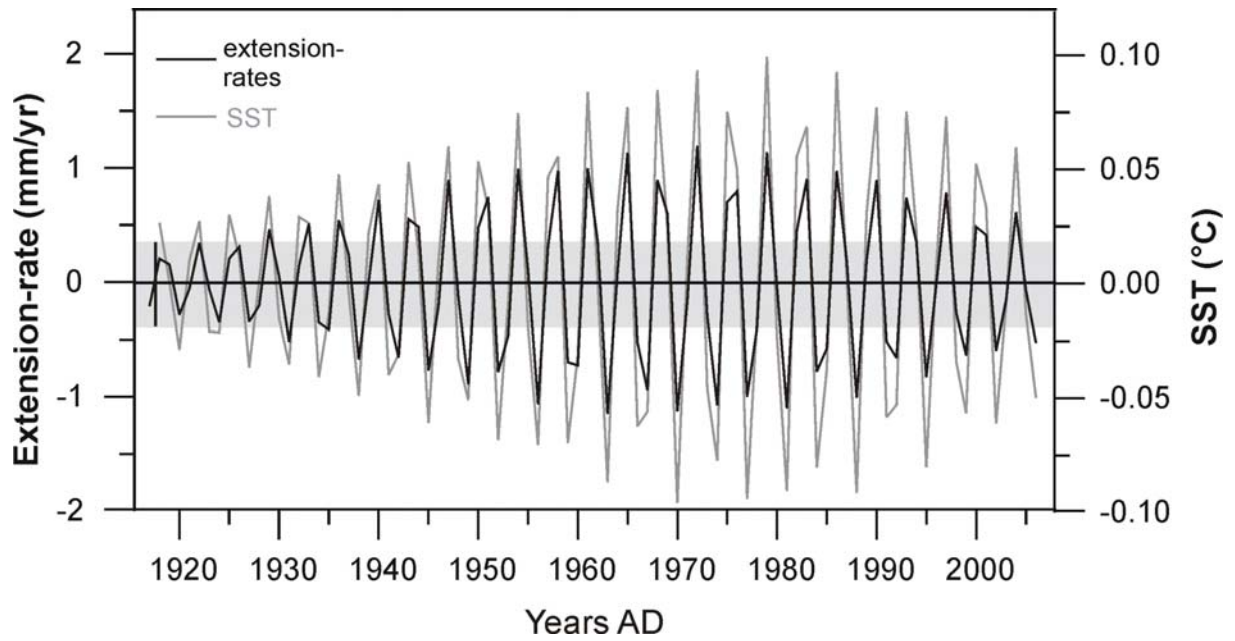
Figure 18: Three to four years band-passed filtered (Gaussian filter) extension-rate and SST records, in order to highlight in-phase relationship between both records and the synchronous developing of their amplitudes through 1917-2006. Shaded area indicates mean sampling resolution of 0.08 mm. Bandwidth is 0.02.
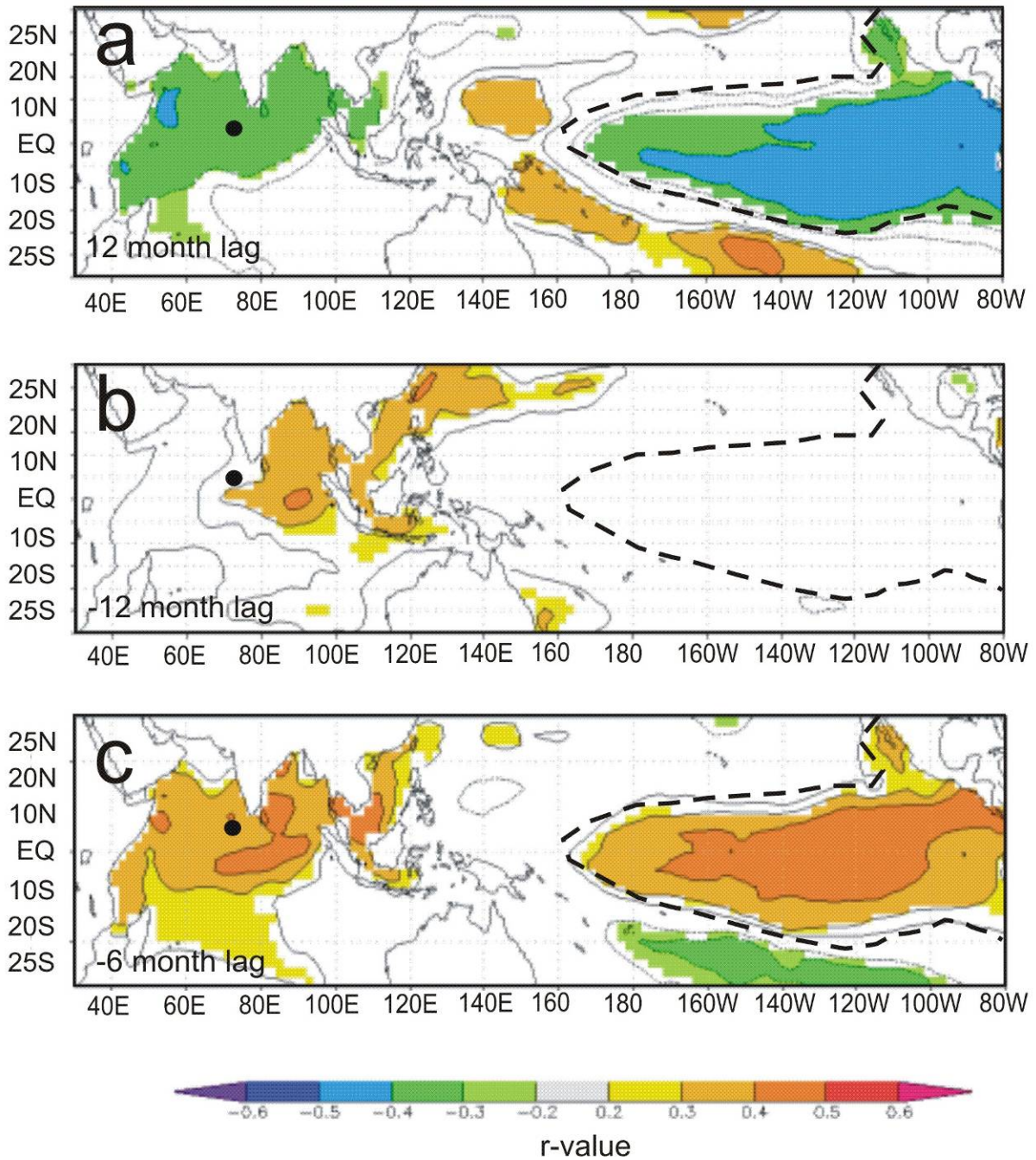
Figure 19: R-values of field correlations between 12-months averaged annual extension-rates and SST (ERSST). (a) The extension-rate record lags SST by 12 months, (b) SST lag extension-rate by 12 months, (c) SST lag extension-rate by 6 months. Black circle indicates Rasdhoo Atoll. A high-pass filter was applied in order to highlight the interannual variability by removing trends or slow variations. Correlations stronger than r = +0.4 or r = -0.4 are significant at 99%, based on a two-sided student t-test. R-values with p >0.10 are masked out. Analysis was run with the KNMI climate explorer web application (van Oldenborgh and Burges, 2001; http://climexp.knmi.nl).
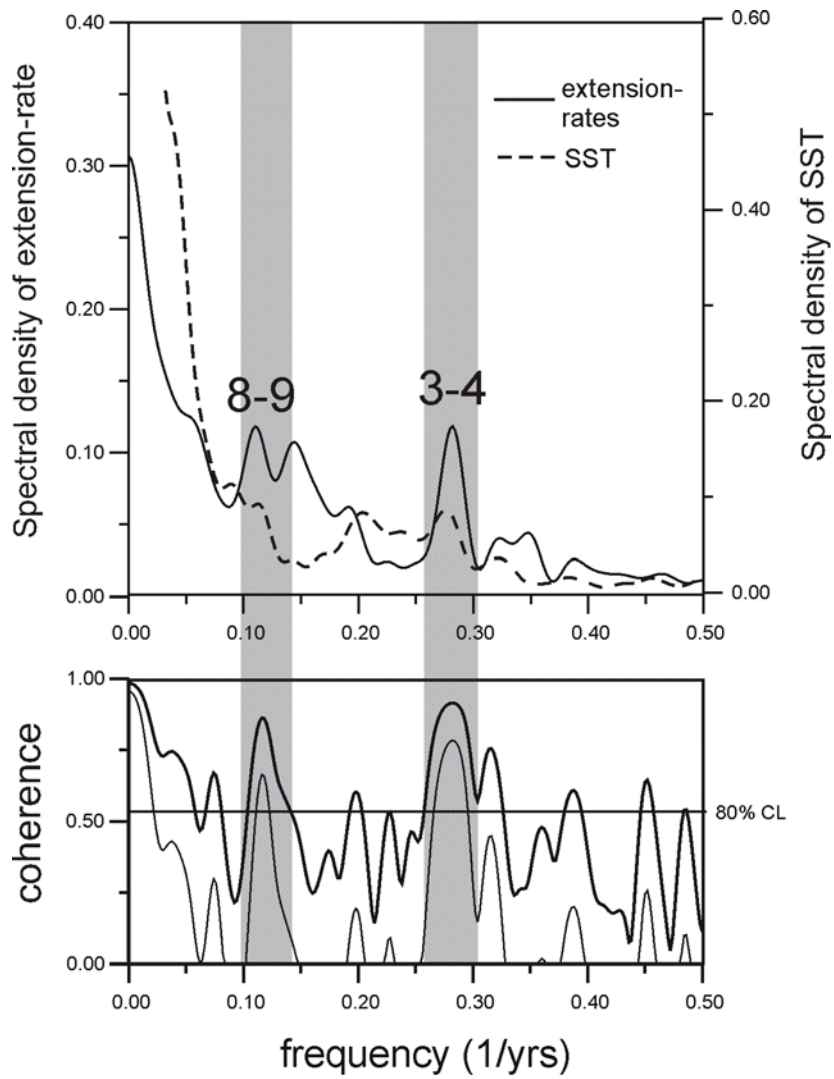
Figure 20: Cross spectrum between annual extension-rate and SST (ERSST) for the central Maldives for 1917-2006. Numbers are given in years. Significant spectral coherence is highlighted by grey shading. See Figure 7c for legend.
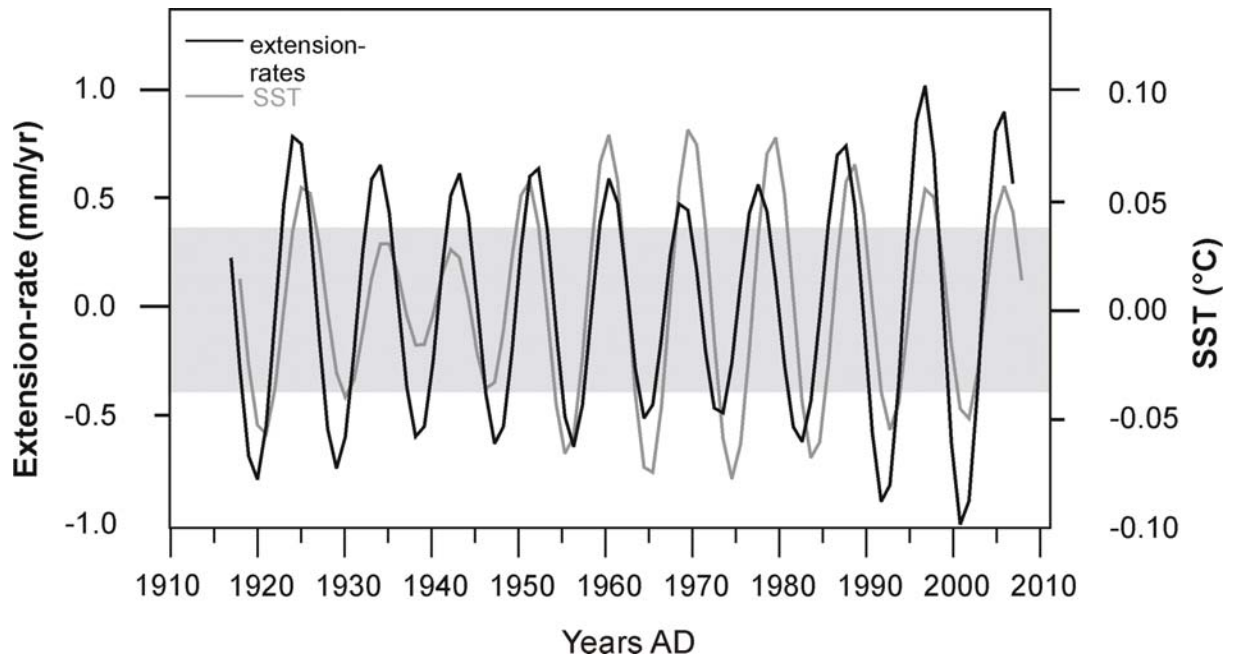
Figure 21: Eight to nine years band-passed filtered (Gaussian filter) extension-rate and SST records, in order to highlight in-phase relationship between both records and the synchronous developing of their amplitudes through 1917-2006. Shaded area indicates mean sampling resolution of 0.08 mm. Bandwidth is 0.02.
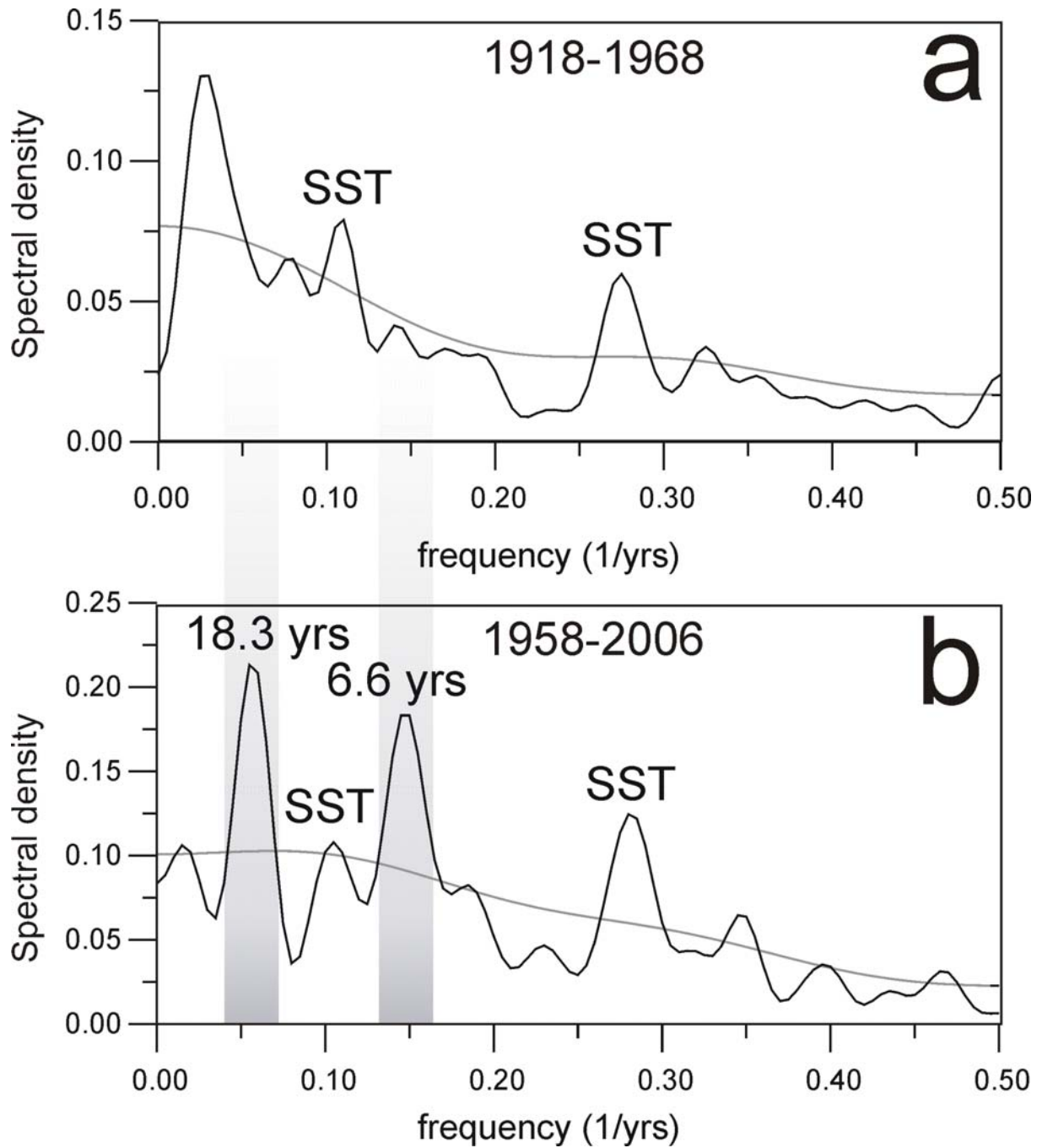
Figure 22: Blackman-Tukey spectra of annual extension-rates for (a) 1918-1968, and (b) 1968-2007. The bandwidth is 0.04 (number of lags: 41). The background (grey) was calculated as a low-resolution spectrum with a bandwidth of 0.3 (5 lags). Grey shaded areas highlight peak found, which are found (b) but not in (a). Predominant SST peaks are indicated.
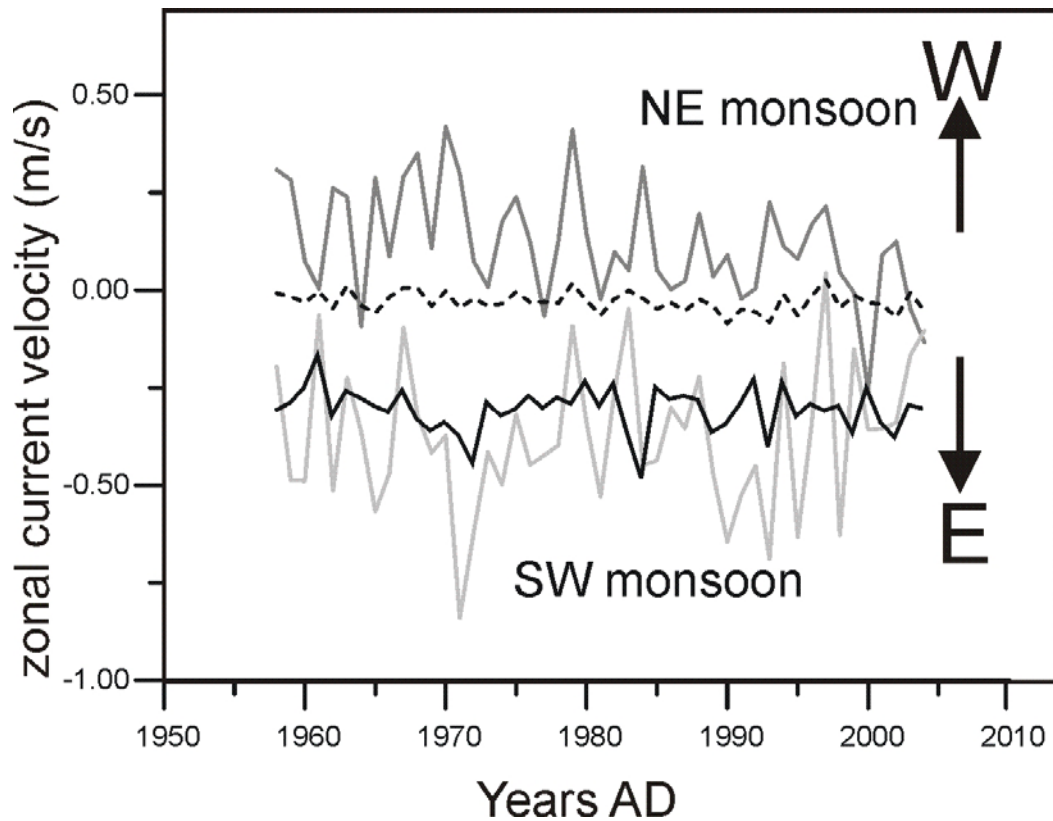
Figure 23: SODA time-series of 0.5°x0.5° gridded mean NE monsoon (November-February) and SW monsoon (May-September) zonal currents for the central Maldives. Light grey: current velocity during SW monsoon; dark grey: current velocity during NE monsoon; dashed line: mean annual current velocity; black: annual current gradient (difference between mean summer and winter current velocity for a given year). Note that positive velocities correspond to zonal velocity vectors orientated towards west, predominant during the NE monsoon season, while negative velocities accordingly correspond to vectors orientated towards east, predominant during the SW monsoon season.
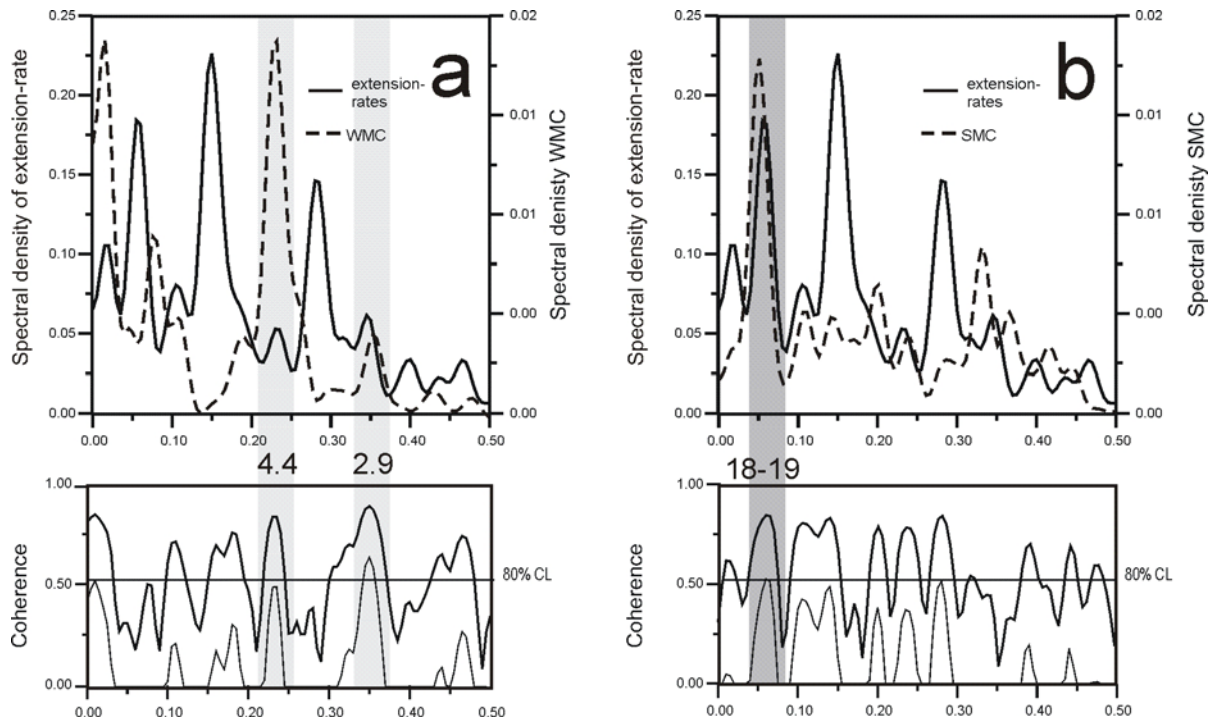
Figure 24: (a) Cross-spectral analysis between the extension-rates and mean winter monsoon current velocities from SODA for 1958-2006. Light grey shaded areas indicate spectral coherence between both time-series. (b) The same analysis for extension-rates with mean summer monsoon currents for the same period. Grey shading indicates spectral coherence. Numbers are given in years. See Figure 7c for legend.
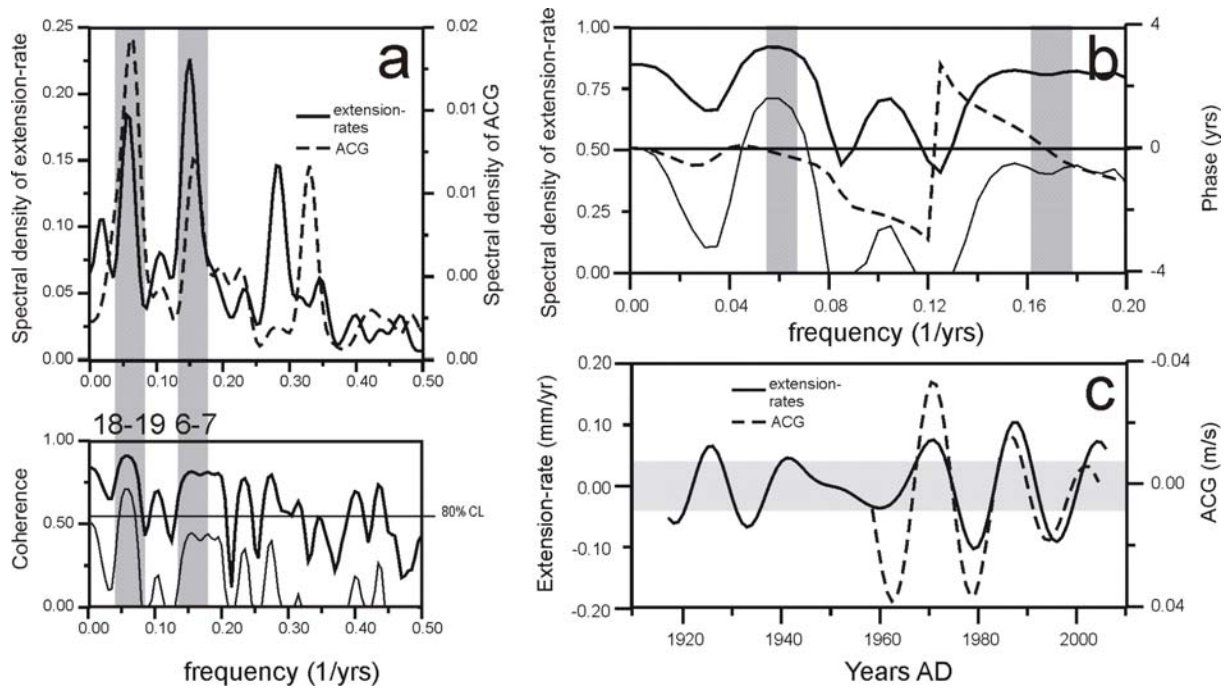
Figure 25: (a) Cross-spectral analysis between the annual current gradient record (ACG; difference between mean summer and winter monsoon current velocity from SODA), and annual extension-rates for 1958-2006. Grey shaded areas indicate spectral coherence between both time-series. Numbers are given in years. See Figure 7c for legend. (b) Enlargement of the coherence spectrum between the ACG record and extension-rates for the frequencies band of 0-0.5/yr, including Blackman-Tukey phase analysis (dashed line). Grey shaded areas indicate spectral coherence between both time-series. (c) Sixteen to eighteen years Gaussian band-pass filtered records of extension-rate and ACG. Note that the absolute values of the velocities were used. Note also the inverse axis of the ACG record. Shaded area indicates mean sampling resolution of 0.08 mm.
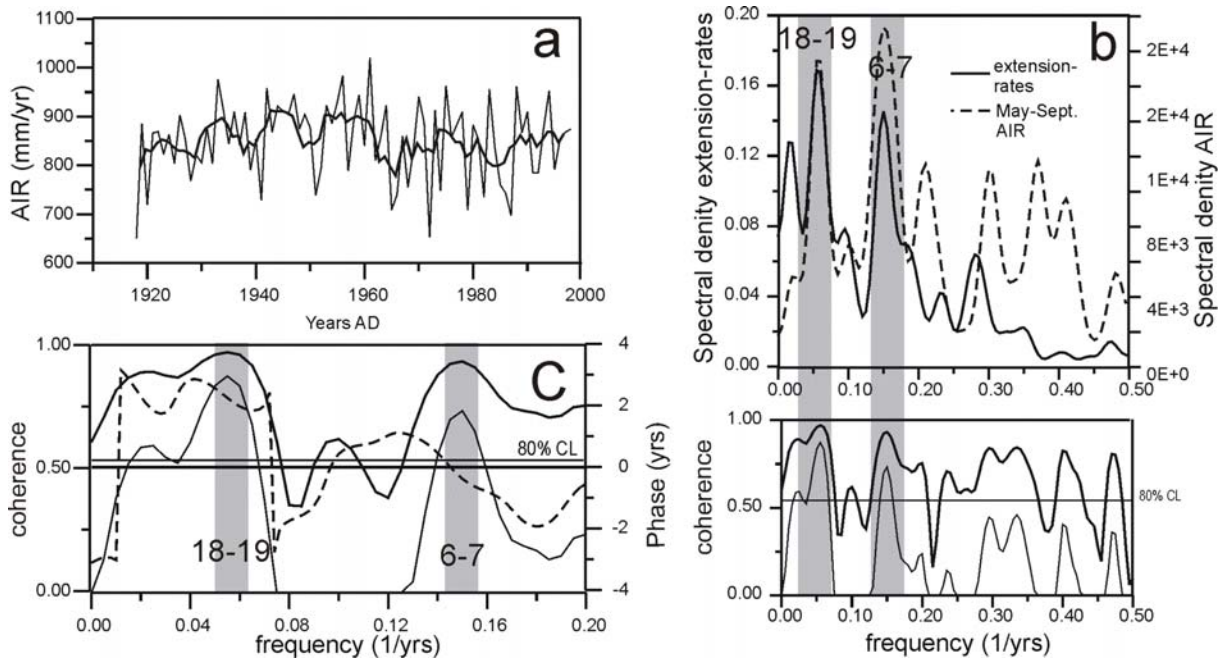
Figure 26: (a) Mean May-September All India Rainfall index (AIR; Sontakke and Singh, 1996) for the period 1917-1998. Bold line indicates 5-yrs running mean time-series. (b) Cross-spectral analysis between extension-rates of C1 and mean May-September AIR index, significant spectral coherence is highlighted by grey shading. Numbers are given in years. See figure 7c for legend. (c) Enlargement of the coherence spectrum between May-Sept. AIR index and extension-rates for the frequencies band of 0-0.5/yr, including Blackman-Tukey phase analysis (dashed line). Grey shaded areas indicate spectral coherence between both time-series.
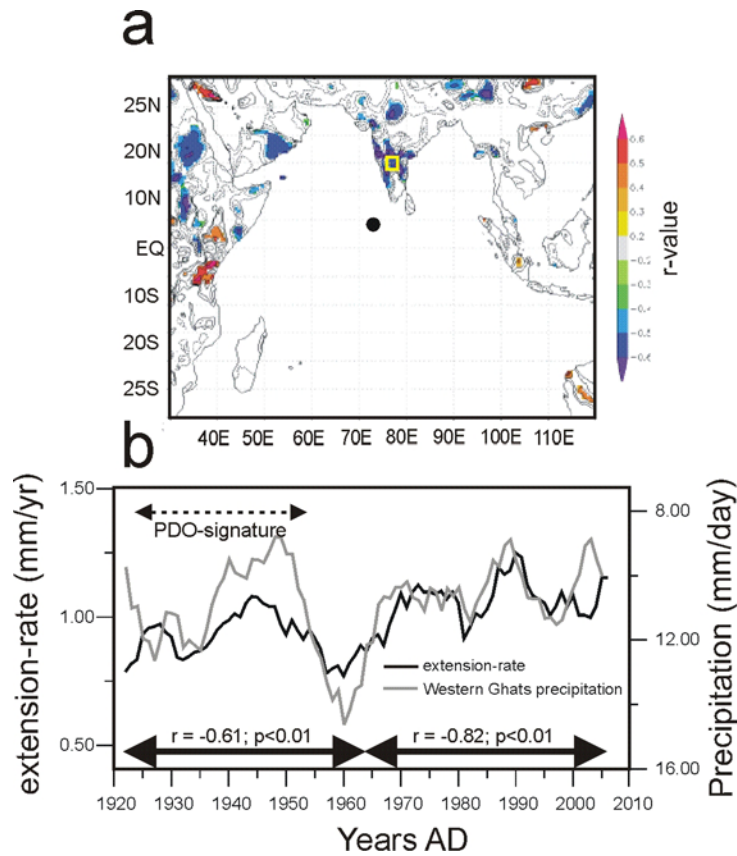
Figure 27: (a) R-values of field correlations between the extension-rate of C1 and May-September CRU TS3 precipitation on land (old world; grid:0.5°x0.5°) for 1922-2006. A low-pass filter (five years average) was applied in order to remove interannual variability. Correlations stronger than r = +0.4 or r = -0.4 are significant at 99%, based on a two-sided student t-test. R-values with p >0.10 are masked out. Blue areas mean strong negative and red strong positive correlation. Analysis was run with the KNMI climate explorer web application (van Oldenborgh and Burges, 2001; http://climexp.knmi.nl). Black dot indicates central Maldives. Rectangle indicates mean Western Ghat region. (b) Five-years running mean record of Western Ghat precipitation (CRU TS3; gridded over 73°E-76°E/13°-15°N) for 1922-2006. Note that correlation is negative and reversed y-axis of precipitation.
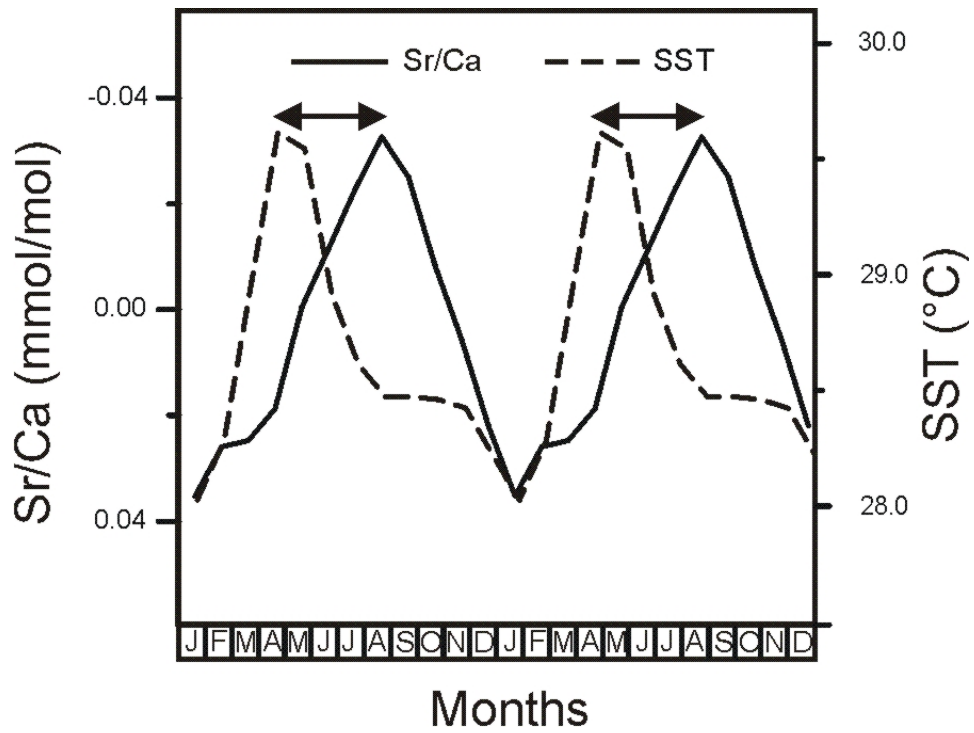
Figure 28: Comparison between two mean seasonal cycles of Sr/Ca and SST (ERSST, 1917-2006). Mean standard deviation is for Sr/Ca 0.06 mmol/mol, and for SST 0.2 °C. Black arrows indicate the temporal offset between Sr/Ca minima and SST maxima.
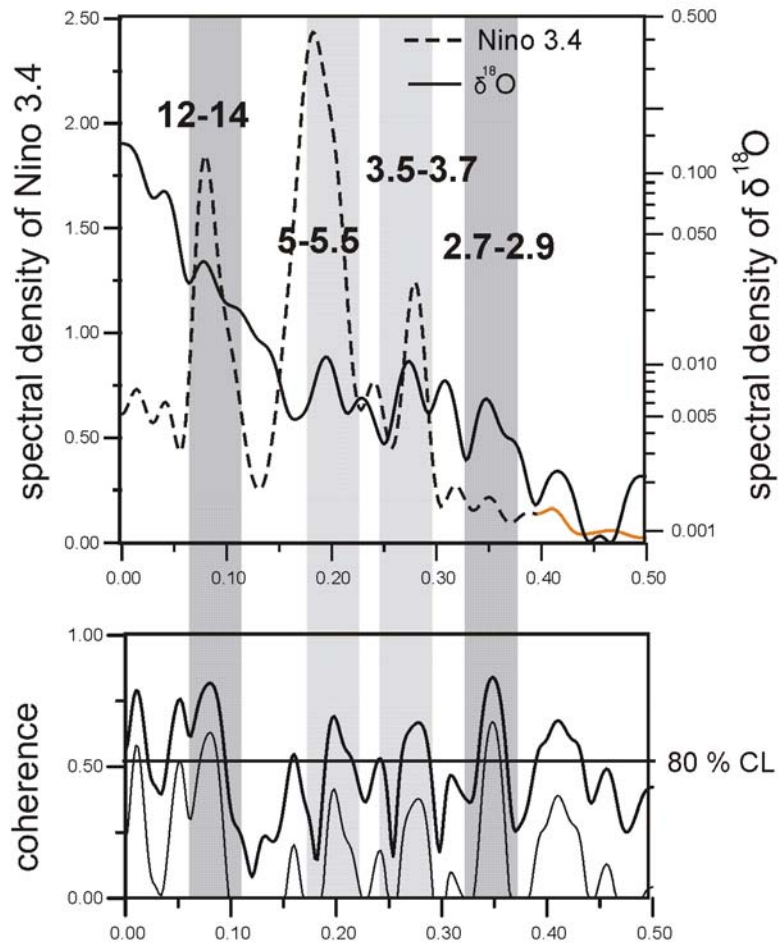
Figure 29: The results of Blackman-Tukey cross-spectral analysis between mean November-February $\delta^{18}O$ and Niño 3.4 for the interval 1917-2006. Note that the right axis of spectral density is chosen to be of logarithmic scale. Numbers in the variance spectrum are given in years. See Figure 7 for legend. Bandwidth is 0.04, number of lags = 41.
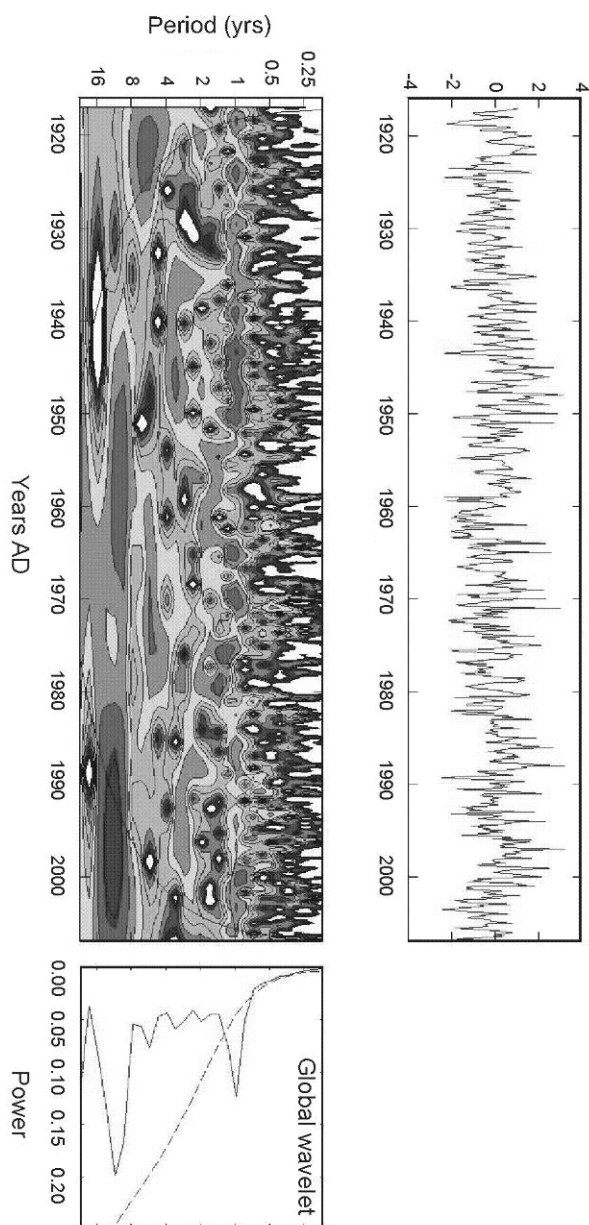
Figure 30: Wavelet power spectrum for the monthly δ¹⁸O record for 1917-2007. Upper panel shows the detrended and normalized time-series without reversed scale. Thick black line indicates the 5 % level of significance. Black line indicates the cone of influence. The Morlet wave function was chosen. This analysis was conducted with the Matlab software package performing cross wavelet transformation at http://www.pol.ac.uk/home/research/waveletcoherence. Note that the field of highest significance reaches out of the cone of influence.
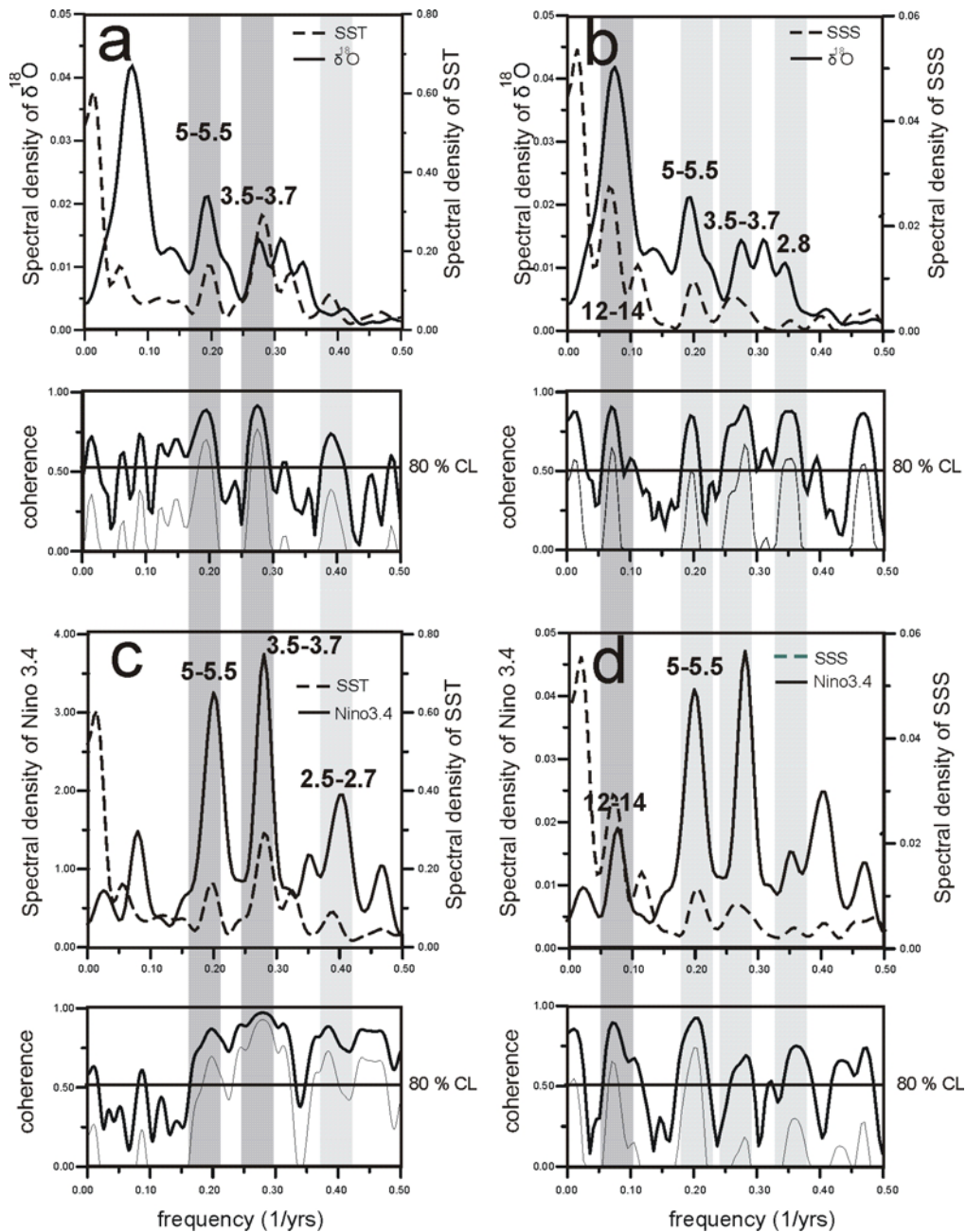
Figure 31: The results of Blackman-Tukey cross-spectral analyses for (a) annual mean δ^{18}O and SST (ERSST), (b) annual mean δ^{18}O and SSS, (c) annual mean SST and Niño 3.4, (d) annual mean SSS and Niño 3.4 for the period 1958 – 2004, for which SODA SSS data are available. Bandwidth = 0.04, number of lags = 41. See Figure 8 for legend. Dark grey shading indicates continuous spectral coherence above 80% CL in (a) and (c), and (b) and (d) respectively. Light grey shading indicates uncontinuous spectral coherence above 80% CL. See Figure 7c for legend.
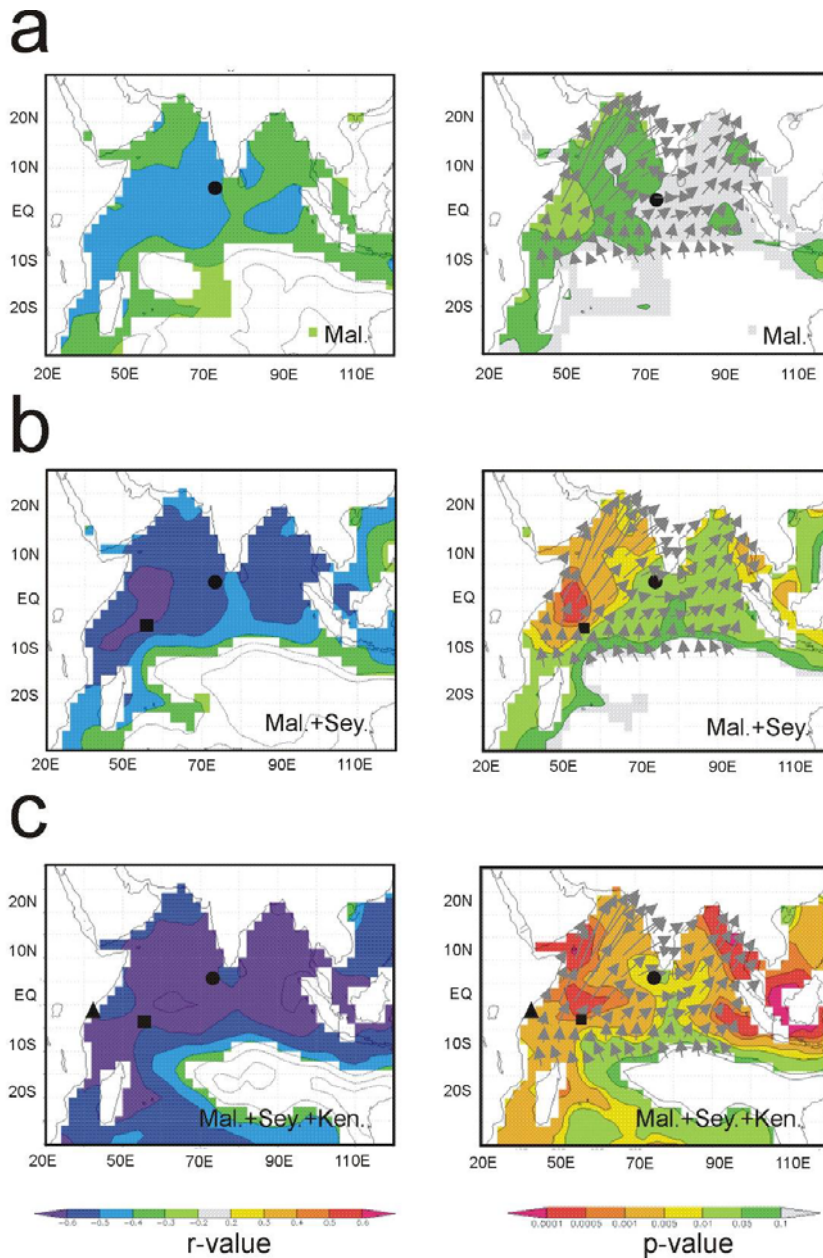
Figure 32: Field correlations of annual mean $\delta^{18}O$ records with 2°x2° gridded instrumental SST records (ERSST) in the NW Indian Ocean for the time span 1917-1995 (12-month running correlation) for (a) C1, (b) a combined record of C1 and the $\delta^{18}O$ record from the Seychelles (Charles et al., 1997), (c) a combined record of C1, Seychelles record, and $\delta^{18}O$ record from Kenya (Malindi, Cole et al., 2000). Left: r-values field; right: corresponding p-values field, circle indicates the location of the central Maldives, square the location of the Seychelles, and triangle the location of Malindi, Kenya. Correlations at or stronger than r = -0.4 are significant at the 99% confidence level based on a two-sided student t-test. The seasonal cycles were removed prior to analysis. Analysis was run with the KNMI climate explorer web application (van Oldenborgh and Burges, 2001; http://climexp.knmi.nl). P-values < 0.1 have been masked out. Arrows in the p-value fields indicate the predominant orientation of the wind field vectors during SW monsoon.
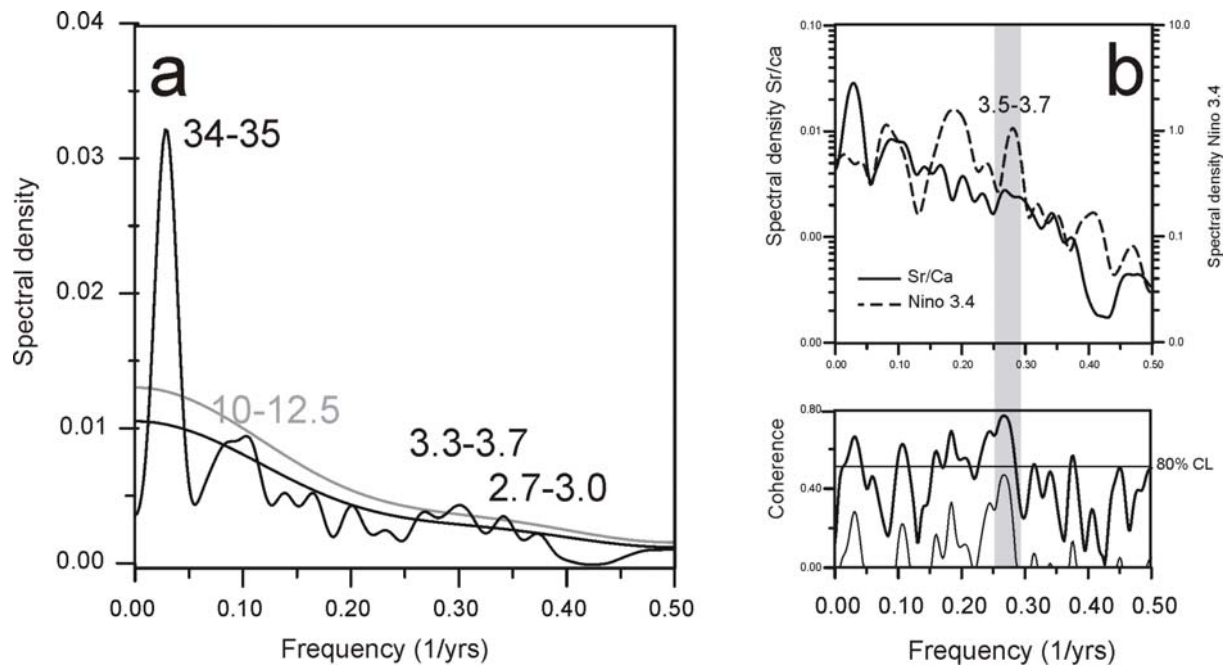
Figure 33: (a) Blackman-Tukey variance spectrum for the annual mean coral Sr/Ca record spanning the years 1917-2006. The high-resolution spectrum was calculated using 41 lags and a bandwidth of 0.04. The low-resolution noise background spectrum was calculated using 5 lags and a bandwidth of 0.3. Those peaks of the spectrum that rise over the low-resolution spectrum by a distance greater than the one-sided confidence interval at the 80% level (indicated by grey line) are marked in black. Those peaks below this level are marked in grey. Numbers are given in years. (b) Blackman-Tukey cross-spectrum between annual mean Sr/Ca and Niño 3.4 for the period 1917-2006. Shaded area indicates the period of highest spectral coherency. Both axes of ordinates are of logarithmic scale. The bandwidth is 0.04 (number of lags: 41). See Figure 7c for legend.
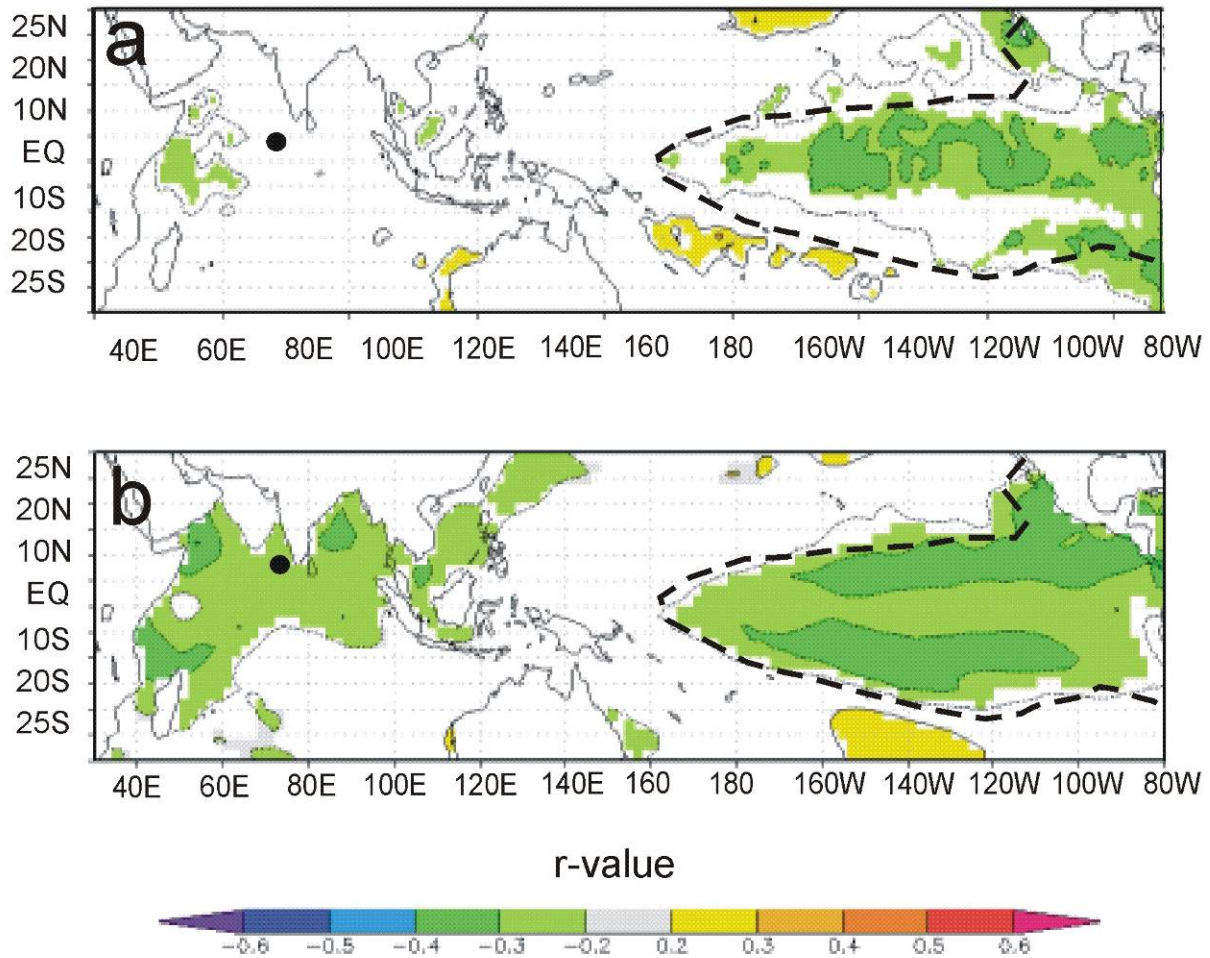
Figure 34: Field correlations of coral Sr/Ca records with (a) 1°x1° gridded instrumental SST records (HadISST1) and (b) 2°x2° gridded instrumental SST records (ERSST) in the Indo-Pacific realm for the time span 1917-2006 (12-months running correlation). A high-pass filter (year-on-year-difference) was used in order to highlight the interannual variability by removing trends or slow variations. SST datasets lack Sr/Ca by 6 months. Analysis was run with the KNMI climate explorer web application (van Oldenborgh and Burges, 2001; http://climexp.knmi.nl). P-values < 0.1 have been masked out. The seasonal cycles were removed prior to analysis. Black dot indicates the central Maldives, and dashed line the area of strongest interannual ENSO-forced SST variability. Compare with Figure 7.
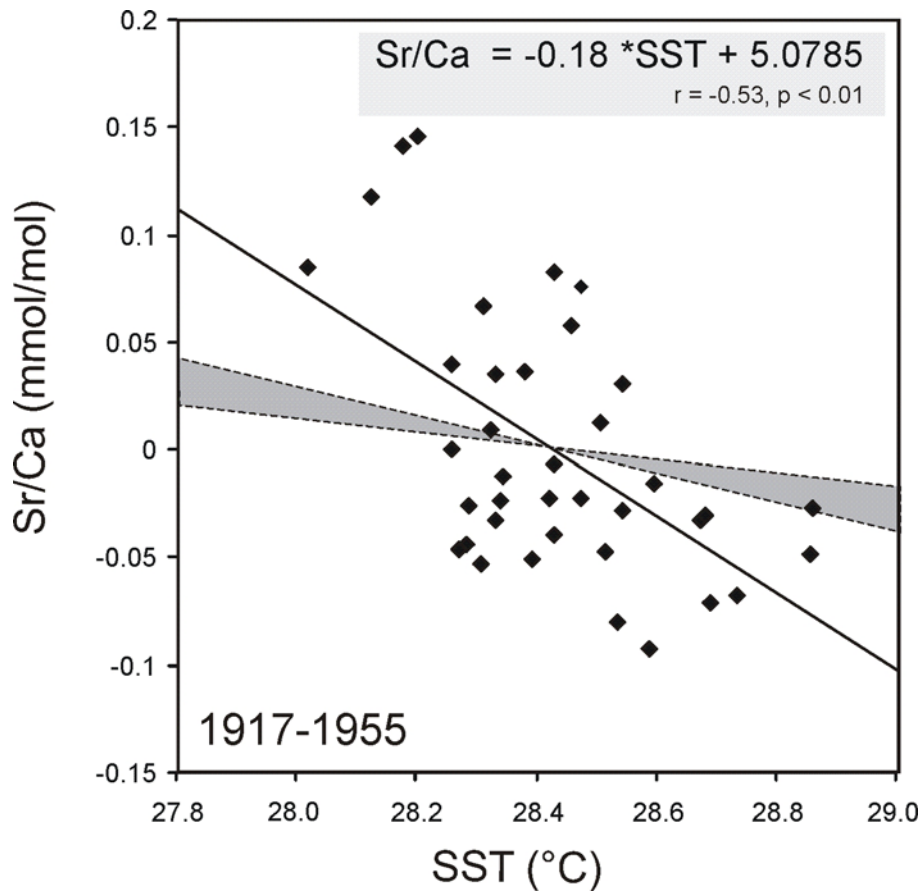
Figure 35: Linear regression between annual mean SST (ERSST) and coral Sr/Ca for the period 1917-1955. The correlation is significant, but the calculated regression slope is outside of the range of published regression slopes for the empirical Sr/Ca-SST relationship (between 0.04 and 0.08 mmol/mol °C^{-1}; Corrège, 2006). If the regression slope was within 0.04 and 0.08 mmol/mol °C^{-1}, and regression line ran through 0 mmol/mol at 28.4 °C, the linear regressions would be situated in the dark grey sector. Note that Sr/Ca values are given in zero mean values.
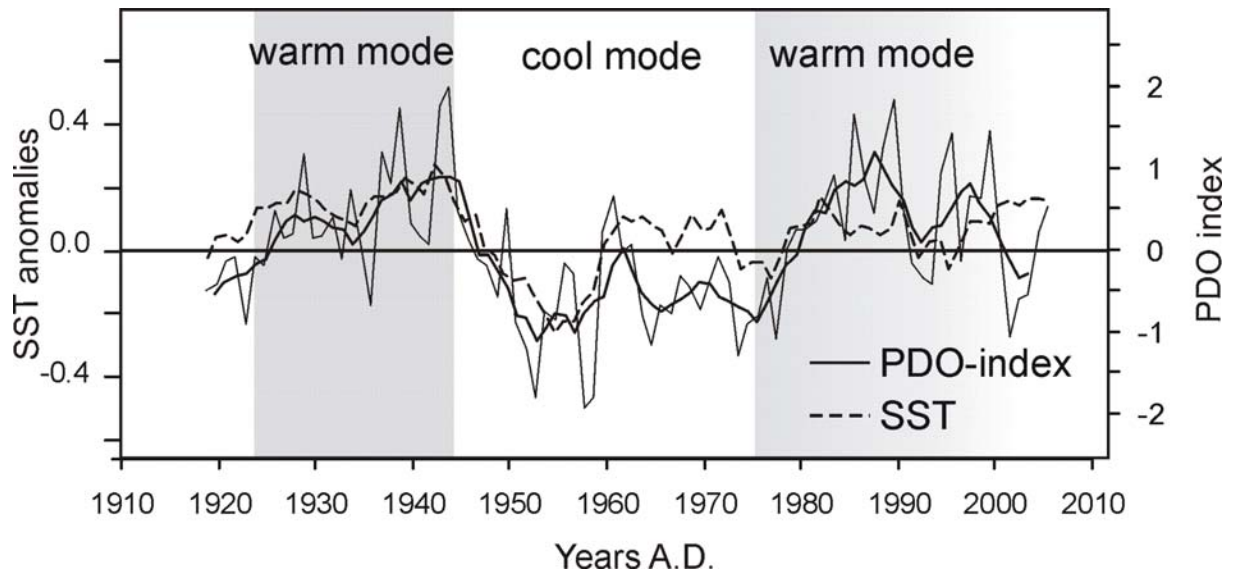
Figure 36: Time-series of annual mean PDO index (solid line; ERSST based), and SST from the central Maldives. Bold line indicates 5-years running mean average. Dashed line: 5-years detrended running mean SST (ERSST) for the central Maldives. Grey shaded areas indicate the warm modes after Mantua et al. (1997).
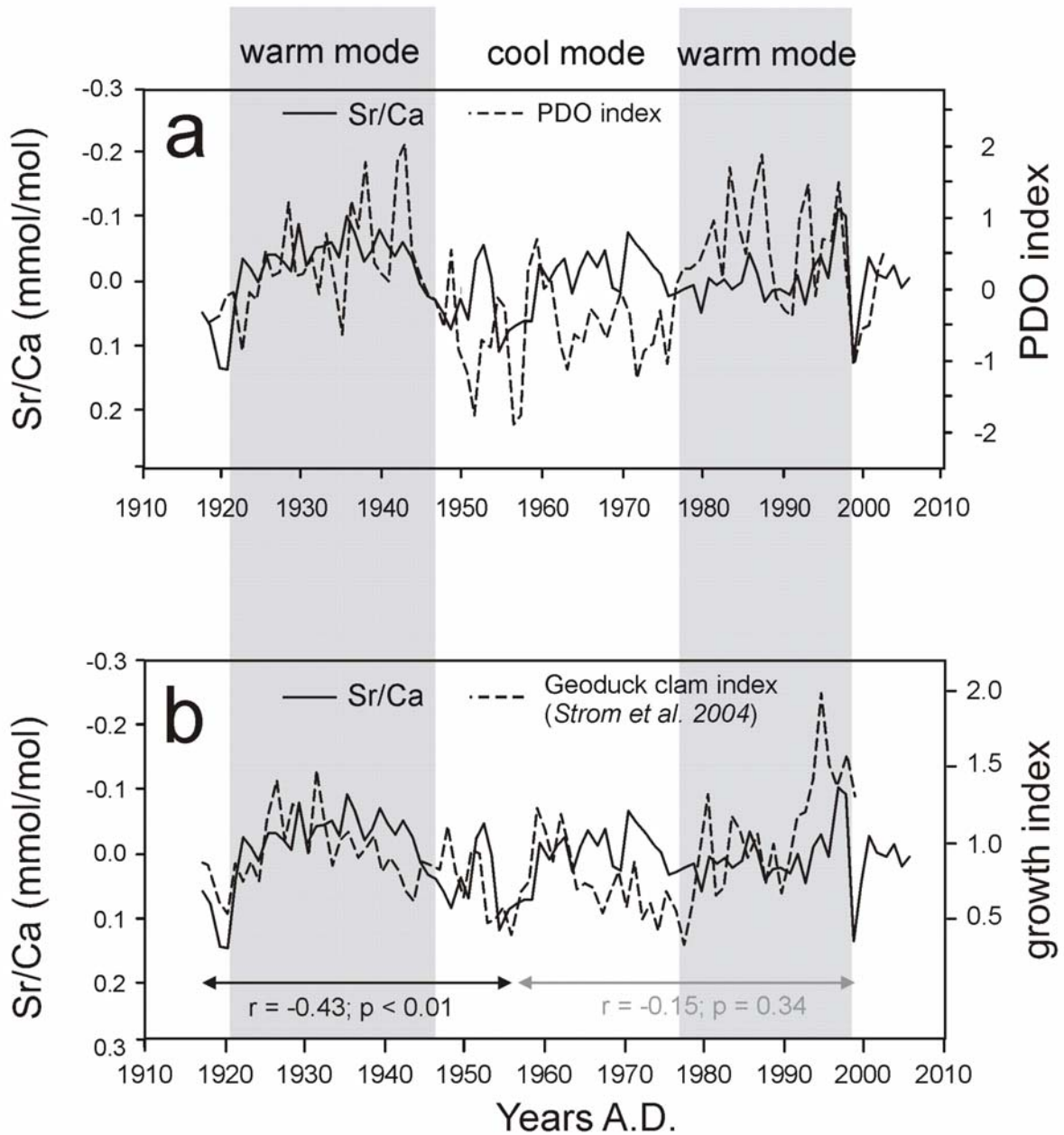
Figure 37: Annual mean records of coral Sr/Ca with (a) the PDO index (based on ERSST) and (b) a growth record of a Geoduck archive (122°W/48°N; 1917-1997) from Strom et al. (2004). Grey shaded areas indicate the warm modes after Mantua et al. (1997).. Note that in (b) the correlation between both time-series is only significant in the lower part of the record.
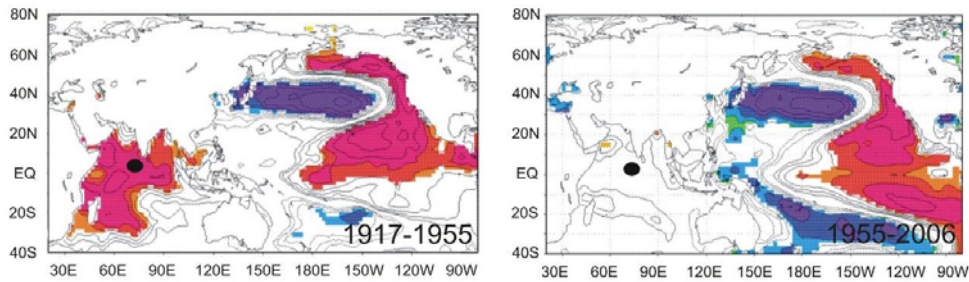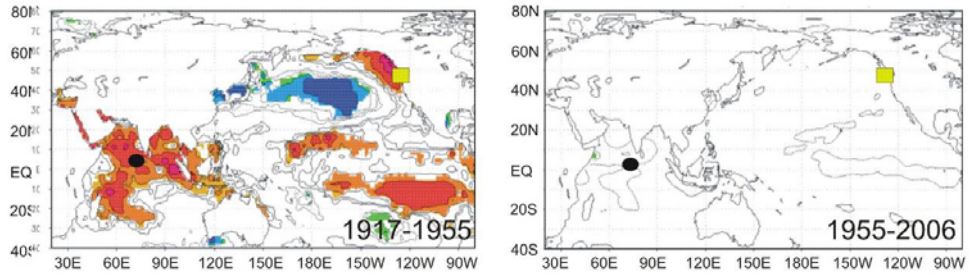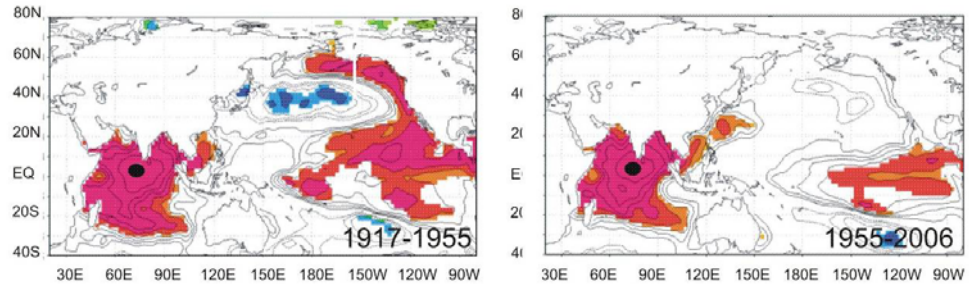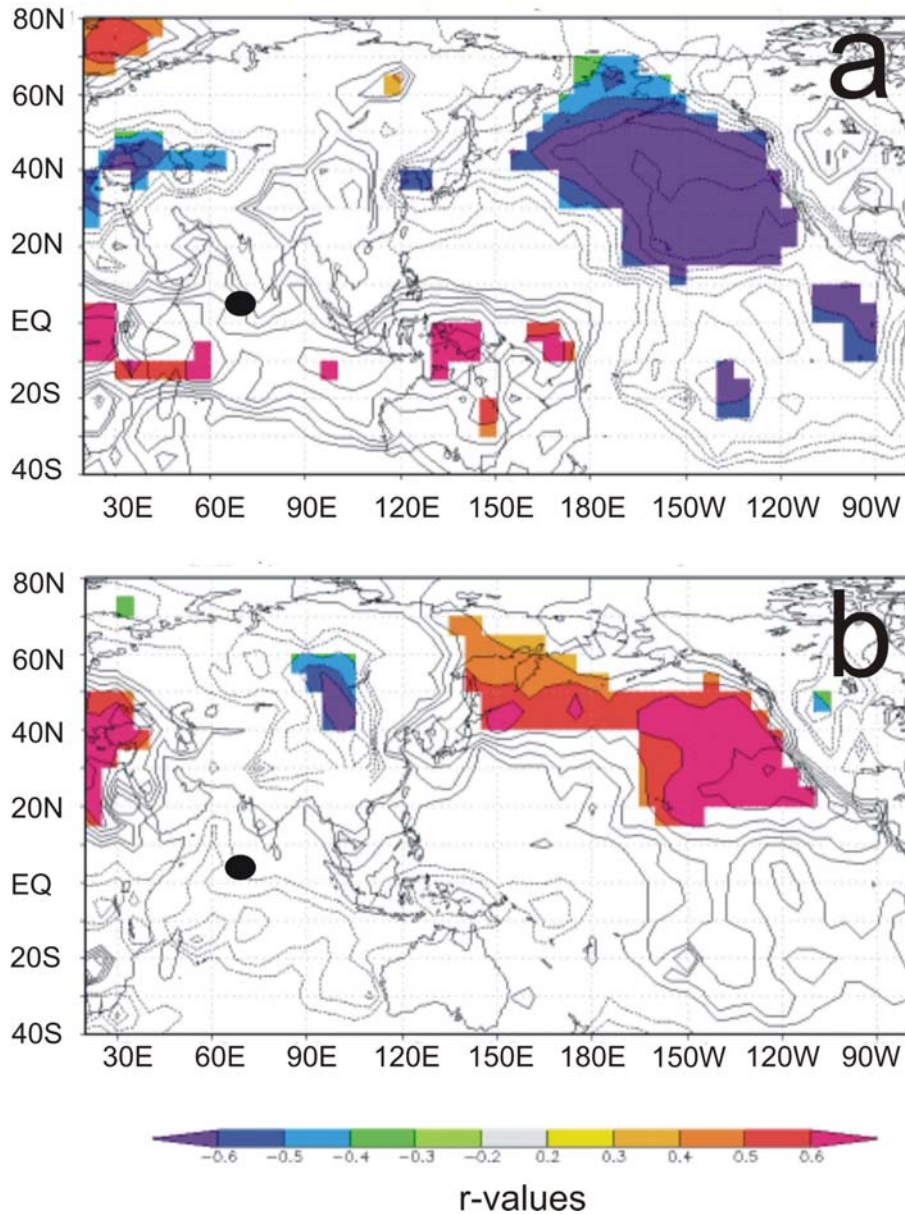
Figure 38: R-values of field correlations between 12-month running-averaged (a) annual mean PDO index (ERSST based) and SST records, (b) annual mean Sr/Ca from the Maldives (black dot) and SST records, and (c) SST from the central Maldives (3°-5°N/72°-74°E) and SST records. ERSST is used to represent SST fields. Correlations stronger than r = +0.4 or r = -0.4 are significant at 99%, based on a two-sided student t-test. R-values with p >0.10 are masked out. The seasonal cycles were removed prior to analysis. Analysis was run with the KNMI climate explorer web application (van Oldenborgh and Burges, 2001; http://climexp.knmi.nl).Yellow square in (b) indicates the site of the Geoduck clam growth record (Strom et al., 2004). Note that for the Sr/Ca values the positive sign was inverted for better comparison.

Figure 39: R-values of field correlations between 12-month running-averaged (a) annual mean PDO index (ERSST based) and SLP, and (b) annual mean Sr/Ca from C1 and SLP. Correlations stronger than r = +0.4 or r = -0.4 are significant at 99%, based on a two-sided student t-test. R-values with p >0.10 are masked out. In order to remove interannual noise, a low-pass filter was applied (3-yrs mean) in order to improve the signal to noise ratio. The seasonal cycles were removed prior to analysis. Analysis was run with the KNMI climate explorer web application (van Oldenborgh and Burges, 2001; http://climexp.knmi.nl). Field correlations were conducted with the HadSLP2 dataset of the MET Office Hadley Centre on a grid basis of 5°x5° (Allan and Ansell, 2006). Black dot indicates the position of the central Maldives.
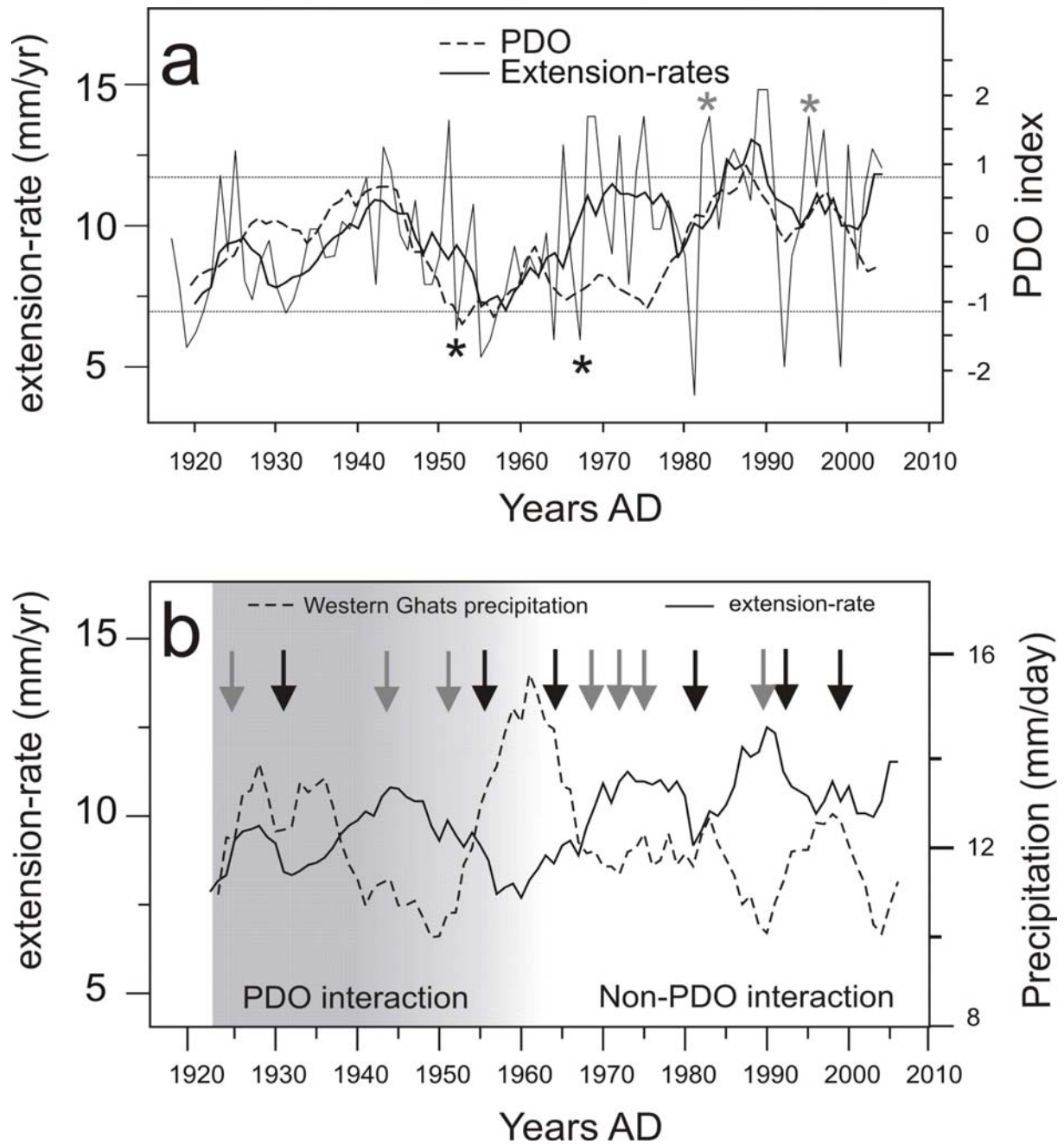
Figure 40: (a) Comparison between mean annual PDO index and annual extension-rates of C1 for 1918-2006. Bold thick line indicates 5-yrs mean average. Black and grey asterisks: negative and positive excursions of annual extension below 7 or above 12 mm (thin dashed line), which do not follow the pattern described in (b). (b) Comparison between 5-yrs means records of Western Ghat Precipitation and extension-rates. In comparison to Figure 27, the rainfall record is not reversely scaled. Black arrows: Years of slow extension (< 7 mm/yr) from (a), in most cases coinciding with stronger monsoon activity. Grey arrow: Years with faster extension (> 12 mm/yr), coinciding with weaker monsoon activity.
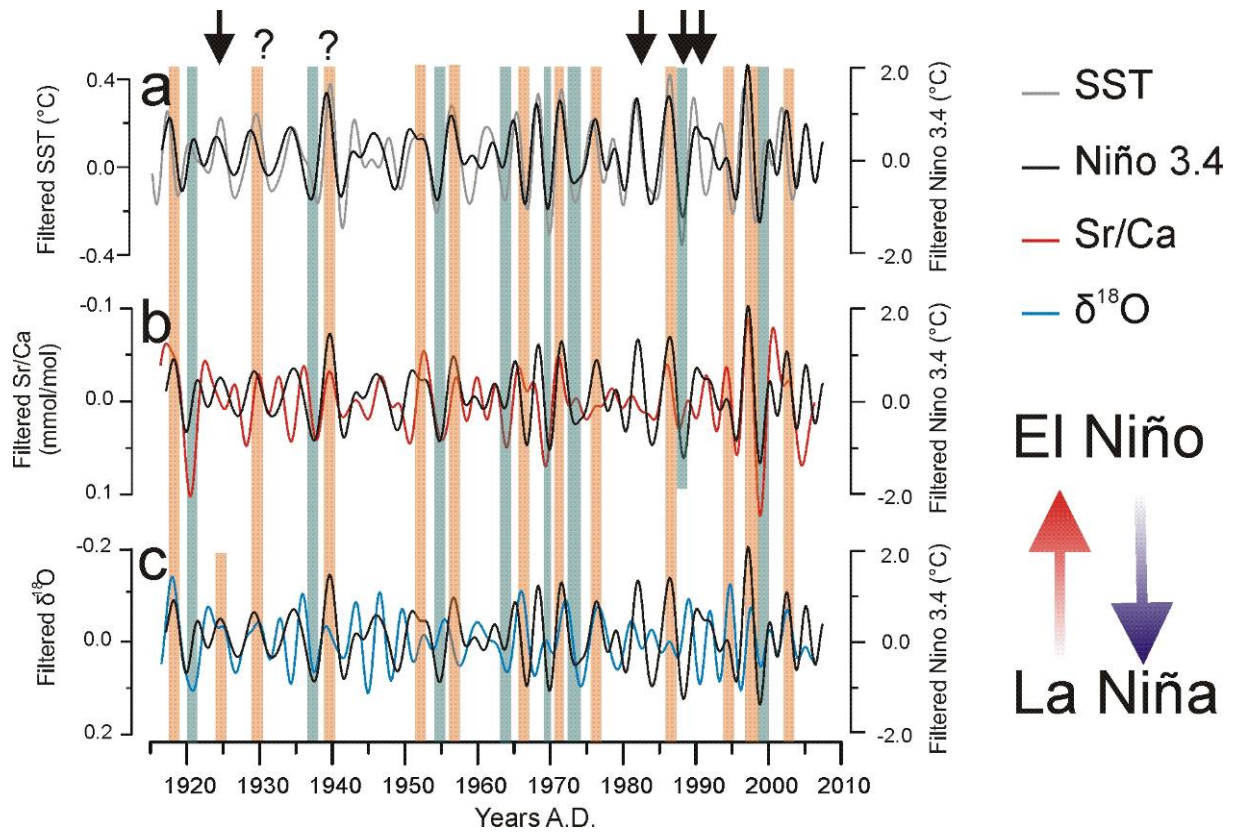
Figure 41: Band-pass filtered records (Hamming filter) of (a) gridded monthly SST (ERSST) and Niño 3.4, (b) monthly Sr/Ca and the Niño 3.4, and (c) monthly $\delta^{18}O$ and the Niño 3.4 to highlight the interannual ENSO band of 2.5-7 yrs. Red and blue shading indicate identified El Niño and La Niña events. Criteria for the identification of an ENSO event are the alignment of a positive anomaly in the proxy with a negative anomaly in Niño 3.4 (La Niña), and vice versa (El Niño), and the existence of a contemporaneous SST anomaly in the gridded SST record of the central Maldives (ERSST). Arrows indicate ENSO events, which are noted in the ENSO tabulation of Kousky and Bell (2000), and evident in gridded SST, but not in Sr/Ca and $\delta^{18}O$, or in only one of them. Question mark indicates possible ENSO events which are not mentioned by Kousky and Bell (2000). For the events after the year 2000, the climate page of the Department of Geoscience, University of Washington (www.atmos.washington.edu) was used. A temporal lag of ~6 months between Pacific and Atlantic is neglected.
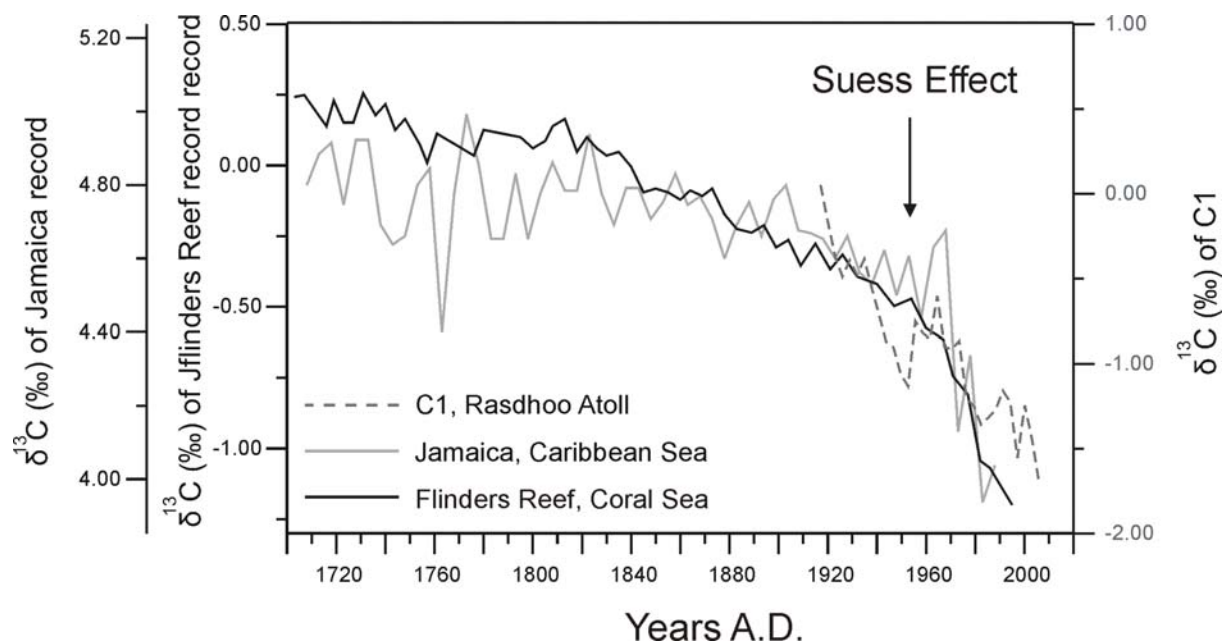
Figure 42: Comparison of $\delta^{13}C$ data for C1 (3-yrs average), a coralline sponge record from Jamaica (5-yrs mean average, *Ceratoporella nicholsoni*, Böhm et al., 2002), and a Porites coral from Flinders Reef in the W Pacific (5-yrs mean average, Pelejero et al., 2005).
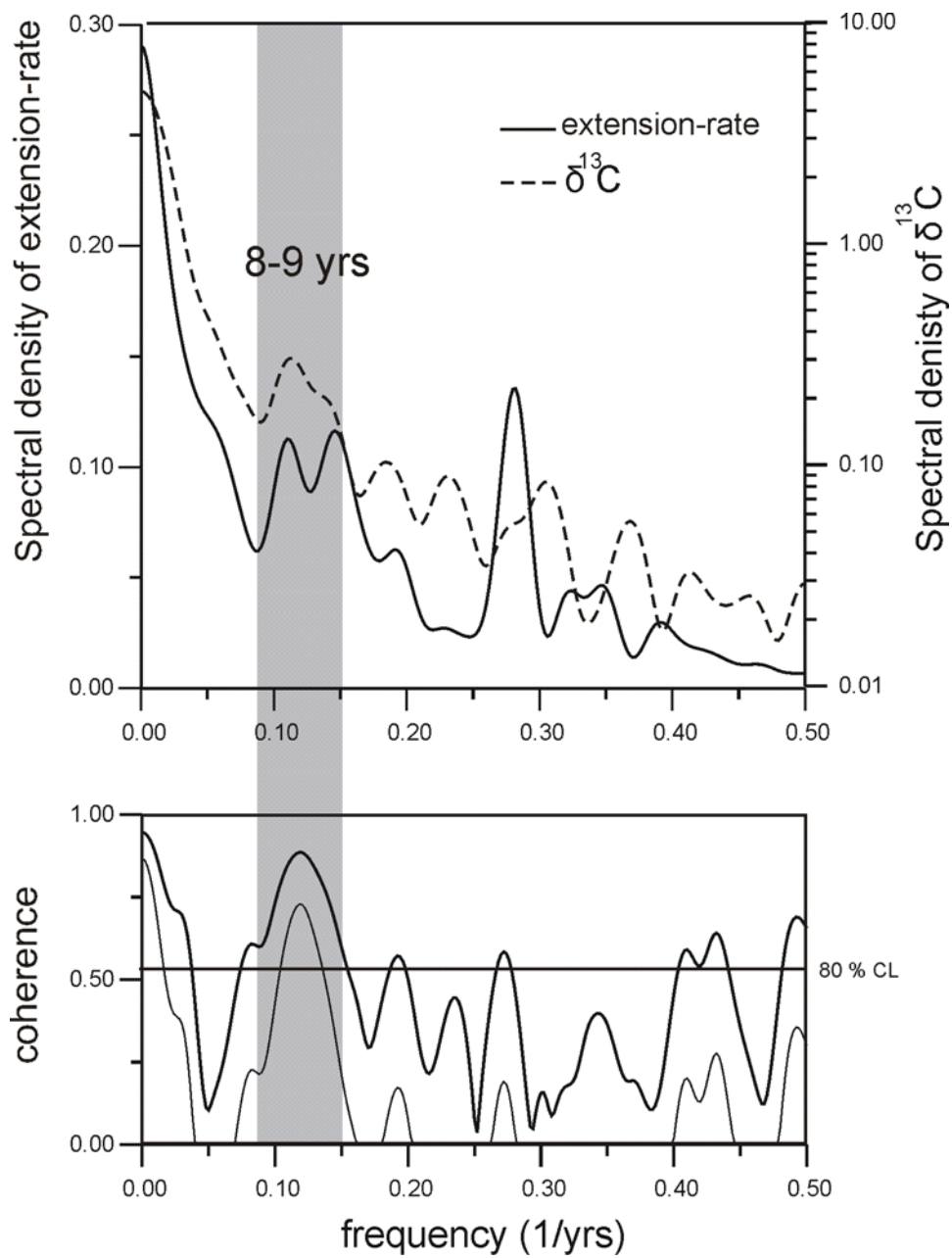
Figure 43: The result of a Blackman-Tukey cross-spectral analysis for annual extension-rate and annual mean $\delta^{13}C$. Grey shading highlights significant spectral density.
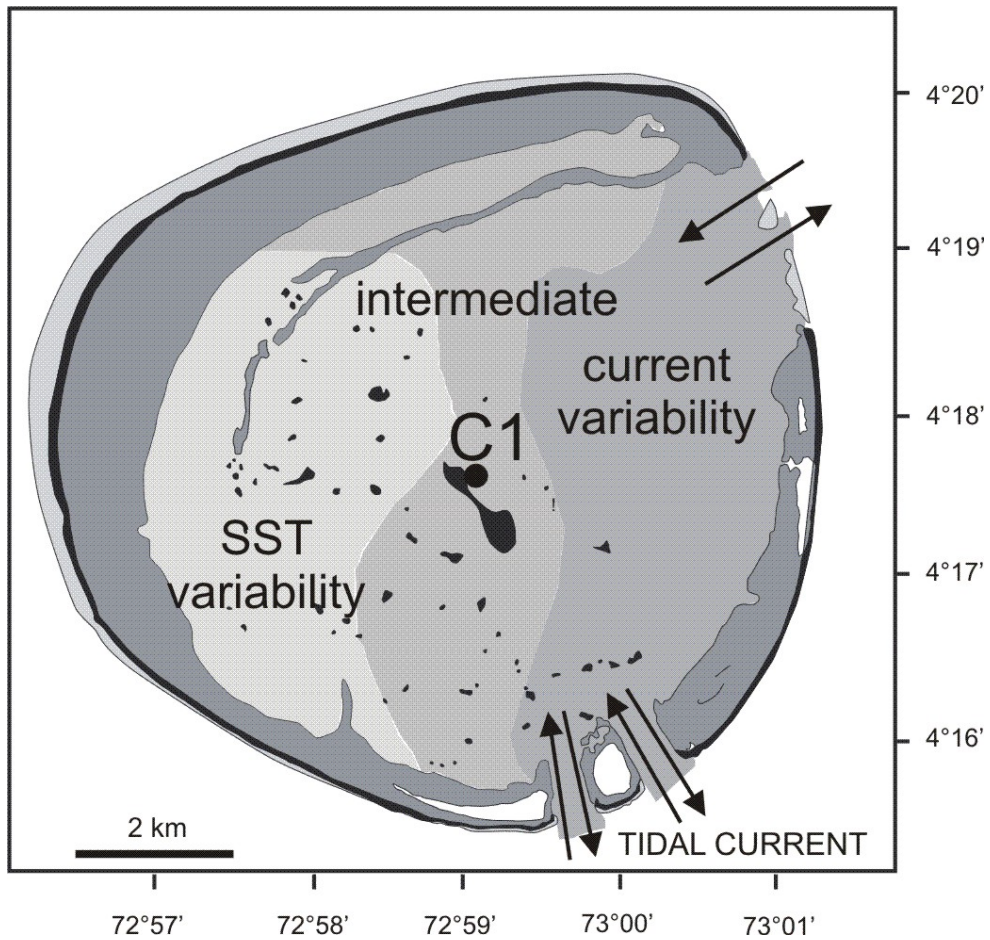
Figure 44: The proposed hypothesis of habitat-dependent "climate facies" for coral records. Dark grey area: hard bottom facies; medium grey area: mollusc wackestone-packestone facies; light grey area: mudstone facies. Redrawn after Gischler (2006): his figures 10 and 12.

Tables

Table 1: Instrumental records of SST, SSS, precipitation and OLR, used in this study. Abbreviations used here and in the text: ERSST: Extended Reconstructed SST; HadISST1: Hadley Centre Global Sea Ice and Sea Surface Temperature; SODA: Simple Ocean Data reanalysis project; COADS: Comprehensive Ocean Atmosphere Dataset. CRU: University of East Anglia Climate Research Unit.

record	grid	time period	reference
ERSSR v.3.	2°x2°; 72°-74°E/ 3°-5°N	1917-2007	Smith and Reynolds 2004; http://www.ncdc.noaa.gov
HadIISST1	1°x1°; 73°-74°E/ 4°-5°N	1917-2007	Rayner et al., 2003; http://metoffice.gov.uk/hadobs
SSS	0.5°x0.5°; 73°-73.5°E/ 4°-4.5°N	1958 - 2004	SODA, Carton et al., 2005; http://apdrc.soest.hawaii.edu/
Precipitation (4°10 N, 73°50E, 2 m; Hulhule Airport)	70 km west of Rasdhoo Atoll	1975-2007	Meteorology Department Male
Wind speed	2°x2°; 73°-74°E/ 4°-5°N	1977-2007	COADS, Woodruff et al., 1998; http://www.cdc.noaa.gov/
Zonal surface currents	0.5°x0.5°; 73°-73.5°E/ 4°-4.5°N	1958 - 2004	SODA, Carton et al., 2005; http://apdrc.soest.hawaii.edu/
OLR	2.5° x2.5°; 72°x74.5°E/ 3.75°-6.25°N	1974-2007	Liebmann and Smith, 1996; http://www.cdc.noaa.gov/
Precipitation South India	3°x2°; 73°E-76°E/ 13°-15°N	1917-2007	Mitchel and Jones, 2005 http://badc.nerc.ac.uk/data/cru

Table 2: $\delta^{18}O$ of ten measured water samples (depth: 1 m), collected on 9th February 2009 in the lagoon (3, 7, 8, 9, 10) and fore reef (1, 2, 4, 5, 6) of Rasdhoo Atoll. The standard deviation of the 10 samples is 0.12‰. The measurement of the $\delta^{18}O$ composition of seawater samples collected at Rasdhoo Atoll follows the method described by Swart et al. (2000). The standard deviation for each single measurement is 0.07‰, and the data are reported relative to VSMOW.

sample number	$\delta^{18}O$	Location
		4°18'0/72°56'0
1	0.52	
		4°17'8/73°00'1
2	0.75	
		4°17'8/72°58'8
3	0.62	
		4°16'7/72°58'1
4	0.62	
5	0.50	4°16'8/73°00'0
6	0.33	4°16'5/72°56'7
7	0.42	4°17'2/73°00'7
8	0.53	4°16'2/72°58'4
9	0.50	4°18'0/72°57'1
10	0.43	4°18'3/73°00'6
mean	0.52	

Table 3: Basic statistics of the monthly and bimonthly coral $\delta^{18}O$ record.

C1	Mean	SD
monthly	-4.92	0.14
min	-5.10	0.11
max	-4.71	0.11
seasonality	0.39	0.13
annual mean	-4.92	0.09

Table 4: Summary of correlation coefficients (r-values) of annual mean coral δ^{18}O and annual mean climate records. Correlations with SSS are for the period 1958-2004. Bold: Significance at 95 %.

	C1	ERSST	HadleySST	SODA SSS
C1	1	…	…	…
ERSST	-0.42	1	…	…
HadleySST	-0. 31	0.93	1	…
SODA SSS	-0.02	-0.41	-0.38	1

Table 5: Regression analyses for annual mean $\delta^{18}O$ and SST datasets for the period 1917-2006.

	Regression equation	r (R^2)	p
ERSST (2°x2°)	$\delta^{18}O$ = -0.13 * SST -1.49	-0.42 (0.20)	<0.0001
HadISST1 (1°x1°)	$\delta^{18}O$ = -0.10 * SST -2.41	-0.31(0.10)	<0.0001

Table 6: Correlations (r-values) between annual mean Sr/Ca, HadISSST1, ERSST, and PDO index for the period 1917-1955, and .1955-2006, respectively. All correlations are significant at the 95 % level.

1917-1955	Sr/Ca	HadISST1	ERSST
Sr/Ca	1	...	...
HadISST1	-0.39	1	...
ERSST	-0.53	0.91	1

1955-2006	Sr/Ca	HadISST1	ERSST
Sr/Ca	1	...	...
HadISST1	-0.21	1	...
ERSST	-0. 30	0.90	1

Table 7: Twice standard variation of gridded SST in the interannual ENSO band of 2.5-7 yrs. Lower and upper limit are indicating the range of estimated SST fluctuations for relative low and high published slopes for the proxy-SST relationship (δ^{18}O: 0.22 ‰/°C and 0.18 ‰/°C, Grotolli and Eakin, 2007; Sr/Ca: 0.08 mmol/mol °C-1 and 0.05 mmol/mol °C-1, Corrège, 2006). As mean slopes 0.20 ‰/°C and 0.06 mmol/mol °C-1 were used (Grotolli and Eakin, 2007; Corrège, 2006). Twice standard deviation for Sr/Ca was 0.06 mmol/mol °C-1, and for δ^{18}O 0.05 ‰/°C.

	lower limit (°C)	mean (°C)	upper limit (°C)
SST		0.3	
δ^{18}O	0.4	0.5	0.6
Sr/Ca	0.9	1.0	1.6

Table 8: Summary of climate variability and non-climatic trends.

Proxy	Climate signals and trends
Extension-rate	QBO, ENSO-forced interannual variability, Indian Ocean SST variability within 8-9 yrs, decadal and interannual monsoon variability, warming trend
$\delta^{18}O$	ENSO-forced interannual variability, ENSO-like decadal variability, monsoon-induced cooling, warming trend
Sr/Ca	ENSO-forced interannual variability, PDO 1917-1955, secular seawater Sr/Ca variations (?)
$\delta^{13}C$	Suess effect

Danksagung

Auch wenn diese Arbeit, dies wir niemand anzweifeln, nicht dem Bereich der Klassischen Mechanik zuzurechnen ist, möchte ich mich hier auf einen wichtigen Satz von Sir Isaac Newton (1643-1727) berufen, welcher im Allgemeinen ihm zugeschrieben wird:

„If I have been able to see further, it is because I have stood on the shoulders of giants "

<div align="right">Brief and Robert Hooke, 5. Februar 1675/76</div>

auf den Malediven geholfen haben. Dazu danke ich Dr. Harold Hudson (Miami), welcher die Korallenkerne bohrte und bei der Lösung vielfältiger technischer Probleme half. Kapitän Haneeff von der Insel Radhoo und seine Dhoni Besatzung danke ich für ihr nautisches Können in den Gewässern der Malediven. Dr. Reinhard Kikinger (Kuramathi Island Biostation) und Bill Allison (Male) halfen bei logistischen Problemen. Ms. Fareesha Adam and Dr. Shiham Adam von der Regierung der Malediven unterstützen die Reise administrativ und halfen bei der Genehmigung.

Dr. Rainhard Kikkinger stellte Aufzeichnungen von Meerwassertemperaturen von Radhoo Atoll für 2005 und 2006 zur Verfügung und sammelte Seewasserproben in der Lagune und um Rasdhoo Atoll. Dr. Peter Swart (Universität von Miami) hat die Sauerstoffisotopie dieser Proben gemessen. Dr. Geert Jan Oldenbourgh bin ich dankbar für Entwicklung und Instandhaltung des KNMI climate explorer (http://climexp.knmi.nl), sowie für die Hilfe bei statistischen Analysen.

Danken möchte ich Frau Anhalt für ihre Hilfe in vielfältiger Weise und für den guten Kaffee, den sie immer bereitstellt.

Abschließend möchte ich Birgit, meiner Frau, unendlich danken, nicht nur für das Korrekturlesen, sondern für ihre seelische und moralische Unterstützung und die viele Geduld. Meinen Eltern und meiner Schwester möchte ich für all das danken, was sie mir ermöglicht haben.

Curriculum vitae

Dipl. Geol. David Markus Ulrich Storz

Marbachweg 272
60320 Frankfurt am Main

Persönliche Angaben

Geburtsdatum:	03.03.1979
Geburtsort:	Filderstadt
Nationalität:	Deutsch
Familienstand:	verheiratet

Schulbildung

08/1985 – 07/1989:	Grundschule Mosbach-Waldstadt
08/1989 – 07/1995:	Realschule Mosbach, Baden
09/1995 – 06/1998:	Technisches Gymnasium Mosbach, Baden
06/1998:	Abitur
08/1998 – 08/1999:	Zivildienst

Hochschulausbildung

10/1999 – 09/2000:	Studium der Mathematik an der Eberhard-Karls-Universität Tübingen
10/2000 – 09/2006:	Studium der Geowissenschaften an der Eberhard-Karls- Universität Tübingen mit dem Schwerpunkt Mikropaläontologie
04/2004 - 08/2005:	Stipendiat der „Studienstiftung des Deutschen Volkes"
07/2005 – 04/2006:	Diplomarbeit am Lehrstuhl für Mikropaläontologie mit dem Titel „Die Saisonalität planktischer Foraminiferen im Bereich einer Sinkstofffallenstation im

subtropischen Nordatlantik zwischen Februar 2002 und April 2004"

06/2006 – 07/2006:	Studienarbeit am Lehrstuhl für Mikropaläontologie, mit dem Titel „Coccolithophoridenfloren entlang eines Transekts im subtropischen Nordatlantik im März 2006 (FS Poseidon Reise 334)"
29.09.2006:	Abschluss des Diplomstudiengangs Geowissenschaften mit der Diplomprüfung und der Gesamtnote 1,1
04/2007 - 03/2010	Wissenschaftlicher Mitarbeiter in der Facheinheit Paläontologie, Arbeitsgruppe Biosedimentologie, Institut für Geowissenschaften, Goethe-Universität Frankfurt, Projekt Gi 222/14. Wissenschaftlicher Betreuer: Prof. Dr. Eberhard Gischler